

AD-753 010

OPTIMAL CONTROL OF THE F-8C IN A FULLY
AUTOMATIC CARRIER APPROACH

Roger J. Bannett

Naval Air Development Center
Warminster, Pennsylvania

7 November 1972

DISTRIBUTED BY:

NTIS

National Technical Information Service
U. S. DEPARTMENT OF COMMERCE
5285 Port Royal Road, Springfield Va. 22151

AD753010

Reproduced by
**NATIONAL TECHNICAL
INFORMATION SERVICE**
U S Department of Commerce
Springfield VA 22151

UNCLASSIFIED

Security Classification

DOCUMENT CONTROL DATA - R & D

AD 753 010

Systems Analysis and Engineering Department
 Naval Air Development Center
 Warminster, Pennsylvania 18974

UNCLASSIFIED

OPTIMAL CONTROL OF THE F-8C IN A FULLY AUTOMATIC CARRIER APPROACH

FINAL REPORT

Roger J. Bennett

7 November 1972

18. TOTAL NO. OF PAGES

135/40

13

A34533-906/2021/F012-04-03

B. PROJECT NO. Work Unit 29

19. ORIGINATOR'S REPORT NUMBER(S)

NADC-SD-7153

20. OTHER REPORT NO(S) (Any other number(s) that may be assigned this report)

17. DISTRIBUTION STATEMENT

Approved for public release; distribution unlimited.

21. SUPPLEMENTARY NOTES

22. SPONSORING MILITARY ACTIVITY

Naval Air Systems Command
 Washington, D. C.

23. ABSTRACT

The report
 This paper presents a detailed exposition of the problems associated with landing high performance jet fighter aircraft on a moving aircraft carrier along with a new procedure for designing a fully automatic flight control system tailored to the aircraft carrier approach. Included in the development is a brief description of the present SPN-42 ACLS (Aircraft Carrier Landing System) and the probable reason for its very limited success. Possible alternatives to the SPN-42 system have suggested a more sophisticated ACLS configuration, in particular, the AMOAC (Automatic Multiloop Optimal Approach Controller) developed herein. The use of an AMOAC system in actual carrier approaches should yield a substantial improvement to present automatic carrier landing capability. The results of Appendix I show that similar closed loop dynamics can be expected for other carrier based, high performance aircraft. In particular, it is felt that the AMOAC design procedure has potential for rapid and straightforward application to the A-5A and the F-4 aircraft.

I-A

UNCLASSIFIED

UNCLASSIFIED

Security Classification

14

KEY WORDS

LINK A

LINK B

ROLE

WT

ROLE

WT

Carrier Landing
Automatic Flight Control
Automatic Carrier Landing System
Optimal Control

I-2

DD FORM 1473 (BACK)
NOV 68
(PAGE 2)

UNCLASSIFIED

Security Classification



DEPARTMENT OF THE NAVY
NAVAL AIR DEVELOPMENT CENTER
WARMINSTER, PA. 18974

Systems Analysis and Engineering Department

REPORT NO. NADC-SD-7153

7 November 1972

Optimal Control of the F-8C in a
Fully Automatic Carrier Approach


FINAL REPORT

AIRTASK A34533-906/2021/F012-04-03
Work Unit 29

Prepared by: R. J. Bannett

Reviewed by: C. A. DeCrescente

Approved by:


W. H. Raber
Director

Approved for public release; distribution unlimited.

I-C

TABLE OF CONTENTS

List of Tables	Page
List of Figures	v
List of Symbols	vi
	viii
I Introduction	
A. Background	1
B. Design Consideration	3
II Theory	
A. Optimal Control Equations	5
B. Design Procedure	11
1. System Roots	13
2. Carrier Approach Simulation	18
3. Guidance Loop Closure	30
C. Desired Closed Loop System	31
1. Phugoid and Short Period Roots	31
2. Numerator Zeros	34
III. Results	
A. Application to the F-8C	36
1. System Synthesis	36
2. Design Evaluation	54
IV. Conclusions	78
V. Literature Cited	80
VI. Bibliography	81
Appendix A - Aerodynamic Parameters	82

	Page
Appendix B - Optimal Control Equations	87
Appendix C - Root Square Locus Equation	91
Appendix D - Carrier Approach Simulation Equations	94
Appendix E - Carrier Motion Dispersion	99
Appendix F - Guidance Loop Equation	101
Appendix G - Open Loop Transfer Matrix	104
Appendix H - AMOAC Design Data	106
Appendix I - Design Limitations of Root Square Locus Technique for the Carrier Approach	113

L I S T O F T A B L E S

		Page
Table I	Inner Loop Closures	43
Table II	Numerator and Denominator Loop Closures	48
Table III	Closed Loop Roots	53
Table IV	Preliminary Systems	54
Table V	Glide Slope Deviations (A/C alone)	59
Table VI	Glide Slope Deviations (A/C plus Actuators and Limiters)	62
Table VII	Aerodynamic Parameters for Various Navy Aircraft	113
Table VIII	Constant Terms of $C_{12}(s)$	115
Table IX	Coefficient Term of $C_{22}(s)$	115
Table X	Coefficient Terms of $N_{22}(s)$	117
Table XI	$N_{22}(s)$ for Various Navy Aircraft	118
Table XII	Roots of $N_{22}(s)$	119
Table XIII	Coefficient Terms of $N_{23}(s)$	121
Table XIV	$N_{23}(s)$ for Various Navy Aircraft	122
Table XV	Roots of $N_{23}(s)$	122
Table XVI	Criteria for Satisfactory Phugoid Control Zero	124

LIST OF FIGURES

	Page
Figure 1 Longitudinal Stability Axes	6
Figure 2 AMOAC Logic Flow Diagram	14
Figure 3 Undisturbed Glide Slope	20
Figure 4 Carrier Approach Environment	21
Figure 5 Carrier Approach Model (Stationary TD)	23
Figure 6 Carrier Approach Simulation Geometry	26
Figure 7 Desirable Closed Loop Roots	33
Figure 8 Pitch Rate Frequency Response	35
Figure 9 Sink Rate Loop Loci	38
Figure 10 Complex Sink Rate Loop Loci	39
Figure 11 Locus of Negative Real Cross Coupling Root	40
Figure 12 Pitch Rate Loop Loci	41
Figure 13 Numerator and Denominator Loci-Case I	45
Figure 14 Numerator and Denominator Loci-Case II	46
Figure 15 Numerator and Denominator Loci-Case III	47
Figure 16 Final Loop Closure-Case I	50
Figure 17 Final Loop Closure-Case II	51
Figure 18 Final Loop Closure-Case III	52
Figure 19 b_2 Root Locus for System 0	56
Figure 20 System 5 Carrier Approach	57
Figure 21 System 6 Carrier Approach	58
Figure 22 System 5 with Actuators and Limiters	60
Figure 23 System 6 with Actuators and Limiters	61
Figure 24 System 5 Guidance Loop Closure	63

	Page
Figure 25 System 6 Guidance Loop Closure	64
Figure 26 System 5 ACLS (K=0.2) 20 feet Low	65
Figure 27 System 5 ACLS (K=0.25) 20 feet Low	66
Figure 28 System 5 ACLS (K=0.3) 20 feet Low	67
Figure 29 System 6 ACLS (K=0.2) 20 feet Low	68
Figure 30 System 6 ACLS (K=0.25) 20 feet Low	69
Figure 31 System 6 ACLS (K=0.30) 20 feet Low	70
Figure 32 System 6 ACLS (K=0.35) 20 feet Low	72
Figure 33 Response Times for Closed Loop ACLS	73
Figure 34 System 6 ACLS (K=0.24) 20.0 feet High	74
Figure 35 System 6 ACLS (K=0.24) 20.0 feet Low	75
Figure 36 System 6 ACLS (K=0.24) 20.0 feet Low with Surble	76
Figure 37 Controller Limitations	77

LIST OF SYMBOLSNon-Dimensional Stability Parameters

C_D	Drag coefficient, total
C_{D_u}	Drag coefficient change due to airspeed perturbation
C_{D_α}	Drag coefficient change due to angle of attack perturbation
$C_{D_{\delta E}}$	Drag coefficient change due to elevator deflection
$C_{D_{\delta F}}$	Drag coefficient change due to flap deflection
C_L	Lift coefficient
C_{L_u}	Lift coefficient change due to airspeed perturbation
C_{L_α}	Lift curve slope
$C_{L_{\delta E}}$	Lift coefficient change due to elevator deflection
$C_{L_{\delta F}}$	Lift coefficient change due to flap deflection
C_m	Pitching moment coefficient
C_{m_u}	Pitching moment coefficient change due to airspeed perturbation
C_{m_α}	Static pitch stability
$C_{m_{\ddot{z}}}$	Damping due to vertical acceleration
C_{m_q}	Damping in pitch
$C_{m_{\delta E}}$	Pitch control surface effectiveness
$C_{m_{\delta F}}$	Flap effectiveness

Dimensional Stability Derivatives

X_u	Longitudinal Force change due to airspeed perturbation
X_w	Longitudinal Force change due to normal velocity perturbation
X_α	Longitudinal Force change due to angle of attack perturbation
$X_{\delta E}$	Longitudinal Force change due to elevator deflection perturbation
$X_{\delta F}$	Longitudinal Force change due to flap deflection perturbation

X_{δ_T}	Longitudinal Force change due to thrust perturbation
Z_u	Normal Force change due to airspeed perturbation
Z_w	Normal Force change due to normal velocity perturbation
Z_{δ_E}	Normal Force change due to elevator deflection perturbation
Z_{δ_F}	Normal Force change due to flap deflection perturbation
Z_{δ_T}	Normal Force change due to thrust perturbation
M_u	Pitching Moment change due to airspeed perturbation
M_w	Pitching Moment change due to normal velocity perturbation
M_α	Pitching Moment change due to angle -of-attack perturbation.
M'_w	Pitching Moment change due to normal acceleration perturbation
M'_α	Pitching Moment change due to angle-of-attack rate perturbation
M_q	Pitching Moment change due to pitching rate perturbation
M_{δ_E}	Pitching Moment change due to elevator deflection perturbation
M_{δ_F}	Pitching Moment change due to flap deflection perturbation.
M_{δ_T}	Pitching Moment change due to thrust perturbation

Matrices and Vectors

A	Coefficient matrix of the homogeneous linearized airframe equation.
A	Simplified coefficient matrix
\tilde{A}	Coefficient matrix including position variables
B	Input matrix of the linearized airframe equation
B	Simplified input matrix
\tilde{B}	Input matrix with state variables plus position variables
D, D'	Control weighting matrix
H	Optimal feedback gain matrix

\hat{H}	Optimal feedback gain matrix including position feedback
I	Identity matrix (nxn)
K, K'	State weighting matrix
L	Controller limit matrix
$M(s)$	Transfer matrix
$M_{CL}(s)$	Closed loop transfer matrix
P	Riccati matrix
$p(t)$	Adjoint vector
$\underline{X}(s)$	Laplace transformed state vector
$\underline{x}(t)$	State vector
$\underline{x}_{fb}(t)$	ACLS state feedback vector
$\underline{x}_g(t)$	Gust input vector
$\underline{x}^*(t)$	Optimal state vector
$\underline{\hat{x}}(t)$	Vector of states plus position variables
$\Delta \underline{x}$	Perturbation of optimal state vector
$\underline{\Delta}(s)$	Laplace transformed control vector
$\underline{\delta}(c)$	Input control vector
$\underline{\delta}_c(t)$	Command input vector
$\underline{\delta}_{fb}(t)$	Feedback control vector
$\underline{\delta}^*(t)$	Optimal control vector
$\Delta \underline{\delta}(t)$	Perturbation of optimal control vector
$\phi_{ij}(t)$	State transition matrix of optimal system

Multiloop Airframe Dynamics

C_{ij} $i-j^{th}$ cofactor of $[I_s - A]$

M_{ij} Generalized uncoupled transfer function; i denotes x_i
and j denotes δ_j

M_{kl}^{u2} Cross coupling function generated by interaction of δ_k
and δ_l upon x_u and x_2

N_{ij} Numerator of M_{ij}

N_{kl}^{u2} Numerator of M_{kl}^{u2}

$\Delta(s)$ Characteristic polynomial of open loop airframe

A_{ij} Carrier motion dispersion transfer function

Performance Index Parameters

k_1 Weighting on sink rate

k_2 Weighting on pitch rate

d_1 Weighting on elevator deflection

d_2 Weighting on flap deflection

b_1 Reciprocal of d_1

b_2 Reciprocal of d_2

Miscellaneous

\bar{c} Mean aerodynamic chord

f Generalized function of n variables (ft)

g Acceleration due to gravity (32.2 ft/sec²)

H_R Height over ramp

H_D Height over desired TDP

h Aircraft vertical position (ft)

\dot{h} Aircraft sink rate perturbation (ft/sec)

h_D Vertical carrier motion induced dispersion (ft)

Δh Vertical glide slope deviation (ft)

i_w	Wing incidence angle	(deg)
I_y	Moment of inertia in pitch	(slug-ft ²)
j	$\sqrt{-1}$	
J	Generalized cost functional of n functions	
J^*	Adjoined cost functional	
k	Constant	
$L(\underline{x}, \underline{u})$	Scalar function of two vectors	
l_z	Thrust moment arm, perpendicular from thrust vector to c.g.	(ft)
m	Mass of airplane	(slugs)
$U(\)$	Error-order function	
q	Dynamic pressure	(lbs/ft ²)
R	Range AFT of TDP	
S_w	Total Wing Area	(ft ²)
$S_y(w)$	Power Spectral Density of y	
s	Laplace Operator	(1/sec)
T	Thrust	(lbs)
T_o	Trim thrust	(lbs)
t	time	(sec)
U_g	Horizontal burble	(ft/sec)
u	Airspeed Perturbation	(ft/sec)
V_o	Trim Flight velocity	(ft/sec)
V_o^*	Aircraft-aircraft carrier closing velocity	(ft/sec)
W	Airplane gross weight	(lbs)
w	Velocity along the z -axis, positive down	(ft/sec)
W_g	Vertical burble	(ft/sec)

X	Nominal glide slope horizontal coordinate	(ft)
X_R	Distance from Ramp to TDP	(ft)
ΔX_D	Horizontal TDP dispersion	(ft)
x	Horizontal distance from aircraft to TDP	(ft)
x_{c_g}	Distance from leading edge of mean aerodynamic chord to center of gravity	(% MAC)
x_{n_T}	Distance from leading edge of mean aerodynamic chord to stick fixed neutral point	(% MAC)
Δx	Horizontal glide slope deviation	(ft)
x_1	Airspeed perturbation	(ft/sec)
x_2	Sink rate perturbation	(ft/sec)
x_3	Pitch attitude perturbation	(rad)
x_4	Pitch rate perturbation	(rad/sec)
z	Nominal glide slope, Vertical coordinate	(ft)
α_{fus}	Fuselage angle of attack	(deg)
α_w	Wing angle of attack	(deg)
γ_o	Flight path angle	(deg)
γ_o^*	Closing Glide Slope angle	(deg)
δ_E, δ_1	Elevator deflection, positive T.E. down	(deg rad)
δ_F, δ_3	Flap deflection, positive T.E. down	(deg rad)
δ_T, δ_2	Thrust change, positive for increase	(lbs)
δ_e	Elevator actuator output	(deg)
δ_f	Flap actuator output	(deg)
δ_t	Engine thrust lag output	(lbs)
ζ_p	Phugoid damping ratio	
ζ_{sp}	Short period damping ratio	
Λ	Thrust to sink rate suitability criterion	

Λ_i	Limit on i-th controller	
σ	Real axis (s-plane)	(rad/sec)
σ_{hd}	Vertical, carrier motion induced dispersion	(ft)
θ	Pitch angle	(rad)
ω	Angular Frequency	(rad/sec)
ω_{cm}	Carrier Motion Spectrum Center Frequency	(rad/sec)
ω_p	Phugoid undamped natural frequency	(rad/sec)
ω_{sp}	Short period undamped natural frequency	(rad/sec)
Ω	Flap to sink rate suitability criterion	
ϵ	Angle between thrust vector and fuselage reference line	(deg)

Abbreviations

ACLS	Automatic Carrier Landing System
AMOAC	Automatic Multiloop Optimal Approach Controller
APC	Approach Power Compensator
c g	Center of gravity
c.m.	Carrier Motion
MAC	Mean Aerodynamic Chord
N.A.	Not Applicable
PI	Performance Index
TDP	Touch Down Point
T.E.	Trailing Edge
WOD	Wind Over Deck

PART I

INTRODUCTION

A. Background

Aircraft carrier landings present one of the most critical problems currently faced by Navy pilots. The relatively small dimensions of the carrier flight deck and the proximity of the water impose severe limitations on the airplane's allowable position errors. The motion of the aircraft carrier in the sea, pitch, roll, heave, etc., further complicates the problem. The random movement of the carrier flight deck and the turbulence created by the carrier interacting with the free air stream both demand precise control of the airplane during the carrier approach. High performance fighter/attack aircraft are designed primarily for operation in the high speed portion of their flight envelopes; the low air speed of the powered approach introduces major control problems. The effectiveness of the control surfaces is severely degraded at approach speeds. Approach air speed is typically below minimum drag air speed. The reversal in the slope of the thrust required curve introduces right half plane zeros into the sink rate to control surface transfer functions, thus radically different control laws are needed in the approach configuration than in the remainder of the flight envelope. The need for improved carrier approach control is borne out by Naval Air Safety Center statistics. In calendar year 1966, the ratio of major accidents in carrier approaches per total flights to major accidents in ground approaches per total flights was approximately ten to one. In calendar year 1967, this figure was approximately six to one.

Past efforts in applying automatic control theory to the carrier approach problem have given rise to the Approach Power Compensator (APC) and SPN-42 Automatic Carrier Landing System (ACLS). The APC concept is based on automatic throttle control used to trim thrust during a power approach. It was originally designed as a pilot aid for manual approaches. For this purpose, it has achieved some success. Subsequent effort has been given to develop an automatic elevator controller to be used along with the APC to maintain longitudinal flight path control. This flight path controller is designated as the SPN-42 ACLS, Mode 1. The SPN-42 system has been under development for more than twelve years and has thus far achieved very limited success. Difficulties have arisen in achieving compatibility of the SPN-42 with the existing APC. The SPN-42 is presently fleet operational for only a single carrier based airplane and there are several compatibility problems with other Navy airplanes.

The SPN-42/APC combination represents a reasonable first attempt to design an automatic carrier landing system. The carrier approach problem, however, is sufficiently complex that it requires a more sophisticated control system. The single command input of the longitudinal portion of SPN-42 elevator deflection and the thrust trimming of the APC are employed to control airspeed, altitude and pitch attitude response for both deterministic and stochastic inputs. This system lacks independence in specifying the various responses for both inputs. In order to alleviate this problem and obtain good response characteristics for the critical variables, a multicontroller, multivariable design can be employed. Reference (a) shows the effect of multiloop control on a manual carrier approach.

This report considers a longitudinal, three controller system incorporating command inputs of elevator, thrust and direct lift control flaps

as a potential advanced ACLS. The control system configuration is a rather general 12-parameter feedback system. Design procedure is based upon the Root Square Locus technique of S. S. L. Chang, and extended to multi-input systems by E. Rynaski and R. Whitbeck, of Cornell Aeronautical Laboratory, in reference (b). For the purpose of this report, good flying qualities will be defined as the best trade-off between (1) minimum dispersion at touchdown and (2) smoothness and regularity of the airplane's stability and control characteristics, and riding qualities. In this regard, the discussion will center around conventional parameters of the characteristic roots of a dynamic system.

The airplane selected for this study is the F-8C in a power approach configuration. Aerodynamic parameters and physical constants for this airplane were obtained from reference (a).

B. Design Considerations

In a multivariable, multicontroller system there are a great number of possible feedback configurations. The determination of the most flexible configuration for the carrier landing problem would require a lengthy investigation involving at least 12 independent feedback parameters; that is, a feedback loop from each measured output θ , $\dot{\theta}$, u , and h to each control input δ_E , δ_F , and δ_T . Such an investigation would be extremely complicated and tax the capabilities of current computing equipment. For this reason, a method was sought to evaluate a 12-parameter feedback configuration as a function of a few independent parameters; namely, four independent variables.

To this date, research on optimal control systems has shown that for linear multidimensional problems the optimal feedback configuration

tends to produce closed loop systems which compare favorably with conventional design criteria. With the introduction of optimal control techniques, the number of independent parameters has been reduced to those required to specify the performance index.

Optimal control techniques dictate the form of the performance index; namely, quadratic forms in the controls and the measured outputs.

$$PI = 1/2 \int_0^{\infty} [a_1 u^2 + a_2 \dot{h}^2 + a_3 \dot{\theta}^2 + a_4 \dot{\theta}^2 + d_1 \delta_E^2 + d_2 \delta_F^2 + d_3 \delta_T^2] dt$$

In adopting this performance measure to the carrier landing problem, some simplifications based on physical control characteristics can be made. The shallow descent angle, which requires more precise control of \dot{h} than u , allows $a_1 = 0$ while the redundancy of controlling $\dot{\theta}$ and θ allows $a_3 = 0$.

Upon normalizing by d_3 , this measure becomes

$$PI = 1/2 \int_0^{\infty} [k_1 \dot{h}^2 + k_2 \dot{\theta}^2 + d_1 \delta_E^2 + d_2 \delta_F^2 + \delta_T^2] dt$$

The optimal feedback control law, that is, that feedback configuration which minimizes PI can now be evaluated as a function of the four parameters k_1 , k_2 , d_1 and d_2 . The remaining problem is to characterize the flying qualities of the resulting closed loop air frame equations as the four parameters of PI are varied. This is accomplished via the Root Square Locus technique of reference (b).

PART II

THEORY

A. Optimal Control Equations

The optimal system is described by three differential equations. The first equation is the constraint imposed by the basic air frame longitudinal equations of motion. The second and third equations are the Euler variational equations of the optimal system which are obtained by using the calculus of variations. A fourth equation, a matrix Ricotti equation, determines the feedback gains.

Air Frame Longitudinal Equations of Motion (Stability Axes)

Figure 1 defines the stability axes system

$$\begin{aligned} \text{Drag: } \dot{u} = & X_u u + X_w w - (g \cos \gamma_0) \theta + X_{\delta E} \delta_E \\ & + X_{\delta T} \delta_T + X_{\delta F} \delta_F \end{aligned} \quad (1a)$$

$$\begin{aligned} \text{Lift } \dot{w} = & Z_u u + Z_w w + V_0 \dot{\theta} + (g \sin \gamma_0) \theta \\ & + Z_{\delta E} \delta_E + Z_{\delta T} \delta_T + Z_{\delta F} \delta_F \end{aligned} \quad (1b)$$

$$\begin{aligned} \text{Pitching Moment } \ddot{\theta} = & M_u u + M_w w + M_{\dot{w}} \dot{w} + M_q \dot{\theta} + M_{\delta E} \delta_E \\ & + M_{\delta F} \delta_F + M_{\delta T} \delta_T \end{aligned} \quad (1c)$$

$$\text{Altitude } V_0 \theta = w + h \quad (1d)$$

where u , w , h , θ , $\dot{\theta}$, δ_E , δ_F and δ_T are incremental quantities and the aerodynamic parameters are as defined in Appendix A.

For the initial portion of this report, actuator lags and nonlinearities will be neglected. In later sections, these effects will be introduced.

Equations (1a, b, c, d) can be rewritten in matrix notation as:

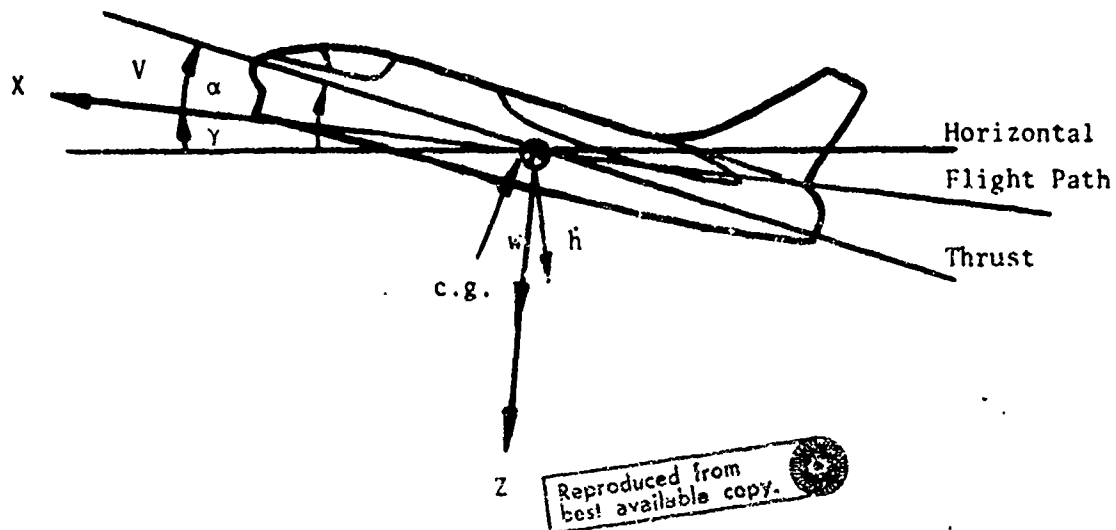


FIGURE 1. LONGITUDINAL STABILITY AXES

$$\begin{bmatrix} \dot{u} \\ \dot{h} \\ \dot{\theta} \\ \ddot{\theta} \end{bmatrix} = \begin{bmatrix} Y_u & -X_w & X_w V_o = g \cos Y_o & 0 \\ -Z_u & Z_w & g \sin Y_o - Z_w V_o & 0 \\ 0 & 0 & 0 & 1 \\ M_u + M_w' Z_u & -(M_w + M_w' Z_w) \left(M_w V_o + M_w' Z_w V_o + \right. \\ & \left. - g M_w \sin Y_o \right) & (M_q + V_o M_w') \end{bmatrix} \begin{bmatrix} u \\ h \\ \theta \\ \ddot{\theta} \end{bmatrix}$$

$$\begin{bmatrix} X_{\delta_E} & X_{\delta_T} & X_{\delta_F} \\ -Z_{\delta_E} & -Z_{\delta_T} & -Z_{\delta_F} \\ 0 & 0 & 0 \\ M_{\delta_E} + M_w' Z_{\delta_E} & M_{\delta_T} + M_w' Z_{\delta_T} & M_{\delta_F} + M_w' Z_{\delta_F} \end{bmatrix} \begin{bmatrix} \delta_E \\ \delta_T \\ \delta_F \end{bmatrix} \quad (2)$$

A more compact form of equation (2) is

$$\dot{\underline{x}} = \underline{A} \underline{x} + \underline{B} \underline{\delta} \quad (3)$$

where \underline{x} = column $(u, h, \theta, \ddot{\theta})$, $\underline{\delta}$ = column $(\delta_E, \delta_T, \delta_F)$ and \underline{A} and \underline{B} are the corresponding matrices of equation (2).

After substituting the values of aerodynamic constants from Appendix A,

\underline{A} and \underline{B} become:

$$A = \begin{bmatrix} -0.0506 & 0.0072 & -33.8 & 0 \\ 0.264 & -0.554 & 127.4 & 0 \\ 0 & 0 & 0 & 1.0 \\ -0.000583 & 0.00465 & -1.051 & -0.390 \end{bmatrix}$$

$$B = \begin{bmatrix} -0.672 & 0.0001595 & -6.72 \\ 19.95 & 0.0002194 & 18.9 \\ 0 & 0 & 0 \\ 2.196 & -4.67 \times 10^{-6} & 0.0357 \end{bmatrix}$$

Euler Equations

The carrier landing problem can be formulated as follows:

Given the air frame constraint equation (3), find $\underline{\delta}$ as a linear function of \underline{x} , linear feedback, such that the PI is minimized for values of k_1 , k_2 , b_1 , and b_2 which result in good airplane flying qualities

Expressing PI in matrix notation yields:

$$PI = 1/2 \int_0^{\infty} [\underline{x}^T K \underline{x} + \underline{\delta}^T D \underline{\delta}] dt \quad (4)$$

$$\text{where } K = \begin{bmatrix} 0 & 0 & 0 & 0 \\ 0 & k_1 & 0 & 0 \\ 0 & 0 & 0 & 0 \\ 0 & 0 & 0 & k_2 \end{bmatrix} \quad \text{and } D = \begin{bmatrix} d_1 & 0 & 0 \\ 0 & 1 & 0 \\ 0 & 0 & d_2 \end{bmatrix}$$

Since the solution of this problem is constrained to satisfy equation (3), a vector function of time $p(t)$, the adjoint variable is introduced. Introduction of the adjoint variables allows the constraint equation to be included under the integral in equation (4) without changing the value of PI.

$$PI = 1/2 \int_0^{\infty} [\underline{x}^T K \underline{x} + \underline{\delta}^T D \underline{\delta} + \underline{p}^T (-\dot{\underline{x}} + A \underline{x} + B \underline{\delta})] dt \quad (5)$$

but
$$-\dot{\underline{x}} + A\underline{x} + B\underline{\delta} = 0$$

or
$$P\dot{I} = PI$$

Using the results of Appendix B yields equations (6a and b).

$$\dot{\underline{p}} = -A^T \underline{p} - K\underline{x} \quad (6a)$$

$$D\underline{\delta} = -B^T \underline{p} \quad (6b)$$

Equations (6a and b) are the Euler equations of the optimal system.

Equations (6a and b) along with equation (3) comprise the necessary conditions for an optimal system. Using a matrix format and eliminating equation (6b) yields:

$$\begin{bmatrix} \dot{\underline{x}} \\ \dot{\underline{p}} \end{bmatrix} = \begin{bmatrix} A - B D^{-1} B^T \\ -K - A^T \end{bmatrix} \begin{bmatrix} \underline{x} \\ \underline{p} \end{bmatrix} \quad (7)$$

Feedback Gains

Once a set of parameter values is determined, it is then necessary to determine the corresponding feedback gains. Equation (6b) indicates that the optimal control $\underline{\delta}(t)$ is a linear combination of the adjoint variables $\underline{p}(t)$.

$$\underline{\delta}(t) = -D^{-1} B^T \underline{p}(t) \quad (8)$$

In order to obtain $\underline{\delta}(t)$ as a linear combination of $\underline{x}(t)$, or linear feedback, it is required that the following relationship be satisfied:

$$\underline{p}(t) = P(t) \underline{x}(t) \quad (9)$$

In which case:

$$\underline{\delta}(t) = -D^{-1} B^T P(t) \underline{x}(t) \quad (10)$$

Appendix B shows that equation (9) is indeed valid and also that the infinite upper limit of integration in PI guarantees that $P(t)$ is a matrix of constant elements. In Appendix C an algebraic equation for P is derived

$$0 = PA + A^T P + K' - PBD^{-1} B^T P \quad (11)$$

In this investigation, the solution of equation (11) was accomplished with a digital computer program developed by Cornell Aeronautical Laboratories. This program implements a scheme based upon the eigen vector expansion of the Hamiltonian matrix. This method was developed by Potter and was first published in reference (c). The P matrix is then substituted into equation (10) to obtain the feedback gain matrix, H .

After computation of the feedback gains, the overall closed loop system can be examined. This is accomplished by calculating the transfer functions of output variable to the command inputs. Starting with the open loop air frame, equation (3), and the equation of the feedback controller which is

$$\dot{\underline{\delta}} = \underline{\delta}c + \underline{\delta}f b \quad (12)$$

where $\underline{\delta}c$ is the command input and $\underline{\delta}f b$ is the feedback controller output given by

$$\underline{\delta}f b = -H \underline{x} \quad (13)$$

the closed loop equations become:

$$\dot{\underline{x}} = (A - BH)\underline{x} + B\underline{\delta}c \quad (14)$$

Laplace transforming equation (14) and solving for $\underline{X}(s)$ yields

$$\underline{X}(s) = [Is - A + BH]^{-1} B \underline{\Delta}(s) \quad (15)$$

From equation (15) it is found that the closed loop transfer matrix

$$Mcl(s) = [Is - A - BH]^{-1} B \quad (16)$$

B Design Procedure

In order to determine which values of k_1 , k_2 , d_1 and d_2 result in good flying qualities, the closed loop roots of the optimal system are determined as a function of these parameters via a digital program implementing the Root Square Locus technique. The program determines a region of parameter values with good short period and phugoid characteristics. This process is discussed in detail in section II B-1 and in Appendix (C). The resulting steady state, matrix Riccati equation is then solved and the complete set of multiloop feedback gains are evaluated. In this manner, the use of optimal control theory has transformed the problem of choosing twelve feedback gains to a lesser problem of choosing four performance index parameters. The design procedure then proceeds along a more conventional, state variable format.

Since the Root Square Locus has been employed only to achieve satisfactory closed loop system roots, it is necessary to investigate the resulting closed loop numerator zeros. Thus, the closed loop transfer matrix is calculated and its component terms investigated along the guidelines established in section II C-2. If the numerator terms cannot meet these guidelines, the performance index parameters are adjusted either by re-employing the Root Square Locus, or on the basis of more immediate intelligence. Upon reaching a satisfactory closed loop transfer matrix, those preliminary feed back gains would be incorporated into a carrier approach simulation.

This simulation is exercised to evaluate the operation of the AMOAC control system in an accurate model of the carrier approach environment. This is accomplished as follows:

a The system is first operated independently of any glide slope positional error information, as an inner loop augmented aircraft, without actuators or aircraft non-linearities and lags. This is done to establish the aircraft's response to airstream velocity disturbances or steady state aircraft carrier burble and pitch induced burble

b The aircraft's control surface and propulsive non-linearities and lags are incorporated into the closed loop system and the resulting simulation exercised again as an inner loop augmented aircraft.

c A glide slope positional error loop of the form

$$h_{fb} = h + k h \quad (17)$$

or upon Laplace transforming

$$H_{fb}(s) = (1 + \frac{k}{s}) H(s) \quad (18)$$

is closed around the augmented aircraft of paragraph b (above). Exercising this simulation demonstrates the capacity of the AMOAC control system to effect accurate glide slope control when combined with the simple outer navation loop described by equation (18)

d. The closed loop system of c is then tested along a turbulence free glide slope toward a desired TDP (touch down point) whose coordinates vary randomly in a manner appropriate to an aircraft carrier in severe sea swell conditions. The resulting vertical touch down dispersion (σ_h) is calculated from the carrier motion power spectral densities and the closed loop transfer matrix

If an unsatisfactory result is obtained from any of the four simulation exercises, the performance index parameters are adjusted and the design procedure re-employed. After satisfactory results are obtained from simulation d, the AMOAC system design is considered satisfactory and the design procedure is terminated. Figure 2 demonstrates a functional block diagram for this design procedure.

Figure 2 breaks down the design process into two phases. The first phase, i.e., system synthesis, employs optimal control theory to obtain a preliminary design configuration. Conventional state variable, analysis techniques are employed in the second phase in order to evaluate the preliminary design.

This second phase is broken up into five separate analyses, each of which must be satisfied before the design is accepted. After each of the five evaluation steps, a decision is made whether to continue to the succeeding step or adjust the multiloop gains. The evaluation procedure is broken into relatively small increments in the hope that only small adjustments of the performance index parameters will be required to retune a preliminary design configuration. The results of this investigation appear to validate this design approach.

1. System Roots

The root locations of the closed loop optimal system vary as functions of the performance index parameters. This section describes how these root locations are determined. The root square locus technique described in Appendix (C) is now adapted for use in the AMOAC design process. In Appendix C, the root square locus equation was derived and is slightly modified here for convenience.

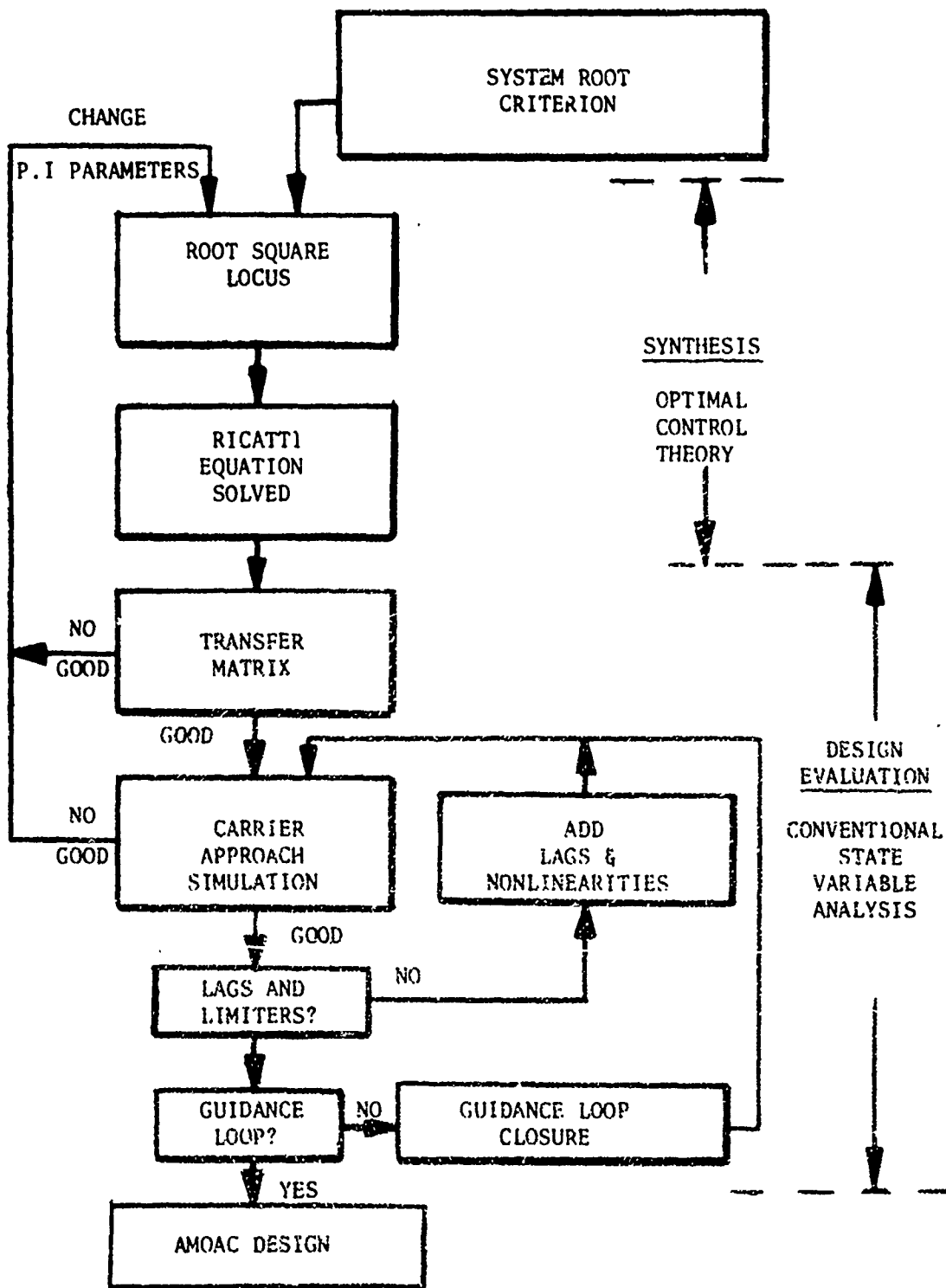


FIGURE 2. AMOAC LOGIC FLOW

$$\det (I + D^{-1} M^T (-s) K' M(s)) = 0 \quad (19)$$

The elements of $M(s)$ are designated as $M_{ij}(s)$, where the first index denotes the measured output, and the second index the control input.

Substituting for D and K' in equation (19) yields:

$$0 = 1 + k_1 \frac{\Delta_{22}}{\Delta(s)} + k_2 \frac{\Delta_{23}}{\Delta(s)} + k_1 b_1 \frac{\Delta_{21}}{\Delta(s)} + k_2 b_1 \frac{\Delta_{24}}{\Delta(s)} + k_1 k_2 b_1 \frac{\Delta_{12}}{\Delta(s)} + \\ + k_1 b_2 \frac{\Delta_{23}}{\Delta(s)} + k_2 b_2 \frac{\Delta_{24}}{\Delta(s)} + k_1 k_2 b_1 b_2 \frac{\Delta_{12}}{\Delta(s)} + k_1 k_2 b_1 b_2 \frac{\Delta_{13}}{\Delta(s)} \quad (20)$$

where $\Delta_{ij} = M_{ij}(s) M_{ij}(-s)$, $\Delta_{12}^2 = \Delta_{41} \Delta_{23} - \Delta_{43} \Delta_{21}$ and $b_i = 1/d_i$.

Each element, $M_{ij}(s)$, of $M(s)$ is of the form

$$M_{ij}(s) = \frac{N_{ij}(s)}{\Delta(s)}$$

where $\Delta(s)$ is the characteristic polynomial of the open loop system. The terms of the form M_{ij}^2 appear to have denominators of $(\Delta(s))^2$; however, reference (b) has shown that the numerator of such terms includes a factor of $\Delta(s)$.

$$M_{ij}^2 = \frac{N_{ij}^2}{(\Delta(s))^2} = \frac{N_{ij}^2}{\Delta(s)}$$

Rearranging equation (20) yields the expression used in this report to determine the closed loop roots.

$$0 = 1 + k_1 \left[\frac{(\Delta_{22} + b_1 \Delta_{21} + b_2 \Delta_{23}) + k_2 (b_1 \Delta_{12} + b_2 \Delta_{23} + b_1 b_2 \Delta_{13})}{\Delta(s) + k_2 (\Delta_{42} + b_1 \Delta_{41} + b_2 \Delta_{43})} \right] \quad (21)$$

Equation (21) has the form of a conventional multiloop, root locus. It consists of an outer loop, closed around parameter k_1 , a numerator and denominator loop each closed simultaneously around k_2 and three inner loops with b_1 and b_2 as parameters.

The three inner loops differ slightly with the conventional root locus format. They are each functions of the same two parameters b_1 and b_2 . Because of the $b_1 b_2$ term, they cannot be broken down into two single parameter loops. Each of the inner loops has a distinct physical interpretation. The first inner loop of the numerator is:

$$0 = N_{22}(s) + b_1 N_{21}(s) + b_2 N_{23}(s) \quad (22)$$

and contains the numerators of all the sink rate transfer functions. This loop weights the importance of elevator, thrust and flaps as primary controllers of sink rate. This loop will be referred to as the sink rate control loop.

The inner loop of the denominator is:

$$0 = N_{42}(s) + b_1 N_{41}(s) + b_2 N_{43}(s) \quad (23)$$

and consists of the numerators of the pitch rate transfer functions and is thus called the pitch rate control loop. This loop weights the contribution of the three control inputs as primary controllers of pitch rate.

The second inner loop of the numerator is:

$$0 = b_1 N_{12}^2(s) + b_2 N_{23}^2(s) + b_1 b_2 N_{31}^2(s) \quad (24)$$

and contains the cross coupling terms. This loop takes into consideration the interaction between any two of the three control actions and is referred to as the cross coupling loop.

Equation (21) is an eighth order polynomial in s , with roots that are symmetric about the $j\omega$ axis. Each term in equation (21) is the product of a polynomial $P(s)$ and another polynomial $P(-s)$. The roots of equation (21) correspond to the closed loop roots of equation (7), i.e., the roots of the optimal system and the adjoint system. If values of the parameters are restricted to be positive, the R matrix of equation (4) is positive definite and the Q matrix positive semidefinite. Under this restriction, PI becomes a Liapunov function for the closed loop system and those open loop roots, $k_1' = k_2' = b_1' = b_2' = 0$, in the left half plane must remain in that plane as the parameters are increased.

Since the basic airframe has stable roots, the part of the root locus in the left half plane must correspond to the closed loop optimal system.

The design procedure followed in this investigation was to first determine values of b_1' and b_2' that provide roots for shaping good numerator and denominator loops. Then k_1' and k_2' was chosen to produce satisfactory phugoid and short period roots.

In order to obtain the roots of equations (22) through (24), a digital program was set up to find roots of an equation of the following form.

$$0 = \hat{T}_1(s) + c_1 \hat{T}_2(s) + c_2 \hat{T}_3(s) + c_1 c_2 \hat{T}_4(s)$$

This program is then used to obtain proper values of k_1' , k_2' , b_1' and b_2' .

2. Carrier Approach Simulation

The heart of the AMOAC design evaluation is the exercise of simulated carrier approaches via digital computer programs which accurately model the carrier approach environment and the closed loop airplane dynamics. This section describes the carrier approach environment, the environmental model used in the simulation, the simulation itself, and its exercise ground rules.

a. Approach Environment

The typical problem of flight mechanics is to determine the motion of an aircraft with respect to its surrounding airstream, when it is subjected to some excitation forces. The longitudinal equations of motion, equation (3), is derived in Part II, Section A in accordance with this format. When this procedure is used to investigate a conventional powered landing approach, however, a new problem arises. This problem is the referral of the aircraft's coordinates to the inertial coordinates of the desired TDP, (touchdown point). If, in addition, the TDP is not stationary with time, the problem is further complicated. A final complexity is the non-uniformity of the airstream velocities. All of these factors together describe the carrier approach problem.

The first consideration in describing the carrier approach environment is the undisturbed glide slope. When the airplane is in the final approach, it tries to fly a straight line flight path to the TDP. In this process, a constant airspeed, V_0 , and a constant angle of attack, α_{Trim} are maintained. This airspeed is essentially the minimum safe airspeed for the airplane based upon stall and other aerodynamic considerations, and α_{Trim} is determined by V_0 and the airplane's weight, W . The value of

sink rate, \dot{h}_o , and consequently the glide slope angle, γ_o ,

$$\gamma_o = \tan^{-1} (\dot{h}_o / V_o) \quad (25)$$

are set by structure, and safety limits at deck contact. The values for these parameters were obtained from reference (a) and are listed in Appendix A.

The aircraft carrier, however, maintains a velocity in the same positive x direction as the airplane. An equivalent situation is a stationary carrier with the airstream moving past the carrier and parallel to it. In this situation, the closure rate of the airplane and the TDP, V_o^* , is $(V_o - WOD)$, where WOD stands for wind over deck, namely, aircraft carrier forward speed. Figure 3 shows this situation. Note that angle of attack and flight path angle are now calculated with respect to the new closure rate.

$$\gamma_o^* = \tan^{-1} (\dot{h}_o / V_o^*) = -4 \text{ deg.} \quad (26)$$

and

$$\alpha_{Trim}^* = \alpha_{Trim} + (\gamma_o^* - \gamma_o) = 7.4 \text{ deg} \quad (27)$$

where V_o^* equals 180 feet per second. The reference system of figure 3 with its origin at the TDP of the stationary carrier, will be used throughout.

As the airstream passes over the carrier, the flow is severely disturbed. This gives rise to a flow pattern which varies with the X and Z coordinates of figure 3 but is stationary with time. The influence of sea waves imparts a random movement to the TDP which further disturbs the airstream. Figure 4 illustrates the carrier approach

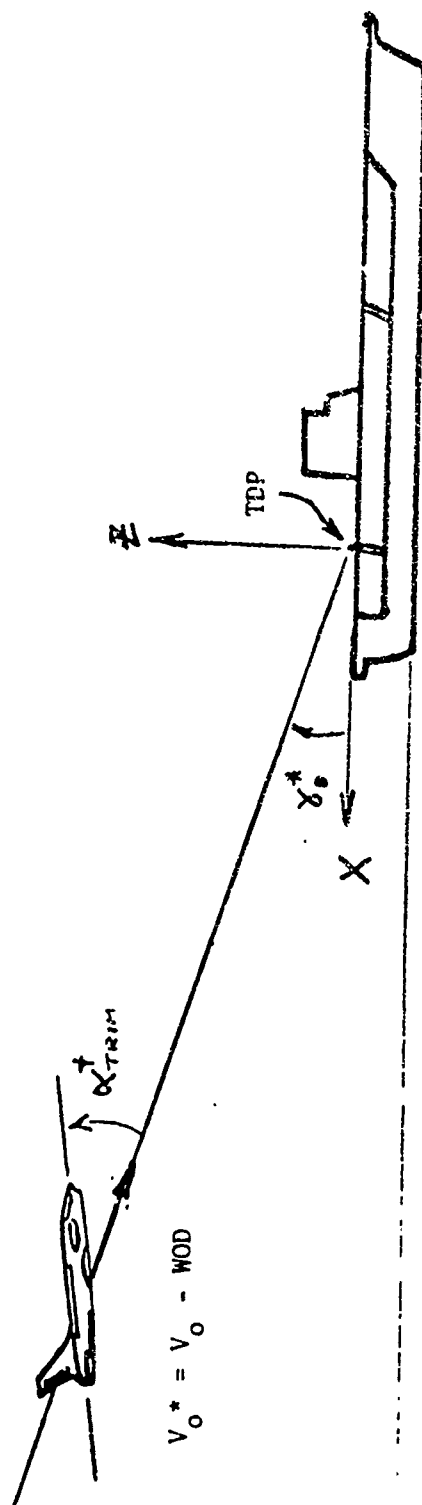


FIGURE 3. UNDISTURBED GLIDE SLOPE

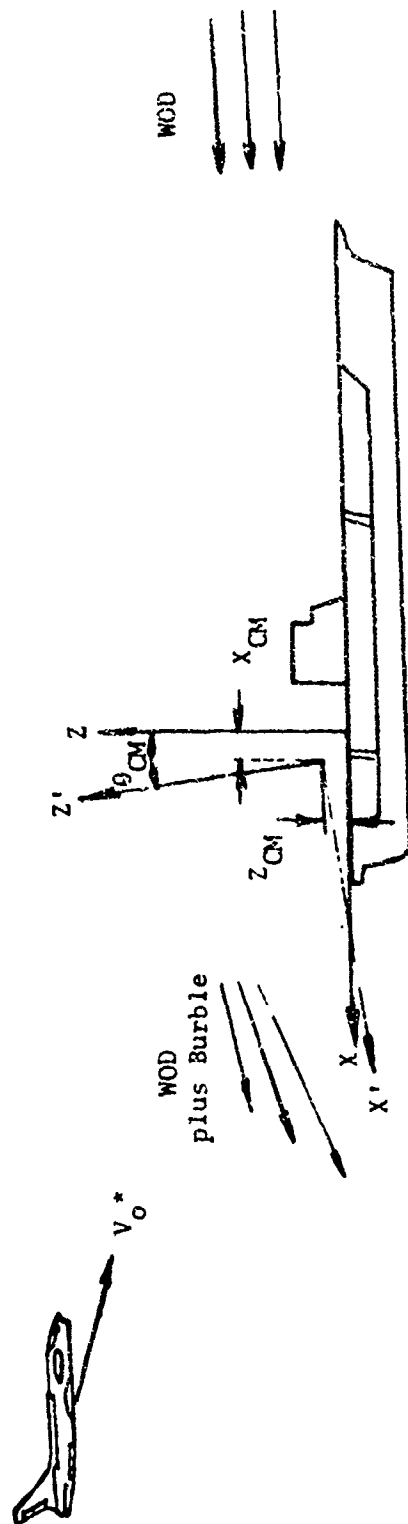


FIGURE 4. CARRIER APPROACH ENVIRONMENT

environment.

The model of the approach environment was broken into two parts. The first part is a model of the airstream variation for points along the undisturbed glide slope. The resulting geometry is shown in figure 5. Carrier burble, i.e., the perturbed portion of the airstream is decomposed into a horizontal component, U_g , and a vertical component, W_g , each of which is a function of the range, R . The results of reference d and e indicate the following form for carrier burble:

$$U_g(R) = \begin{cases} -23.0e^{-R/330} + 17.5e^{-R/75} & \dots R \leq 2000 \text{ ft.} \\ -23.0e^{-R/330} + 17.5e^{-R/75} + \\ + (1.8 - 0.0009R)\sin(26.0 - 0.024R) & R > 2000 \text{ ft} \end{cases} \quad (28)$$

$$W_g(R) = \begin{cases} -7.0e^{-R/1154} \cos(R/255) & \dots R \leq 2306 \text{ ft.} \\ -7.0e^{-R/1154} \cos(R/255) + \\ + (4.15 - 0.0185R)\sin(26.0 - 0.024R) & R > 2306 \text{ ft} \end{cases} \quad (29)$$

This model is quite conservative. The maximum values of U_g and W_g are 14 feet per second and 11 feet per second respectively. Both maximum values occur nearly midway between the ramp and the TDP.

The second phase of the approach environment model consists of a description of the random carrier motion. Reference d indicates the form of typical power spectral densities for an aircraft carrier in pitch, θ_{cm} , heave, z_{cm} and surge, x_{cm} for a severe sea state. The particular model used in this report is:

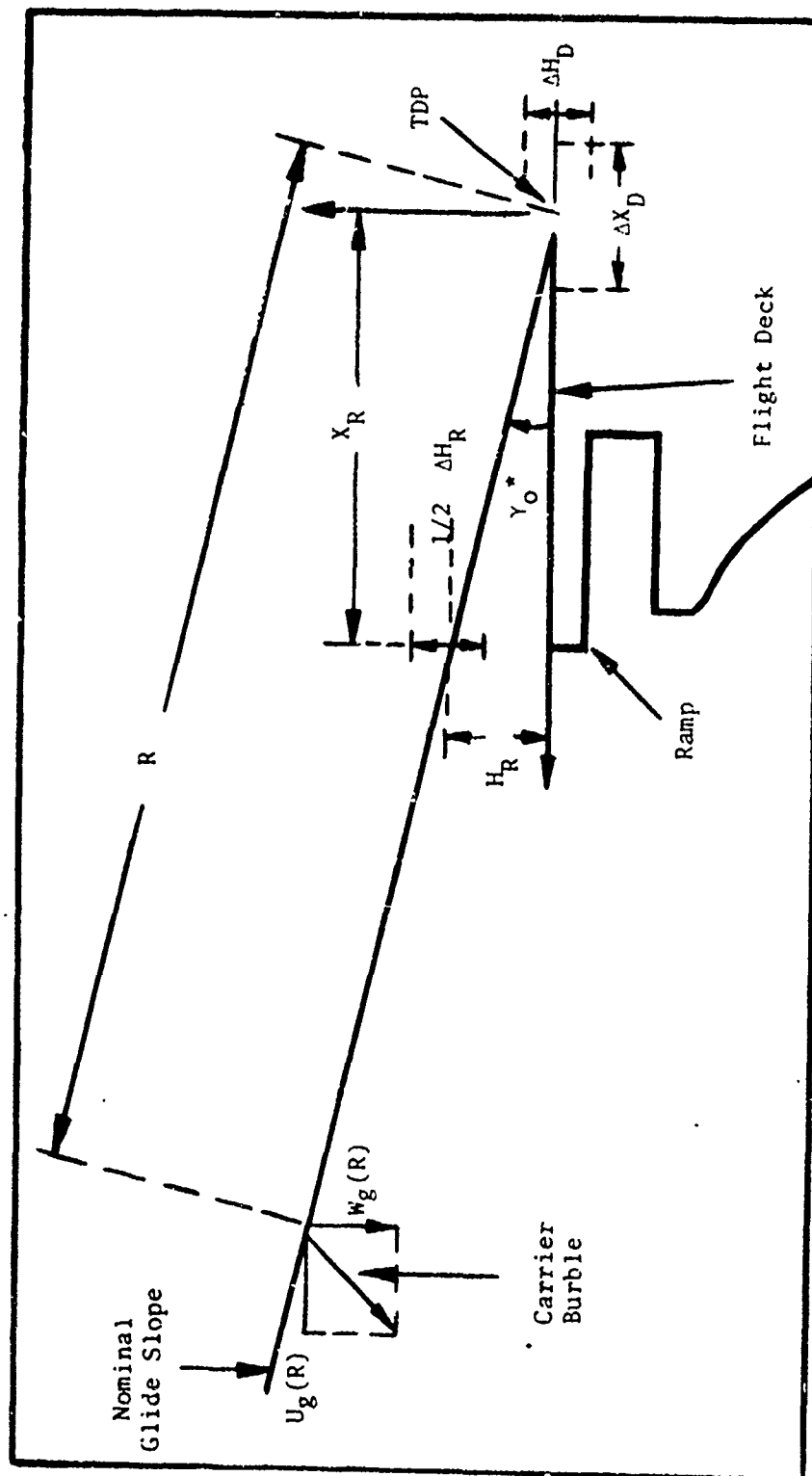


FIGURE 5. CARRIER APPROACH MODEL (STATIONARY TD)

$$\text{Surge, } x_{cm} \quad \bar{x}_{cm} = E [x_{cm}] = 0.0 \text{ feet} \quad (30a)$$

$$\sigma_{x_{cm}}^2 = E [(x_{cm} - \bar{x}_{cm})^2] = 1.0 \text{ feet}^2 \quad (30b)$$

$$S_{x_{cm}}(\omega) = \frac{0.2023\omega^2}{0.05883\omega^2 + (0.5776 - \omega^2)^2} \quad (30c)$$

$$\text{Heave, } z_{cm} \quad \bar{z}_{cm} = E [z_{cm}] = 0.0 \text{ feet} \quad (31a)$$

$$\sigma_{z_{cm}}^2 = E [(z_{cm} - \bar{z}_{cm})^2] = 2.0 \text{ feet}^2 \quad (31b)$$

$$S_{z_{cm}}(\omega) = \frac{0.4198\omega^2}{0.01795\omega^2 + (0.5476\omega^2)^2} \quad (31c)$$

$$\text{Pitch, } \theta_{cm} \quad \bar{\theta}_{cm} = E [\theta_{cm}] = 0.0 \text{ degree} \quad (32a)$$

$$\sigma_{\theta_{cm}}^2 = E [(\theta_{cm} - \bar{\theta}_{cm})^2] = 1.0 \text{ degrees}^2 \quad (32b)$$

$$S_{\theta_{cm}}(\omega) = \frac{0.2217\omega^2}{0.06516\omega^2 + (0.6084 - \omega^2)^2} \quad (32c)$$

Where $S_x(\omega)$ denotes the power spectral density of x and is defined as:

$$S_x(\omega) = \int_{-\infty}^{\infty} e^{j\omega\tau} \left[\lim_{T \rightarrow \infty} \frac{1}{2T} \int_{-T}^T x(t)x(t-\tau) dt \right] d\tau \quad (33)$$

b. Approach Simulator

The approach simulation is also a two part procedure. The first part evaluates the response of the augmented aircraft to the carrier disturbed airstream as modelled in equations (28) and (29). Terminal errors due to carrier deck motion are determined in the second phase of the approach simulation.

i. Carrier Burble Response

Figure 5 is an accurate representation of the geometry and environment model used in this digital simulation. The axis system originates at the stationary TP point with the Z axis in the positive vertical direction and X axis along the flight deck pointed aft. The nominal glide slope emanates from the TDP inclined by the angle $\gamma_0^* = 4$ degrees from the X axis. The carrier burble along the glide slope is characterized by two functions of range, R, according to equations (28) and (29).

The aircraft's linearized equations of motion are solved about the nominal glide slope to yield instantaneous values of sink rate and airspeed, relative to a stationary airstream. These values are then integrated and added to the nominal glide slope to yield the aircraft's position. The carrier burble is then computed and incorporated into sink rate and airspeed and these quantities used in evaluating the equations of motion.

The perpendicular distance between the nominal glide slope and the aircraft's position, h_e is then generated. This position error is multiplied by a preselected gain and added to the sink rate feedback term. This procedure simulates a crude navigation command based upon shipboard telemetry. This navigation guidance is most likely not the best available but it can demonstrate the performance capability of AMOAC in a closed loop ACLS (aircraft carrier landing system)

Figure 6 illustrates the geometry used in generating the aircraft's flight path. An accurate description of the simulation mechanics is given in Appendix D.

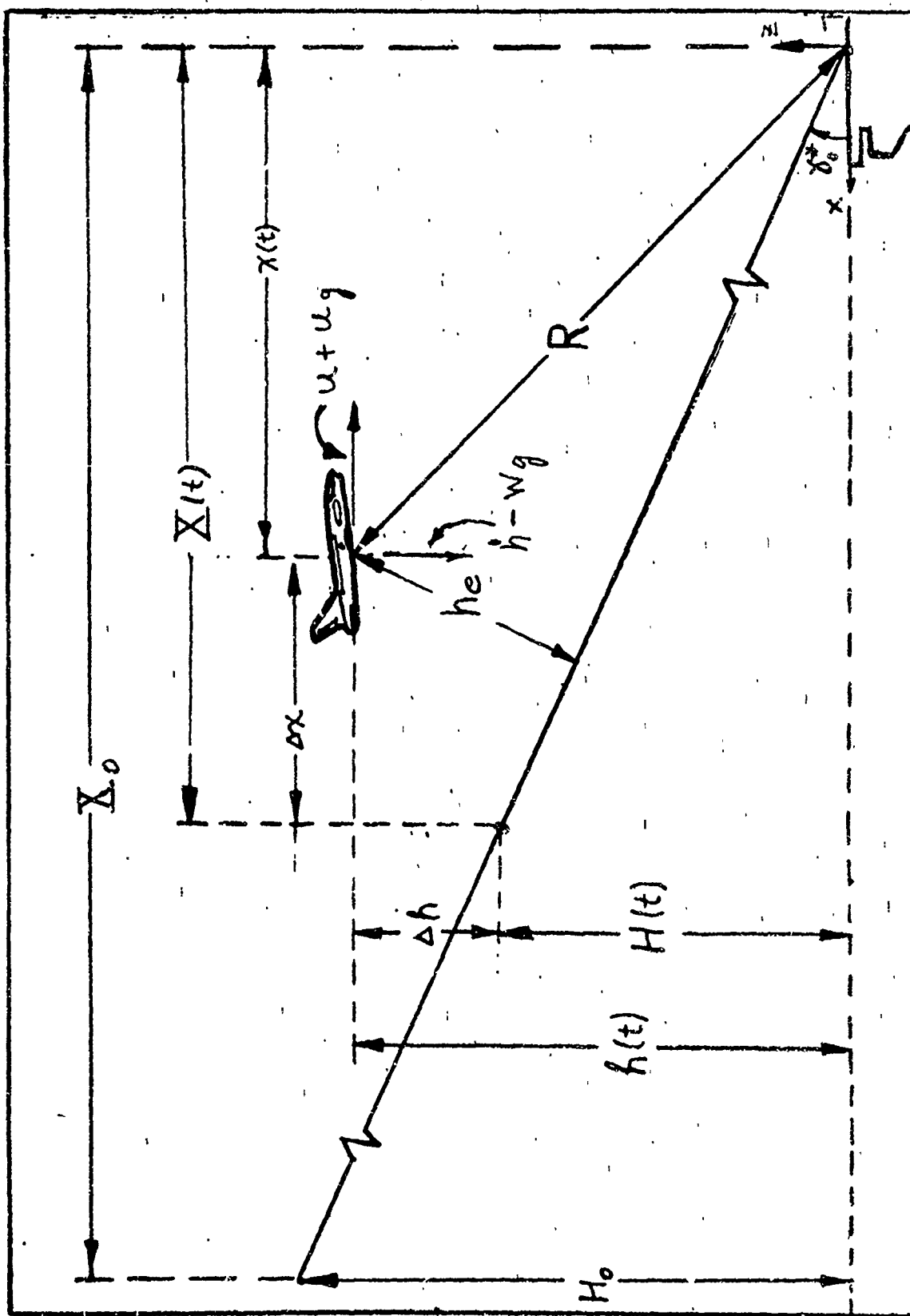


FIGURE 6. CARRIER APPROACH SIMULATION GEOMETRY

One important aspect of the aircraft's response is its vertical clearance of the aft extreme of the flight deck, namely, its height over the ramp, H_R , second in importance only to the TDP dispersion, ΔX_D . However, due to the point mass nature of the translational dynamics and the lack of hook and cable contact geometry in this simulation, the ΔX_D considerations were replaced by a vertical error tolerance over the TDP, ΔH_D . In this manner, it is possible to assess the flight path response of AMOAC in a realistic environment, with a minimum of detailed geometry. In evaluating the performance of the augmented aircraft, an unsatisfactory error in H_R , ΔH_R , was chosen to be any excess of one-half of the nominal H_R . The value of ΔH_D was chosen to be the vertical distance along the glide slope that corresponds to the horizontal distance between two consecutive arresting cables. For modern carriers X_R is approximately 200 feet with 40 feet between arresting cables. Thus, satisfactory performance requires:

$$\left| \Delta H_R \right| \leq 7.0 \text{ feet} \quad (34)$$

$$\left| \Delta H_D \right| \leq 2.8 \text{ feet} \quad (35)$$

ii. Carrier Motion Induced Dispersion

This computation yields the mean square error in vertical position over the TDP induced by random motion of the aircraft carrier according to equations (30), (31) and (32). The necessary equations are derived in Appendix E assuming shipboard telemetry provides the ship's motion information to the aircraft control system. The following is a condensation of the results of Appendix E. It is first necessary to introduce an augmented state variable $\hat{\underline{x}}$

$$\tilde{\underline{x}} = \text{column } (x, h, u, \dot{h}, \theta, \dot{\theta}) \quad (36)$$

Associated with $\tilde{\underline{x}}$ is the following equation of motion

$$\dot{\tilde{\underline{x}}} = \tilde{\underline{A}} \tilde{\underline{x}} + \tilde{\underline{B}} \underline{\delta} \quad (37)$$

where

$$\tilde{\underline{A}} = \begin{bmatrix} 0 & 0 & 1 & 0 & 0 & 0 \\ 0 & 0 & 0 & 1 & 0 & 0 \\ \hline 0 & 0 & & & & \\ 0 & 0 & & & & \\ 0 & 0 & & & & \\ 0 & 0 & & & & \end{bmatrix} \quad \underline{A}$$

and

$$\tilde{\underline{B}} = \begin{bmatrix} 0 & 0 & 0 \\ 0 & 0 & 0 \\ \hline & & \\ & & B \end{bmatrix}$$

and the control law

$$\underline{\delta} = -\tilde{\underline{H}} \tilde{\underline{x}}$$

where

$$\tilde{\underline{H}} = [\underline{H}] \begin{bmatrix} 0 & 0 & 1 & 0 & 0 \\ 0 & K & 0 & 1 & 0 \\ 0 & 0 & 0 & 0 & 1 \end{bmatrix} \quad (38)$$

If σ_h denotes the mean square error in vertical aircraft position due to carrier motion, then

$$\text{where } \sigma_h^2 = \int_0^\infty S_h(\omega) d\omega \quad (39)$$

$$S_h(\omega) = |\Lambda_{21}(\omega)|^2 S_{x_{cm}}(\omega) + |\Lambda_{22}(\omega)|^2 S_{z_{cm}}(\omega) + |\Lambda_{25}(\omega)|^2 S_{\theta_{cm}}(\omega)$$

$$\Lambda(\omega) = [j\omega I - \tilde{\underline{A}} + \tilde{\underline{B}}\tilde{\underline{H}}]^{-1} [j\omega I - \tilde{\underline{A}}]$$

A digital program performs the necessary computations.

c. Simulation Exercises

In the evaluation of a preliminary AMOAC design, the carrier approach simulation is exercised several times.

At first, a simple aircraft model is used, i.e. no control actuators, lags or nonlinearities, and there is no navigation loop closure, i.e., no h_e feedback. This run is used to determine the dynamic response of the aircraft's variables and controllers to the carrier approach environment. The ability to control the aircraft's rate responses, i.e., sink rate, airspeed, flight path and pitch rate as well as the various control expenditures are the prime concern of this run. If it is discovered that a variable is inadequately controlled or a controller is used too much or too little, its respective performance index parameter can be adjusted. The root square locus is then used to determine a new preliminary design.

The next exercise of the approach simulation evaluates the effects of controller actuators, lags and non-linearities. The aircraft model is updated to include these controller dynamics and non-linearities, and the carrier approach is run and evaluated along the same ground rules as the previous run.

After a preliminary design is checked out successfully in the previous two exercises, the AMOAC control system is incorporated into the ACLS system described in the previous section and the simulation is again exercised. In this case, two runs are made. The first run utilizes a twenty foot initial vertical glide slope error and no burble. A successful design is called upon to null out all errors, i.e., position, rates

and controller deflections, within 10 seconds or 1800 feet along the glide slope. For the purpose of this simulation, nulling out errors refers to reducing initial errors to 10 percent and maintaining that level or less. Airspeed and sink rate, which are initially zero, must be maintained within one foot per second and one-half foot per second respectively for an error to be called null.

The aircraft is then started 20 feet off the nominal glide slope and the closed loop ACLS is allowed to land the aircraft in the presence of the burble. The ΔH_D and ΔH_R requirements are then checked. Successful runs lead the computation of carrier motion induced dispersion which completes the simulation exercises.

The choice of a guidance loop, i.e., closed loop ACLS, is accomplished with the aid of the analysis of the next section.

3. Guidance Loop Closure

In the process of evaluating the AMOAC system's ACLS capabilities, the introduction of a guidance loop became necessary. The guidance scheme was chosen to be a simple, single position feedback loop. In particular, the perpendicular deviation from the nominal glide slope, i.e., h_e of figure 6 was weighted with a gain k , and added to the h feedback term.

$$\dot{h}_{fb} = \dot{h} + k \dot{h}_e \quad (40)$$

For the purposes of analysis and selection of a proper value for k , the h_e term was considered approximately equal to the vertical glide slope error. For a 4 degree slope, the resulting error is less than one-half of one percent. With this approximation, equation (40)

becomes:

$$\dot{h}_{fb} = \dot{h} + k \int_0^t \dot{h} dt \quad (41)$$

In appendix F equation (41) is incorporated into the optimal closed loop system equations, equation (3) and 13), and the following result is obtained:

$$0 = s \det(Is - A + BH) + k \sum_{i=1}^4 N_{2i}(s) h_{i2} \quad (42)$$

A digital program is used to solve equation (42) for the closed loop ACLS system roots. The value of k is then determined according to the deviation of ACLS roots from the basis AMOAC roots and system response speed of the ACLS guidance modes.

This value of k is then incorporated into the ACLS simulation for purely demonstration and evaluation purposes. This particular guidance loop is most likely not the best available. Even better performance can be expected with a more complex guidance procedure.

C. Desired Closed Loop System

Physical considerations of the carrier approach problem impose severe constraints on the location of the closed loop denominator and numerator roots.

1. Phugoid and Short Period Roots

In the final phase of the approach, i.e., 10 seconds aft of the ramp, the airplane should be capable of precise response to altitude command inputs in order to stay in phase with carrier deck motions. This requirement indicates a phugoid bandwidth of a magnitude comparable to the center frequency of the carrier deck vertical motion spectrum ω_{cz} . For adequate altitude control, a phugoid damping ratio δf between 0.2 and 0.4 is required.

An aircraft carrier moving through a calm sea at 30 knots sets up vertical gust turbulence with a low frequency spectrum. The carrier's pitching and heaving motion creates additional vertical turbulence of a higher frequency. The value of ω_{cm} used in this report is 0.6 radians per second, the average of the values found in references (d) and (e). The vertical gust spectrum data were taken from reference (e) which indicates vertical turbulence of amplitude 1.75 feet per second centered at 0.3 radians per second, and additional turbulence of 4.15 feet per second amplitude centered at 2.3 radians per second. In order to meet the requirements on terminal altitude control and avoid serious vertical gust problems, the phugoid roots should lie in the smaller shaded region of figure 7. Thus, the desired phugoid roots are characterized by:

$$0.2 \leq \zeta_p \leq 0.4$$

$$0.47 \leq \omega_p \leq 0.75$$

The short period roots should have a bandwidth smaller than the high frequency vertical gusts and a natural frequency great enough to provide ample separation from the phugoid roots, i.e., $\omega_{sp}/\omega_p \geq 2.5$. For satisfactory pitch control, the short period roots should have a damping ratio of between 0.55 and 0.85, as shown in the larger shaded region in figure 7 i.e. desired short period roots are characterized by:

$$0.55 \leq \zeta_{sp} \leq 0.85$$

$$1.88 \leq \omega_{sp} \leq 2.63$$

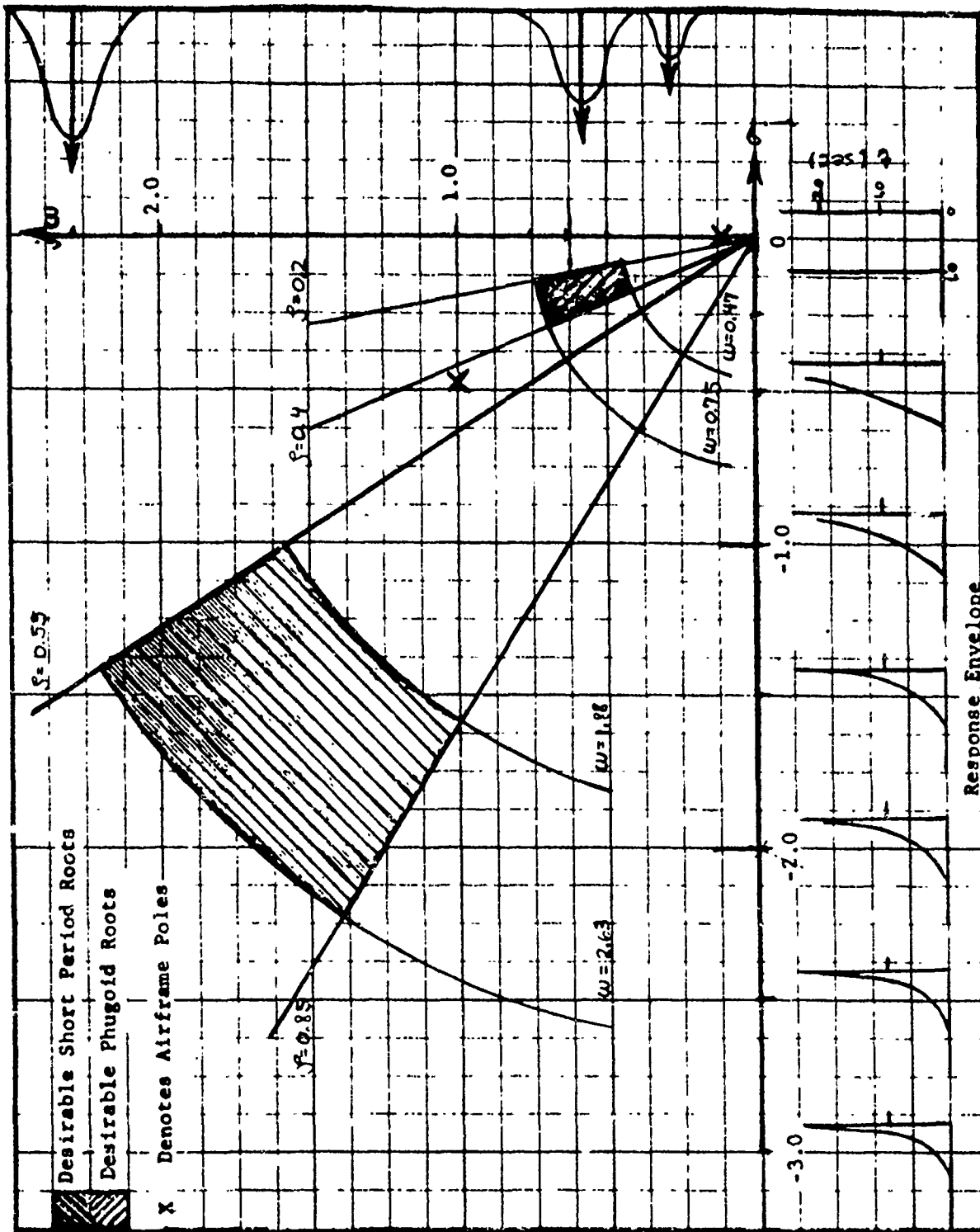


FIGURE 7. DESIRABLE CLOSED LOOP ROOTS

2. Numerator Zeros

In order to determine the significance of the numerator terms of the closed loop system, it is assumed that pitch rate is controlled primarily by the elevator deflection, airspeed primarily by thrust and sink rate by flaps and thrust together. Accordingly, primary interest is given to those transfer functions.

In evaluating the zeros of the sink rate and airspeed transfer functions, serious attention is given to the necessary quick glide slope response and the non-minimum phase nature of the open loop system. For these reasons, the airspeed and sink rate transfer functions are required to have all left half plane zeros. In addition, the magnitude of these zeros was limited to three radians per second in order not to lose needed phase lead. The pitch rate requirements are less critical and therefore more straightforward. As the phugoid and short period roots are moved to higher frequencies, the pitch rate zeros must also be moved to higher frequencies. This procedure insures a flatter frequency response and makes pitch rate response less sensitive to carrier pitch induced disturbances. This phenomenon is illustrated in figure 8. Thus, the magnitudes of the two pitch rate zeros are required to be of the same order as the natural frequency of the closed loop phugoid and short period roots respectively.

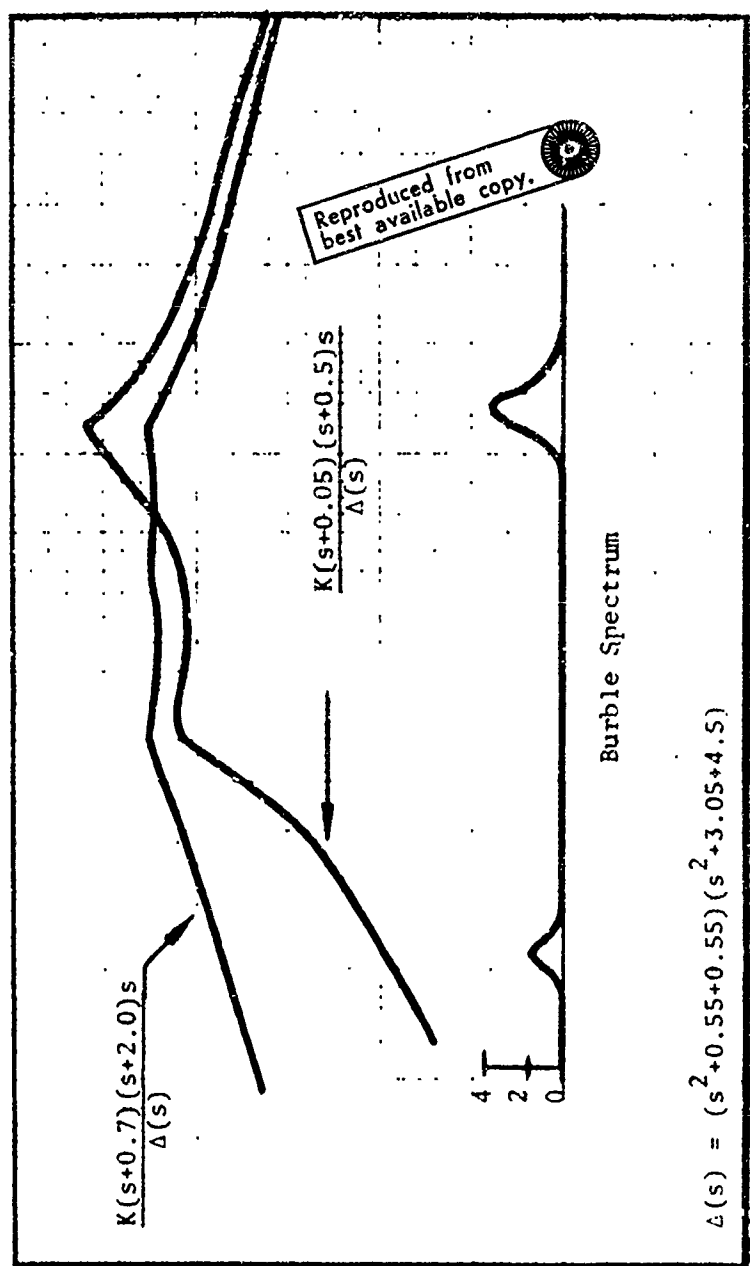


FIGURE 8. PITCH RATE FREQUENCY RESPONSE

PART III

RESULTS

A. Application to the F-8C1. System Synthesis

The effects of the performance index parameters upon the roots of the closed loop optimal system are most readily shown in a series of root locus plots. Figure 9 through 12 show the loci of the roots of the three inner loops; i.e., the sink rate, pitch rate, and cross coupling loops, as functions of b_1 and b_2 . Root loci for the numerator and denominator loops appear in figures 13, 14, and 15. The loci of the outer loop roots, or the final closed loop airframe roots are shown in figures 16, 17 and 18. Due to the symmetry of the root square locus plots, only the upper left-hand quarter of the s-planes is shown.

In the carrier approach, the primary task is flight path control, with pitch attitude control as an important secondary consideration. In order to fulfill the primary task, considerable attention must be given to shaping the phugoid locus, without degrading the short period response. The rationale behind particular loop closures is to position the phugoid roots while maintaining satisfactory short period damping and bandwidth, according to section II C.

Inner Loops

The three inner loops have b_1 and b_2 as common parameters and therefore must be closed simultaneously.

Sink Rate Loop

(43a)

$$\frac{\Lambda}{N_{22}(s)} + b_1 \frac{\Lambda}{N_{21}(s)} + b_2 \frac{\Lambda}{N_{23}(s)}$$

Cross Coupling Loop

$$b_1 \hat{N}_{12}^4(s) + b_2 \hat{N}_{23}^4(s) + b_1 b_2 \hat{N}_{31}^4(s) \quad (43b)$$

Pitch Rate Loop

$$\hat{N}_{42}(s) + b_1 \hat{N}_{41}(s) + b_2 \hat{N}_{43}(s) \quad (43c)$$

Substituting values from Appendix G, the inner loops become

Sink Rate Loop

$$4.8 \times 10^{-8} \langle s + 2.86 \rangle \langle s^2 + 0.50s + 0.51 \rangle + 398 b_1 \langle s + 0.23 \rangle \\ \langle s + 3.82 \rangle \langle s + 3.40 \rangle + 3.57 b_2 \langle s + 0.034 \rangle \langle s^2 + 0.38s + 1.29 \rangle$$

Cross Coupling Loop

$$1.51 \times 10^{-7} b_1 \langle s(s + 2.44) \rangle + 9.24 \times 10^{-9} b_2 \langle s(s + 0.12) \rangle + \\ 178.9 b_1 b_2 \langle s(s + 0.04) \rangle$$

Pitch Rate Loop

$$2.18 \times 10^{-11} \langle s(s + 0.31) \rangle \langle s + 0.89 \rangle + 4.84 b_1 \langle s(s + 0.52) \rangle \\ \langle s + 0.063 \rangle + 1.27 \times 10^{-3} b_2 \langle s(s + 3.18) \rangle \langle s + 0.008 \rangle$$

where $\langle F(s) \rangle$ denotes $F(s) F(-s)$.

Figure 9 shows the loci of roots for the sink rate loop for various combinations of b_1 and b_2 . Figure 10 is an enlargement of the region of interest of figure 9. The loci of the cross coupling loop roots is shown in figure 11 and figure 12 is a locus of the pitch rate loop roots.

The sink rate and cross coupling closed loop roots form the open loop poles and zeros, respectively, of the numerator loop. Pitch rate closed loop roots are the open loop zeros for the denominator loop. The cross coupling loop reflects second order interactions between control input

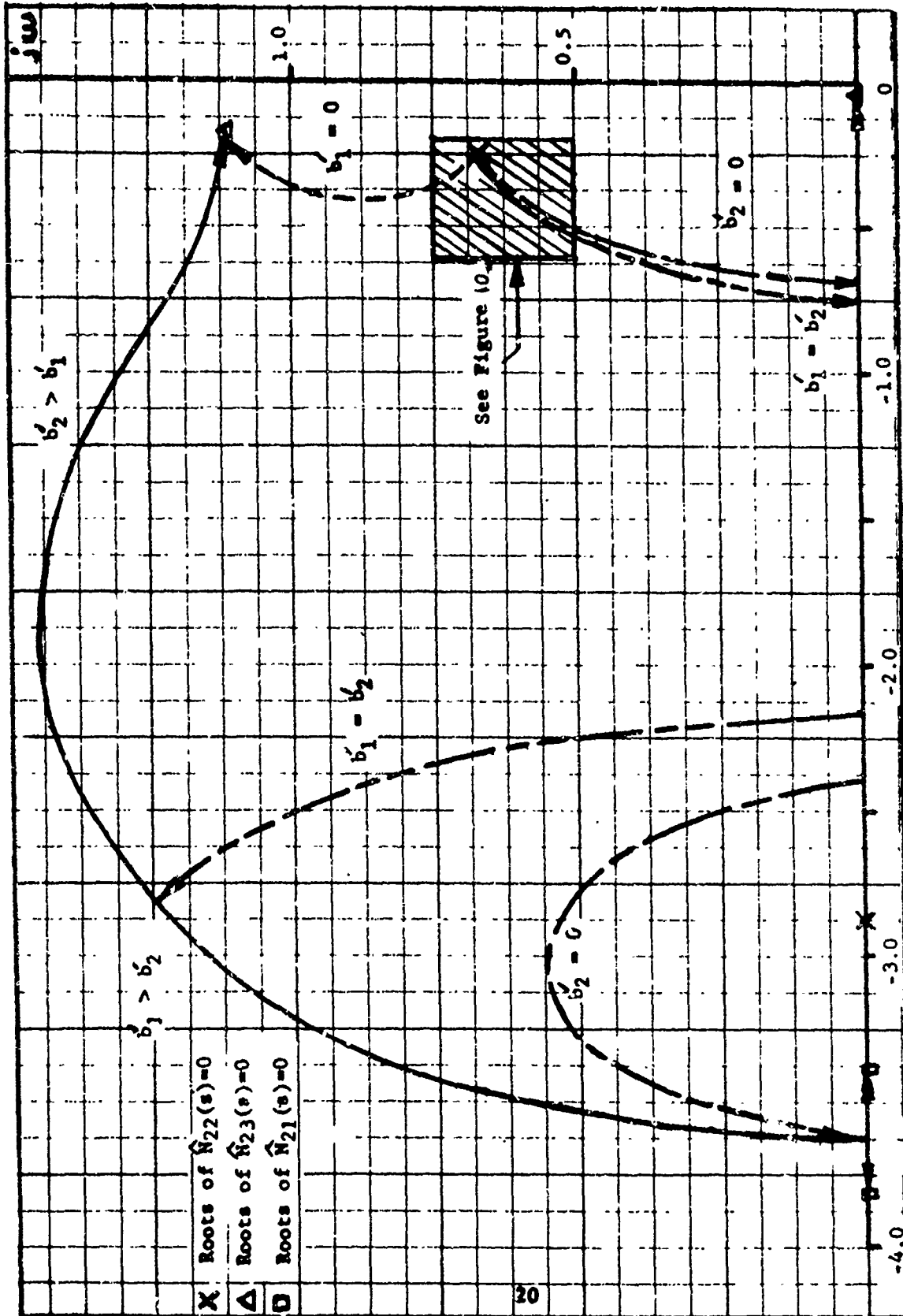


FIGURE 9. SINK RATE LOOP LOCI

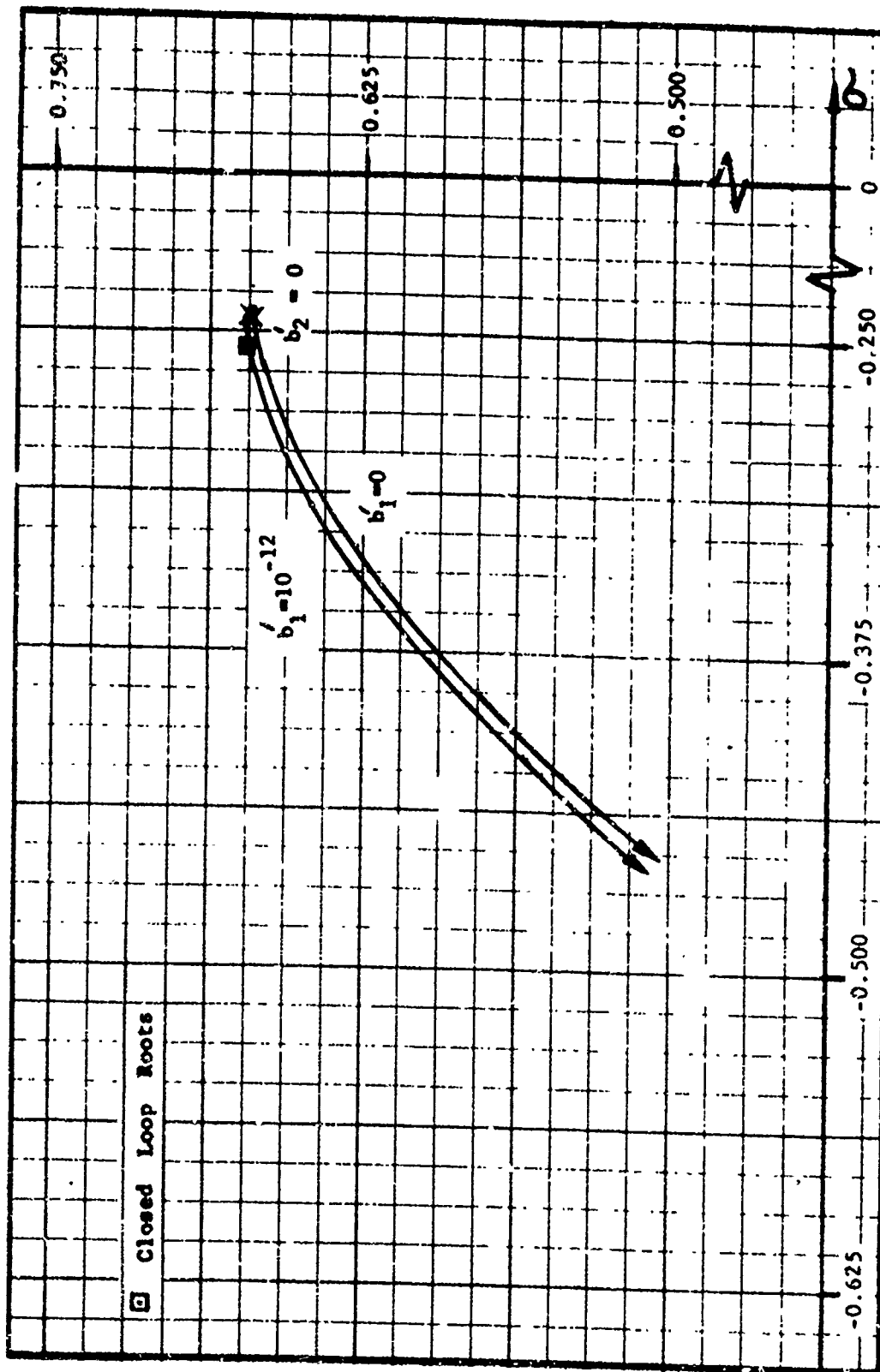


FIGURE 10. COMPLEX SINK RATE LOOP LOCUS

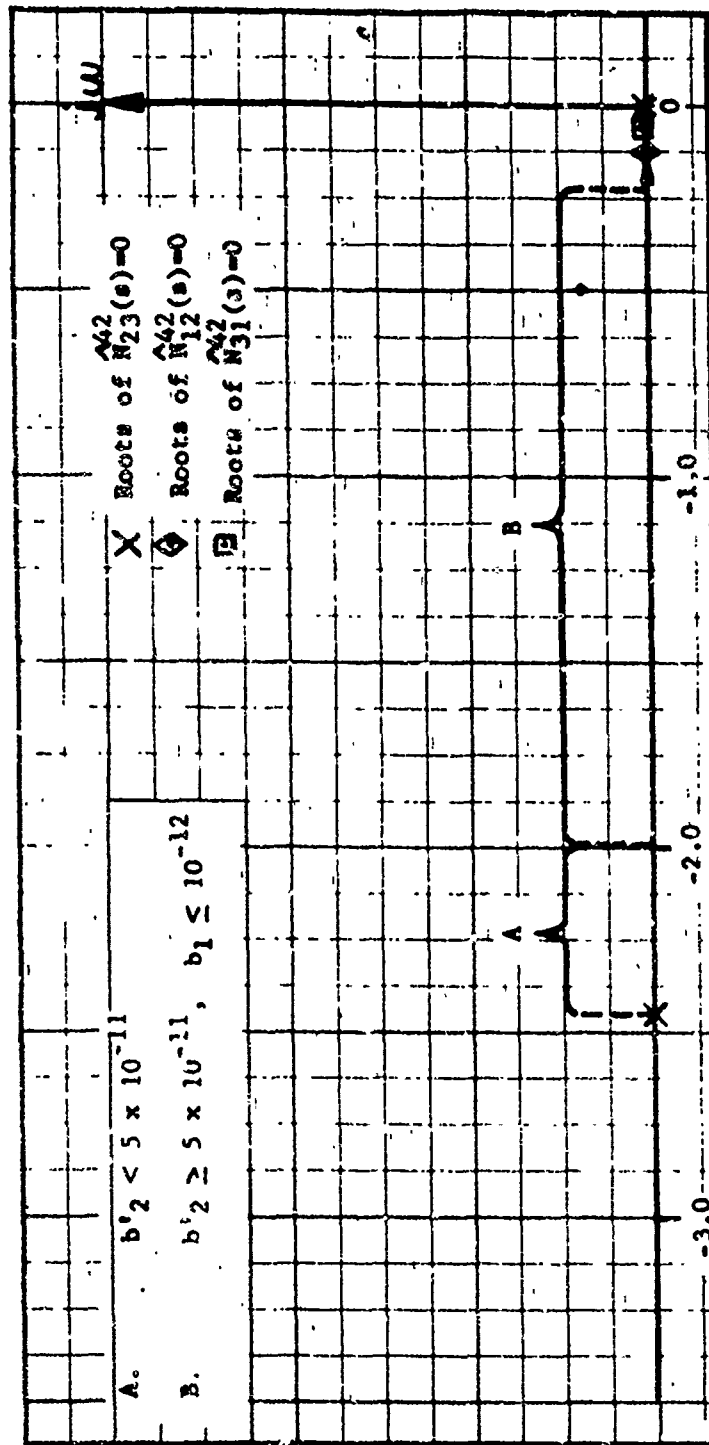


FIGURE 11. LOCUS OF NEGATIVE REAL CROSS COUPLING ROOT

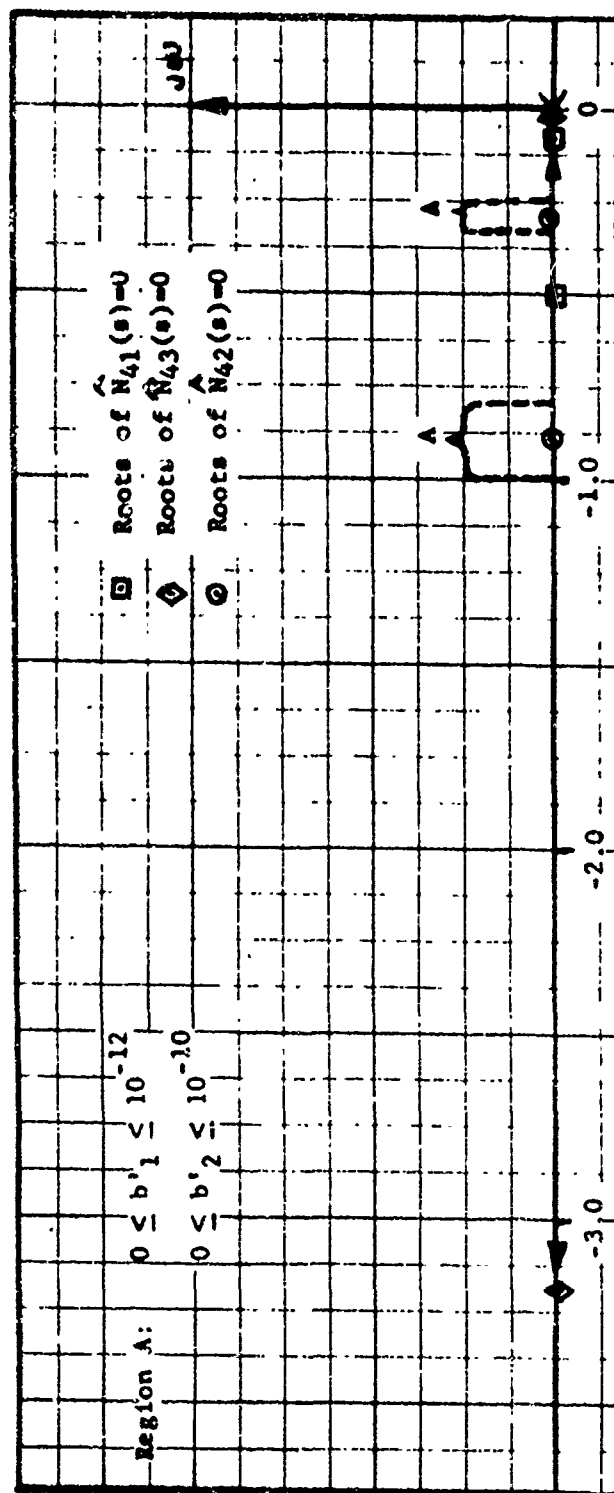


FIGURE 12. PITCH RATE LOOP LOCI

pairs, whereas the sink rate loop reflects a primary interaction between sink rate and the control inputs. For this reason, it was assumed that the cross coupling roots would affect the numerator loop much less than would the sink rate loop roots.

In light of this assumption, the closed loop sink rate roots can be considered as identical to the closed loop numerator roots. Figure 9 shows the entire range of possible roots for the sink rate loop. With b_1 and b_2 equal to zero, there is a complex root pair from the sink rate to thrust transfer function called phugoid control zeros, and a negative real root at $s = 2.86$ rad/sec. Since the phugoid airframe roots exhibit a small natural frequency, a complex pair of zeros will be required to adequately shape the phugoid mode. The much larger natural frequency of the short period mode allows for satisfactory shaping with a single real zero.

Satisfactory placing of the phugoid roots must include a large increase in speed of response, increased damping, a bandwidth close to the carrier deck motion center frequency and adequate separation from the short period roots. These physical considerations limit the complex sink rate root to the shaded region of figure 9. Figure 10 is an enlarged version of this desirable region.

Figure 12 shows the loci of the pitch rate loop roots. For all values of b_1 and b_2 there are three negative real roots; one root at $s = 0$, another root between $s = 0.31$ and $s = 0.008$ rad/sec and a third root between $s = 3.12$ and $s = 0.89$ rad/sec. Constraining b_1 and b_2 to the same values as in figure 10 limits the two negative real roots to the indicated region in figure 12. Using any values of b_1 and b_2 in this limited region

will result in quite similar denominator loop root loci.

Three sets of closed loop roots were chosen to illustrate the effect of large ranges of b_1 and b_2 on subsequent loop closures. Table 1 lists the parameter values and the inner loop roots for these three cases.

CLOSED LOOP ROOTS					
Case	b_1	b_2	Sink Rate	Pitch Rate	Cross Coupling
I	10^{-13}	10^{-13}	$-0.255 \pm j0.669$ -2.86	0.0, -0.305 -0.885	0.0, -2.372
II	10^{-12}	5×10^{-11}	$-0.342 \pm j0.646$ -2.34	0.0, -0.293 -0.844	0.0, -1.210
III	10^{-12}	10^{-10}	$-0.362 \pm j0.655$ -1.98	0.0, -0.287 -0.860	0.0, -0.917

TABLE 1 INNER LOOP CLOSURES

Numerator and Denominator Loops

After selecting values for b_1 and b_2 it is now possible to determine a value for k_2 .

Numerator Loop

$$(\text{Equation (43a)}) + k_2 (\text{Equation (43b)}) \quad (44a)$$

Denominator Loop

$$\Delta(s) + k_2 (\text{Equation (43c)}) \quad (44b)$$

Substituting values from Table 1 and Appendix G

Case I

Numerator Loop

$$4.808 \times 10^{-8} \langle s^2 + 0.510s + 5126 \rangle \langle s + 2.86 \rangle + 1.602 \times 10^{-20} k_2 \langle s(s + 2.372) \rangle$$

Denominator Loop

$$\langle s^2 + 0.96s + 1.27 \rangle \langle s^2 + 0.012s + 0.022 \rangle + 2.23 \times 10^{-11} k_2 s^2 + 0.305s \langle s + 0.885 \rangle$$

Case II

Numerator Loop

$$6.625 \times 10^{-8} \langle s^2 + 0.683s + 0.534 \rangle \langle s + 2.34 \rangle + 6.2 \times 10^{-19} k_2 \langle s(s + 1.21) \rangle$$

Denominator Loop

$$\langle s^2 + 0.96s + 1.27 \rangle \langle s^2 + 0.012s + 0.022 \rangle + 2.670 \times 10^{-11} k_2 s(s + 0.844) \langle s + 0.292 \rangle$$

Case III

Numerator Loop

$$8.41 \times 10^{-8} \langle s^2 + 0.724s + 0.558 \rangle \langle s + 1.98 \rangle + 1.09 \times 10^{-19} k_2 \langle s(s + 0.917) \rangle$$

Denominator Loop

$$\langle s^2 + 0.96s + 1.27 \rangle \langle s^2 + 0.012s + 0.022 \rangle + 2.68 \times 10^{-11} k_2 \langle s(s + 0.287) \rangle \langle s + 0.860 \rangle$$

Figures 13, 14 and 15 show the numerator and denominator loci for Cases I, II and III respectively. In all three cases, it is noted that the denominator locus experiences much greater excursions than the numerator locus for equal increments in k_2 .

For Cases I and III, the open and closed loop numerator roots are nearly identical while the denominator roots experience a definite excursion, i.e., the phugoid root travels approximately 15 percent of its total locus. This evidence validates the assumption of the previous section; that is, the closed loop numerator zeros are approximately the sink rate zeros.

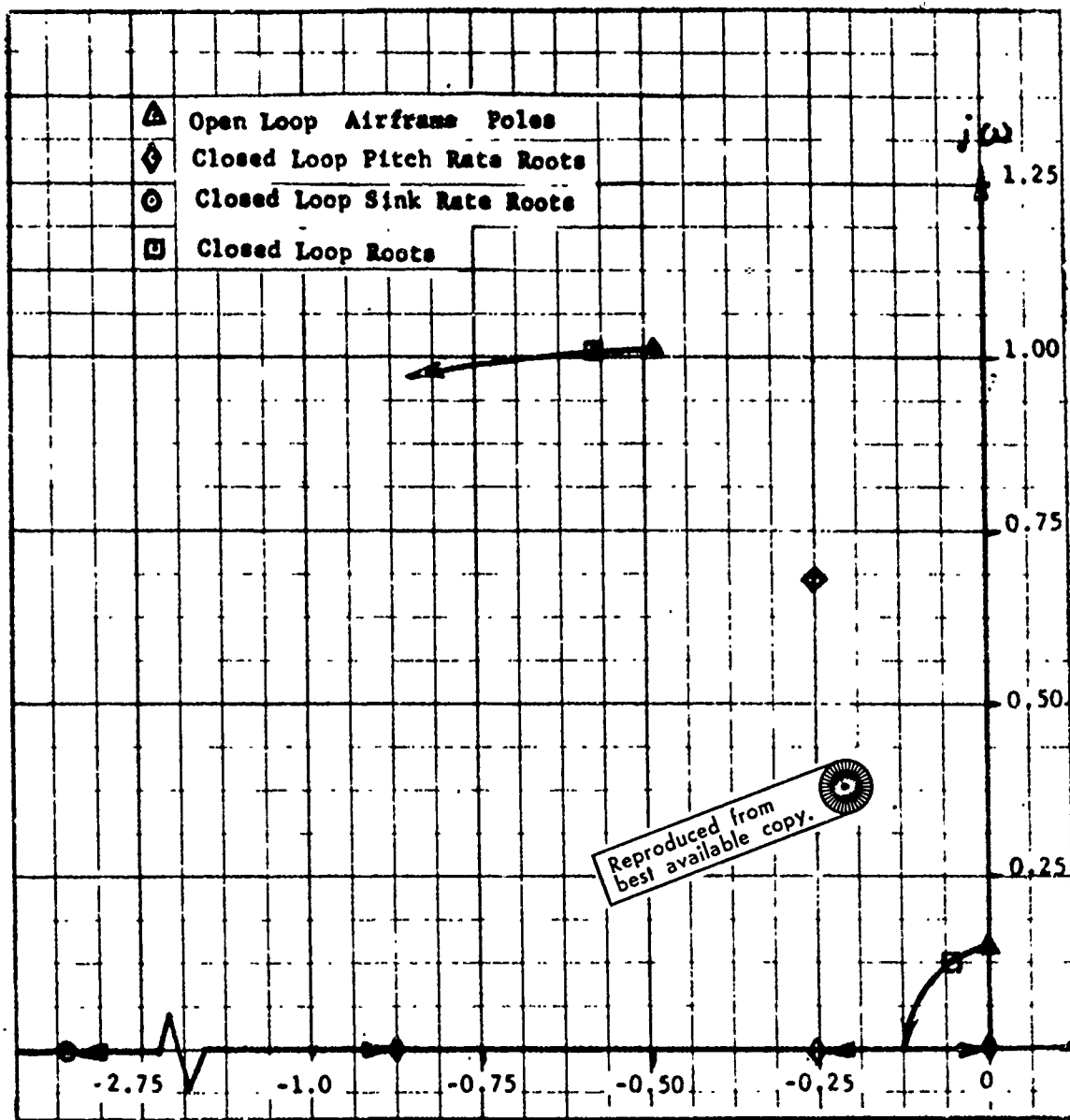


FIGURE 13. NUMERATOR AND DENOMINATOR LOCI - CASE I

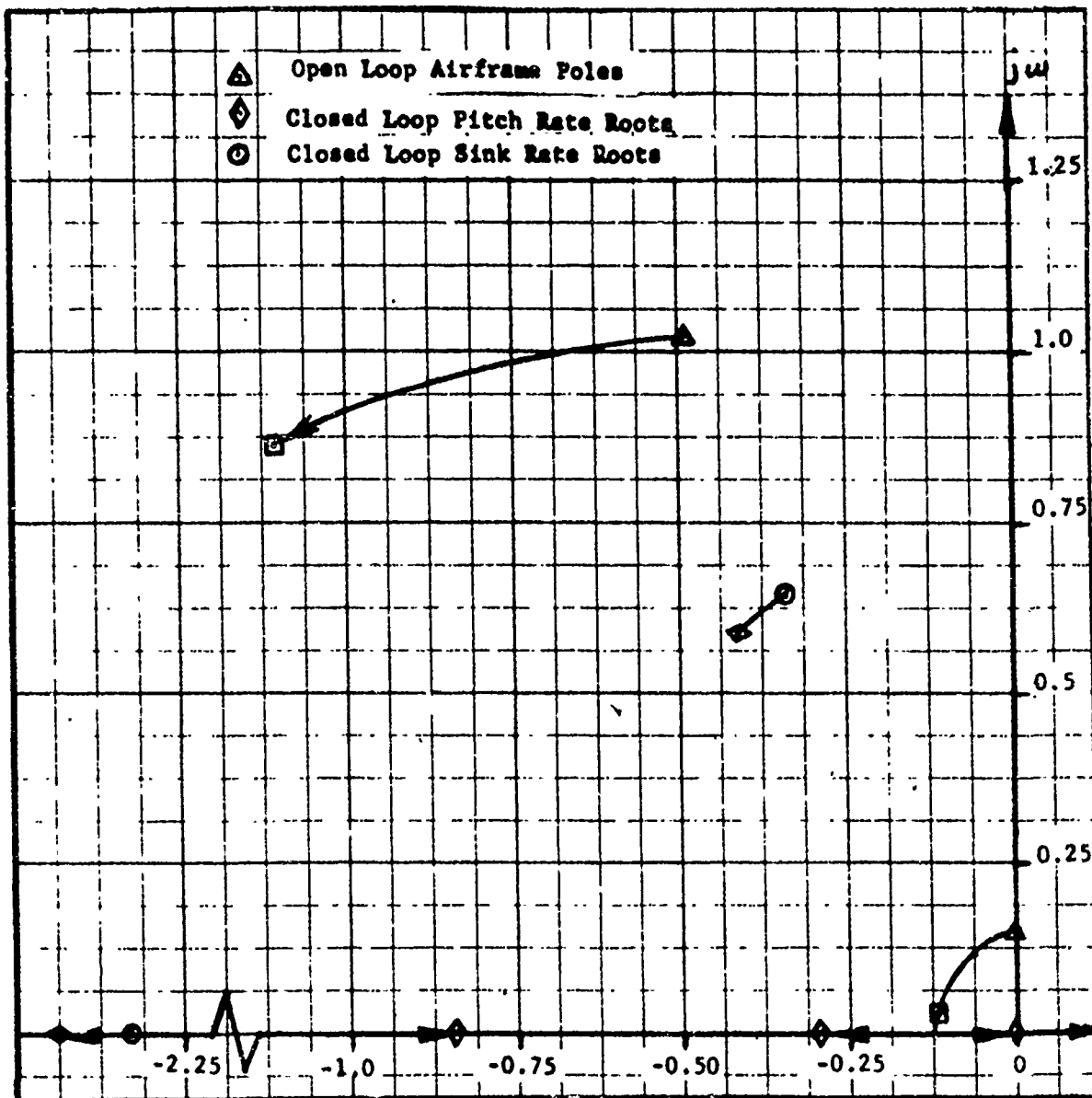


FIGURE 14. NUMERATOR AND DENOMINATOR LOCI - CASE II

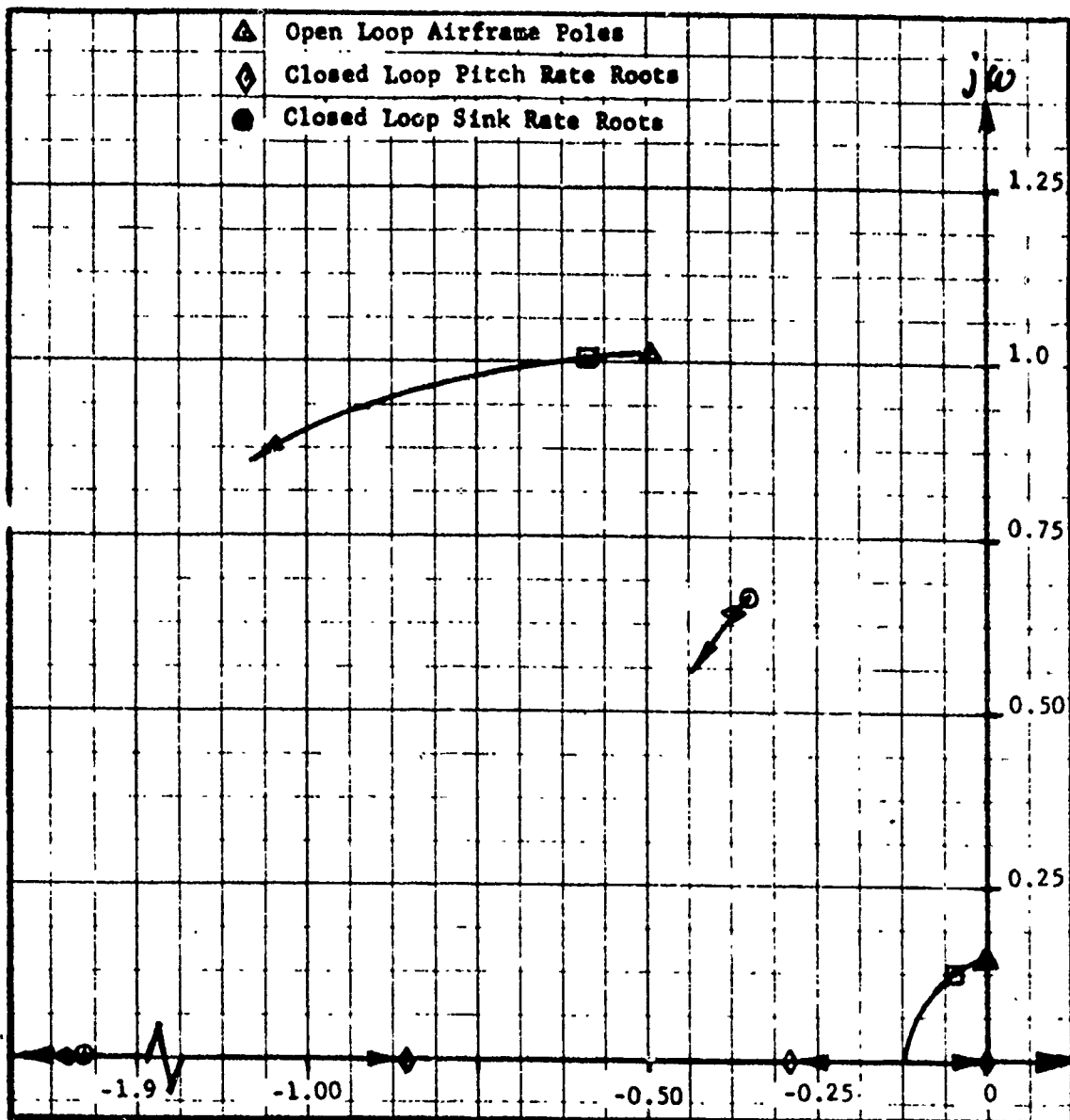


FIGURE 15. NUMERATOR AND DENOMINATOR LOCI - CASE III

Noting the limited region in which the phugoid locus lies and relatively slow movement of the complex numerator root, the phugoid locus in the outer loop closure can be expected to be largely independent of the k_2 closure. The short period locus displays markedly different behavior than the phugoid locus. Evidently, values of k_2 can have a considerable effect on the short period locus in the outer loop closure. In order to demonstrate this conjecture, Cases I and III are closed around small values of k_2 and Case II is closed about a larger value of k_2 , as shown in Table II.

Case	k_2	CLOSED LOOP ROOTS	
		Numerator	Denominator
I	10^{10}	$-0.256 \pm j0.668$ -2.86	$-0.053 \pm j0.134$ $-0.573 \pm j1.019$
II	10^{11}	$-0.419 \pm j0.574$ -2.47	$-0.114 \pm j0.038$ $-1.105 \pm j0.857$
III	10^{10}	$-0.372 \pm j0.644$ -2.00	$-0.053 \pm j0.133$ $-0.587 \pm j1.016$

TABLE II. NUMERATOR AND DENOMINATOR LOOP CLOSURES

The closed loop roots can now be specified with a single loop closure.

OUTER LOOP

$$(\text{Equation 44b}) + k_1' (\text{Equation 44a}) \quad (45)$$

Substituting values from Table II

Case I

$$\langle s^2 + 0.106s + 0.0205 \rangle \langle s^2 + 1.146s + 1.367 \rangle + 4.81 \times 10^{-8} k_1' \langle s + 2.86 \rangle \langle s^2 + 0.512s + 0.512 \rangle$$

Case II

$$\langle s^2 + 0.228s + 0.0146 \rangle \langle s^2 + 2.21s + 1.955 \rangle + 6.63 \times 10^{-8} k_1' \langle s + 2.47 \rangle \langle s^2 + 0.838s + 0.515 \rangle$$

Case III

$$\langle s^2 + 0.106s + 0.0203 \rangle \langle s^2 + 1.164s + 1.377 \rangle + 8.42 \times 10^{-8} k_1' \langle s + 2.0 \rangle \langle s^2 + 0.744s + 0.553 \rangle$$

Figures 16, 17 and 18 show the loci of the closed loop roots for Cases I, II and III respectively. The closed loop short period and phugoid roots are shown for various values of k_1' . For convenience of comparison, Table III lists these roots and their corresponding values of b_1' , b_2' , k_1' and k_2' .

The phugoid locus of the outer loop closure is most greatly affected by the complex closed loop numerator zero. This zero is essentially the same as the closed loop sink rate zero. Thus, the closed loop phugoid locus can be shaped effectively by the sink rate loop closure. The short period roots of the outer loop move considerably more slowly along their locus than do the phugoid roots. This places greater emphasis on the initial part of the short period locus than upon latter parts. Therefore, the short period locus is greatly affected by the closed loop denominator roots.

The design procedure used in this report allows a great deal of independence in placing the closed loop short period and phugoid roots. The closed loop phugoid locus is shaped primarily by the sink rate loop closure, i.e. the values of b_1' and b_2' , while the closed loop short period locus is influenced more by the denominator loop closure, i.e. the value of k_2' .

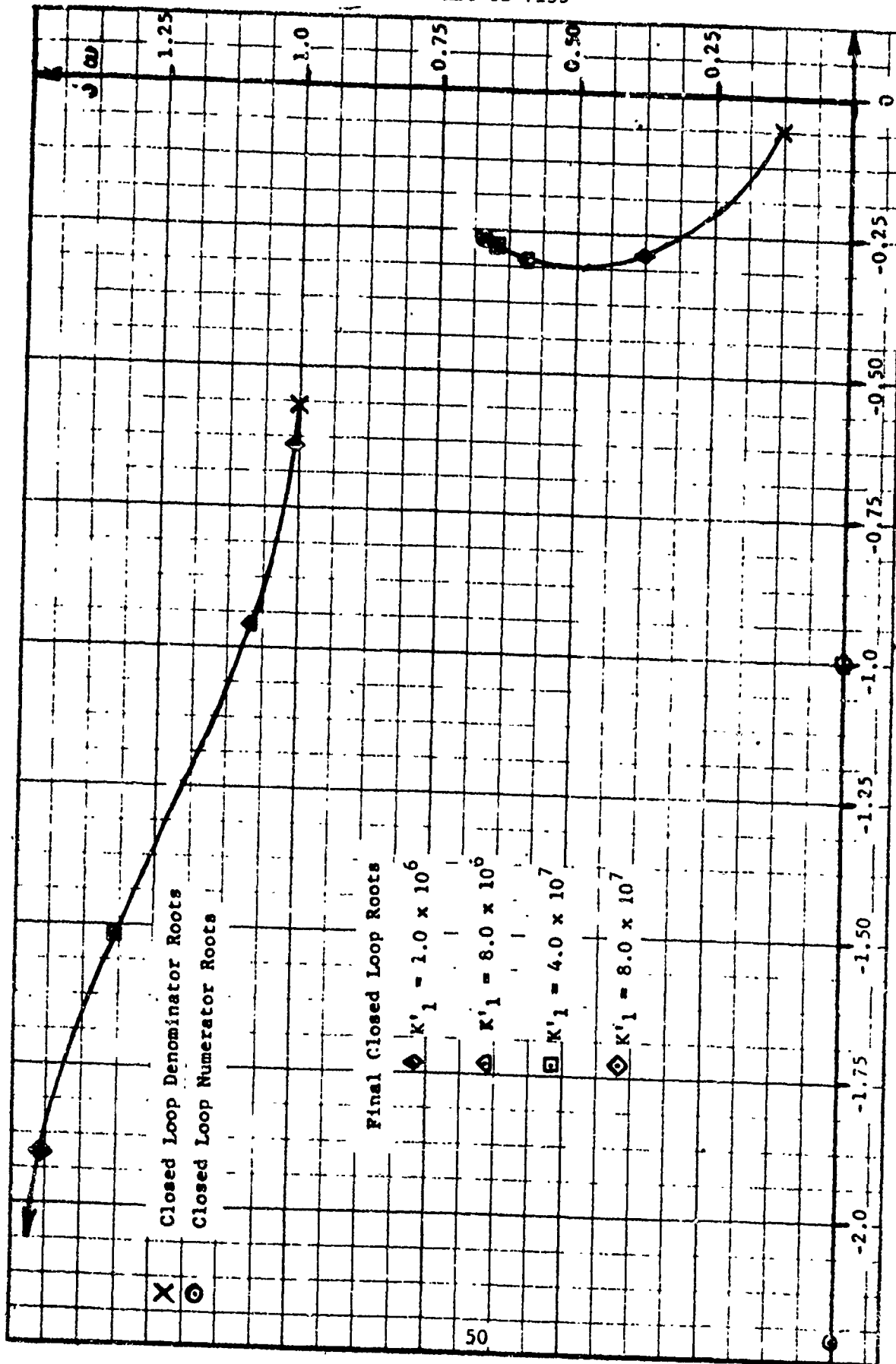


FIGURE 16. FINAL LOOP CLOSURE - CASE I

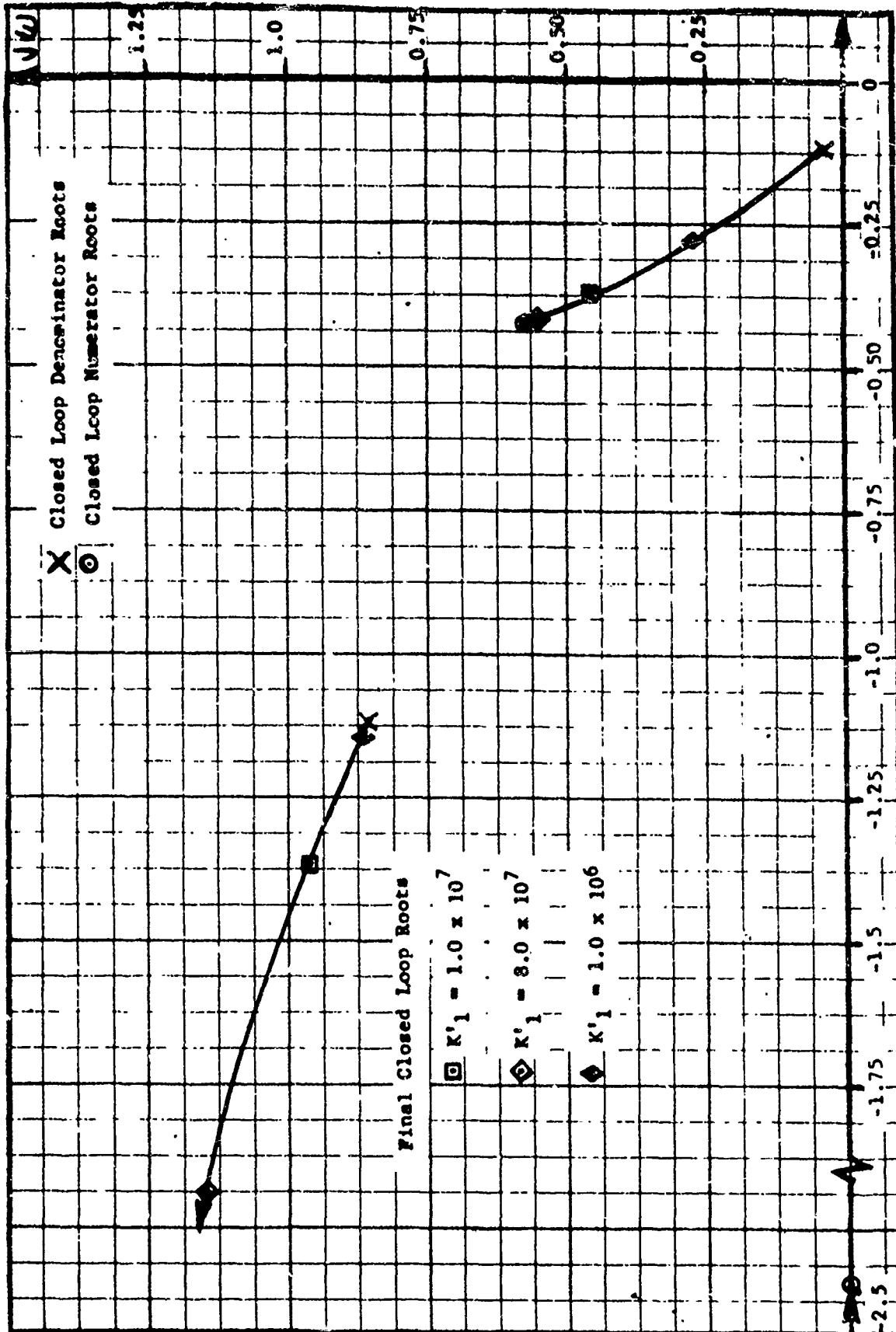


FIGURE 17. FINAL LOOP CLOSURE - CASE II

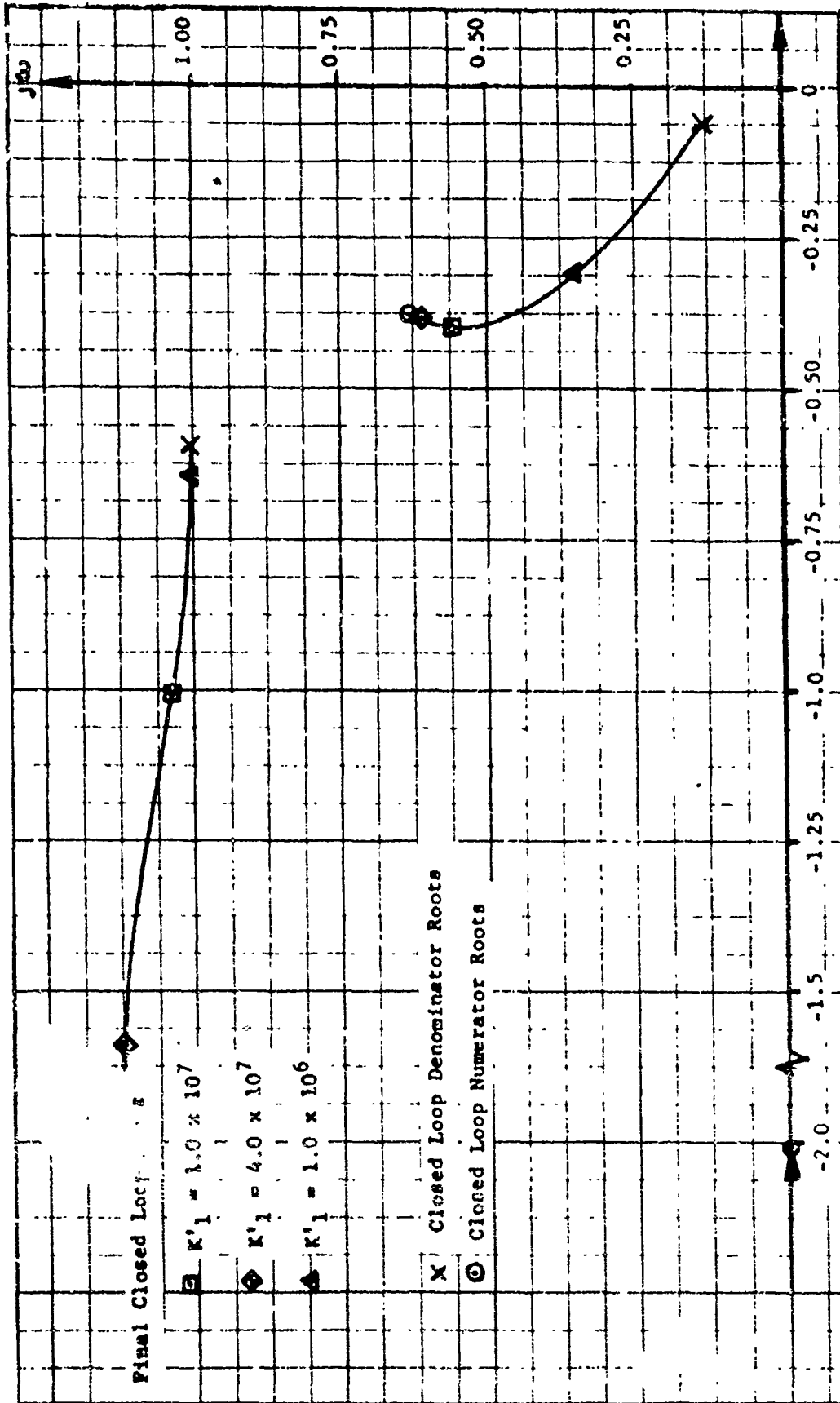


FIGURE 18. FINAL LOOP CLOSURE - CASE III

Item	b_1	b_2	k_1	k_2	ζ_p	$\zeta_{p\omega}$	Phugoid Band Width	ζ_{sp}	$\zeta_{sp\omega}$	Short Period Band Width	ω_{sp/ω_p}
1	10^{-13}	10^{-13}	10^{10}	10^6	0.590	0.280	0.384	0.529	0.631	1.015	2.518
2	10^{-12}	10^{-10}	10^{10}	10^6	0.646	0.305	0.361	0.533	0.640	1.017	2.541
3	10^{-12}	5×10^{-11}	10^{11}	10^6	0.695	0.275	0.285	0.794	1.138	0.871	3.619
4	10^{-13}	10^{-13}	10^{10}	8×10^6	0.448	0.297	0.592	0.659	0.949	1.082	2.170
5	10^{-12}	10^{-10}	10^{10}	1×10^7	0.561	0.387	0.572	0.689	1.006	1.057	2.113
6	10^{-12}	5×10^{-11}	10^{11}	1×10^7	0.626	0.377	0.469	0.814	1.362	0.973	2.780
7	10^{-13}	10^{-13}	10^{10}	4×10^7	0.380	0.267	0.652	0.756	1.531	1.324	2.875
8	10^{-12}	10^{-10}	10^{10}	4×10^7	0.518	0.379	0.625	0.813	1.586	1.135	2.669
9	10^{-13}	10^{-13}	10^{10}	8×10^7	0.369	0.262	0.660	0.798	1.906	1.438	3.363
10	10^{-12}	5×10^{-11}	10^{11}	8×10^7	0.596	0.412	0.555	0.879	2.157	1.169	3.551
11	Open Loop Airframe				0.033	0.005	0.149	0.427	0.483	1.024	7.597

TABLE III CLOSED LOOP ROOTS

2. Design Evaluation

In this section, the preliminary design of the previous section is evaluated and modified according to the procedure in section II in order to achieve the design of a fully automatic approach controller for the longitudinal axis of an F-8C aircraft. In the following discussion various candidate design configurations will be introduced. In order to minimize confusion, each of the preliminary designs will be designated by a system number. This number is a chronological ordering of the candidate designs. The baseline system is number zero with six other candidates systems comprising the entire list.

The results of the previous section indicates a baseline system suitable for initializing the AMOAC design procedure. The particular system is Item 7 of table III. For convenience, table IV below, contains a list of the seven preliminary designs along with their respective performance index parameters.

System No.	$b_1 = 1/d_1$	$b_2 = 1/d_2$	k_1	k_2
0	10^{-13}	10^{-13}	4×10^7	10^{10}
1	10^{-13}	10^{-12}	4×10^7	10^{10}
2	10^{-13}	2×10^{-12}	4×10^7	10^{10}
3	10^{-13}	10^{-11}	4×10^7	10^{10}
4	10^{-13}	2×10^{-11}	4×10^7	10^{10}
5	10^{-13}	10^{-10}	4×10^7	10^{10}
6	10^{-13}	2×10^{-10}	4×10^7	10^{10}

TABLE IV - PRELIMINARY SYSTEMS

For each system listed in table IV, a feedback gain matrix and a closed loop transfer matrix has been calculated as described in section I C.

These data are listed in Appendix H.

Inspection of the transfer matrix of system 0 reveals that the sink rate to thrust transfer function has right half plane zeros. However, the other requirements were fulfilled. These non-minimum phase zeros are a complex pair, close to the imaginary axis, close in magnitude to the left half plane sink rate to flap zeros. For this reason, it was felt that a greater use of flaps as opposed to thrust would result in left half plane sink rate zeros. To accomplish this, the performance index weighting of flap deflection was decreased while the other parameters remained unchanged.

The parameter b_2 , the reciprocal of d_2 was varied from the system 0 value of 10^{-13} through four orders of magnitude to a value of 10^{-9} . The root square locus was used to monitor movement of the closed loop system roots. This root locus plot is shown in figure 19.

Six different values of b_2 were chosen to define the six candidate designs designated system 1 through system 6. Inspection of the transfer matrices of these closed loop systems eliminated consideration of candidate systems 1, 2, 3 and 4 since each of these systems contained right half plane zeros in their sink rate to thrust transfer functions. System 5 and system 6, however, satisfied the criteria specified for satisfactory numerator roots.

The next design step is the exercise of a carrier approach, simulating the simplified aircraft model, with AMOAC augmentation by each of the two candidate systems respectively, as described in section II B-2. Figures 20 and 21 contain the time histories of the carrier approach employing system 5 and system 6 respectively. Inspection of these time histories

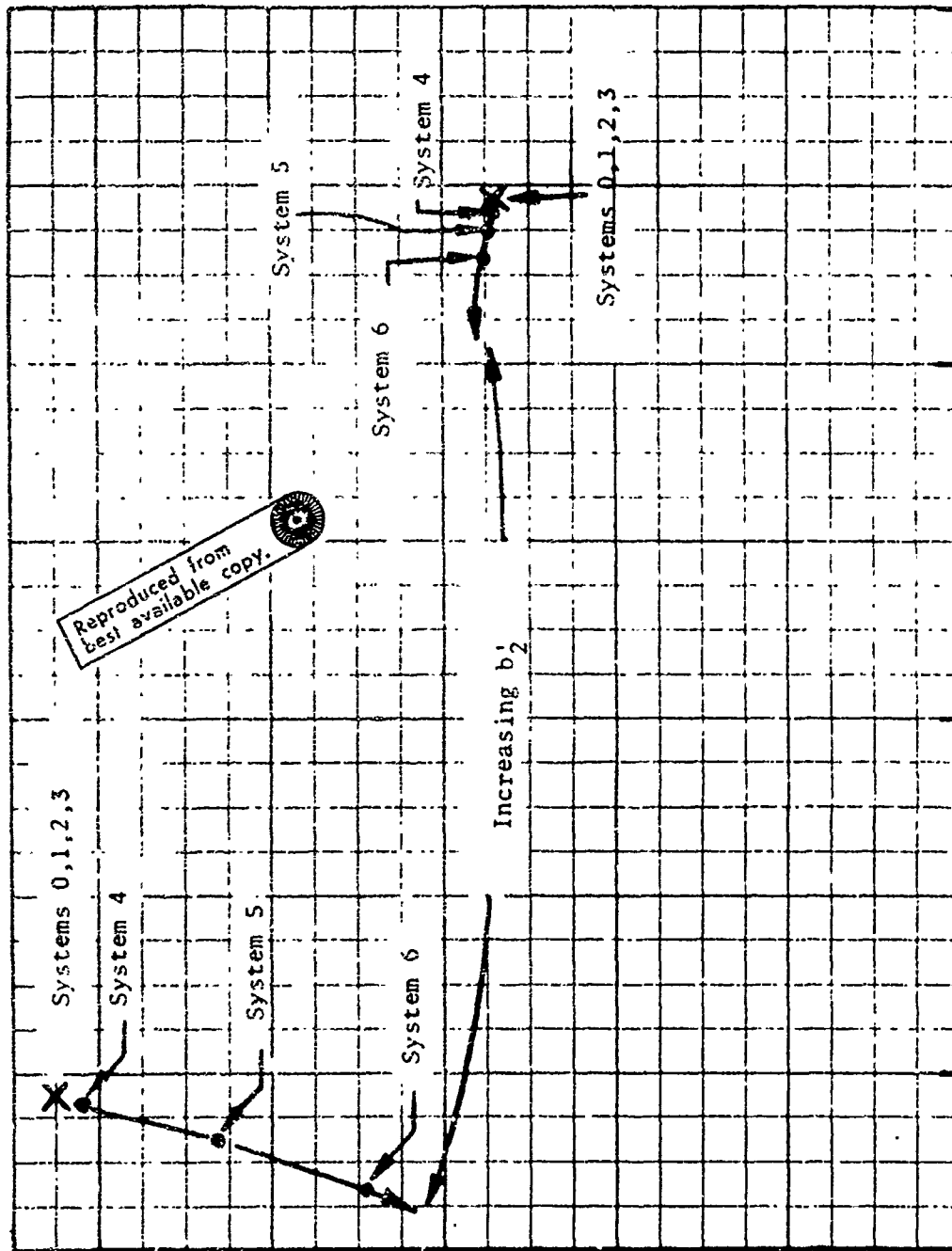
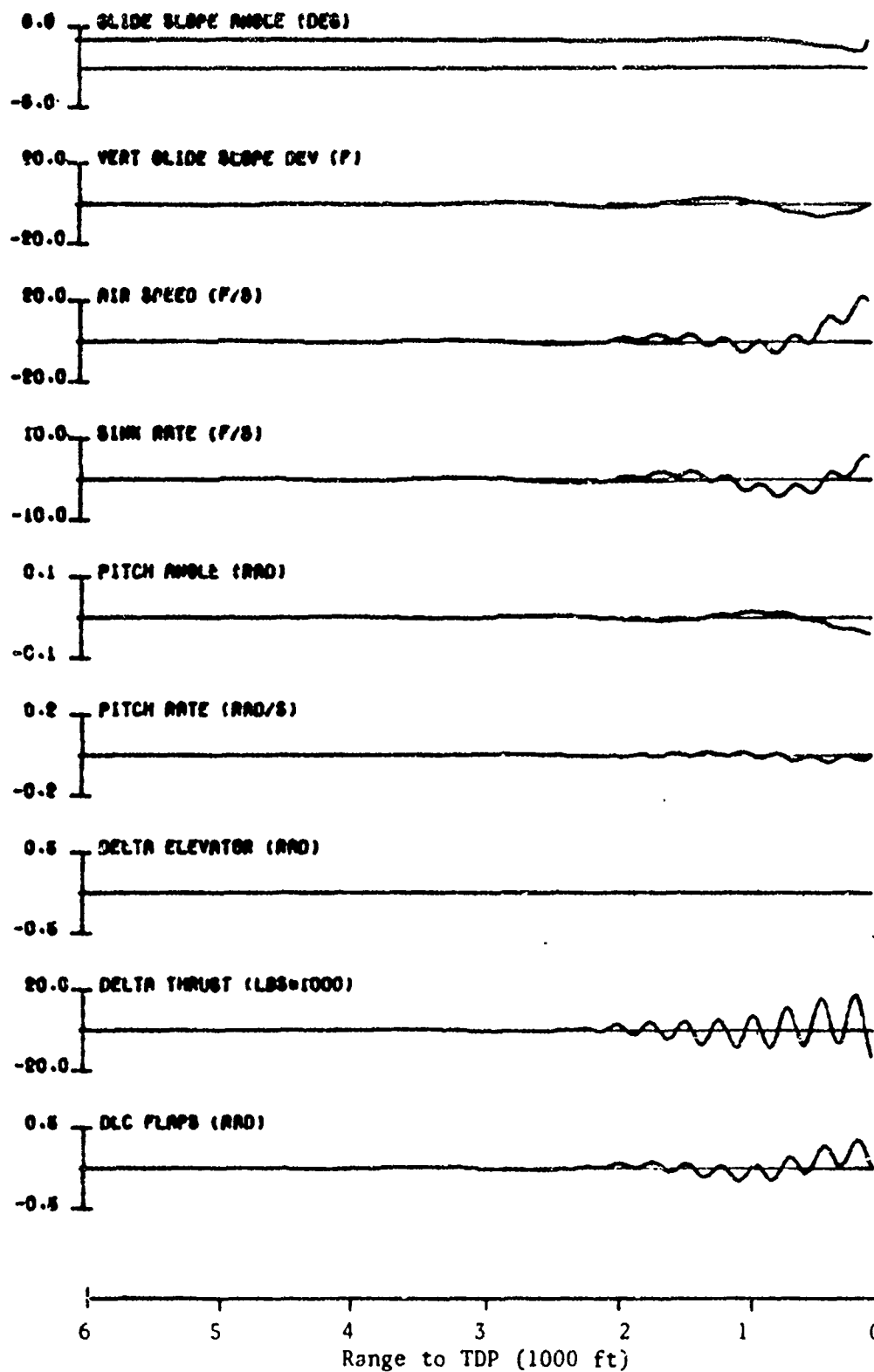
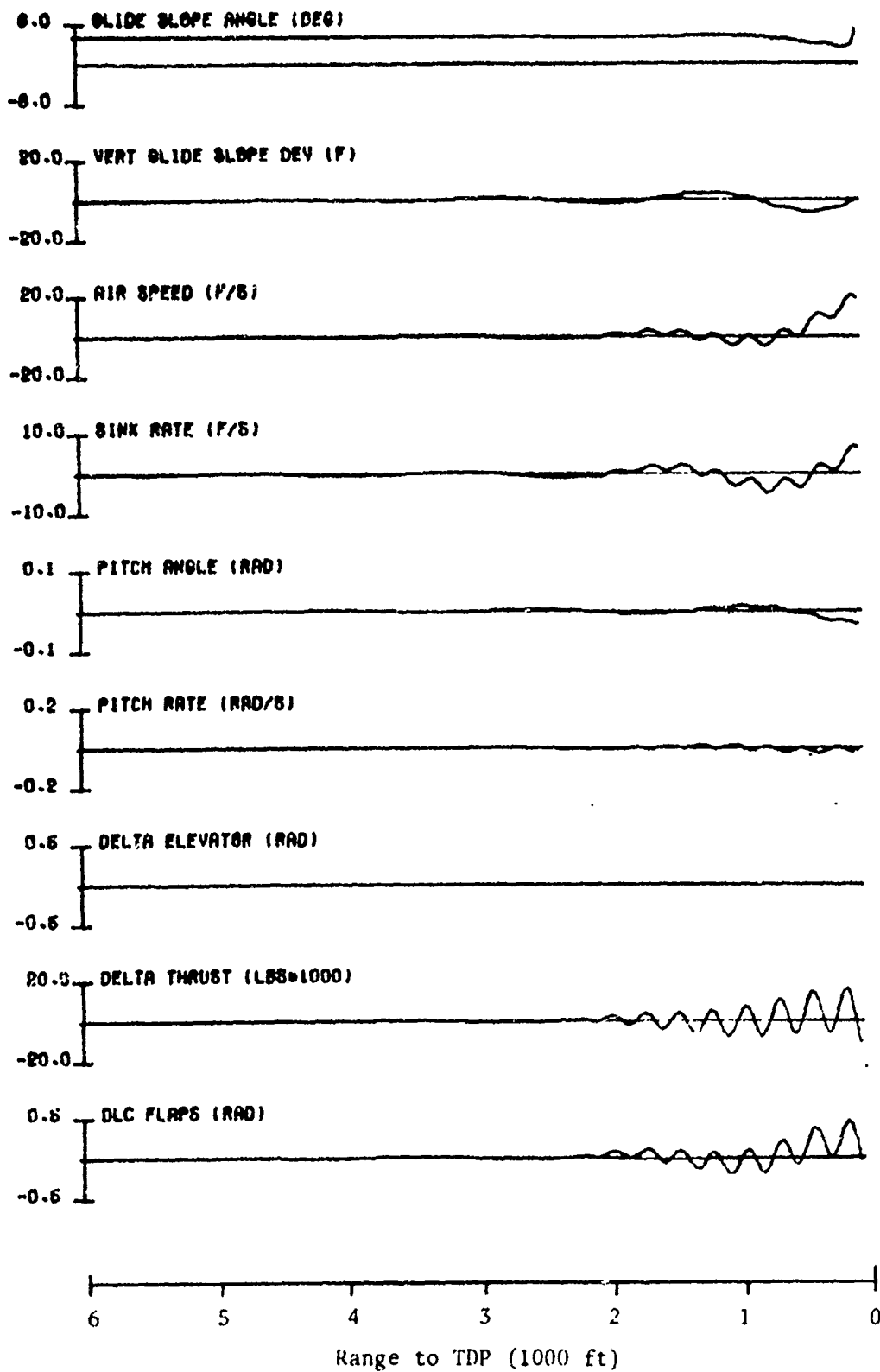


FIGURE 19. b_2 ROOT LOCUS FOR SYSTEM 0



FIGURE(20) SYSTEM 5 CARRIER APPROACH



FIGURE(21) SYSTEM 6 CARRIER APPROACH

shows a generally acceptable response. The glide slope angle shows no appreciable degradation up until one hundred feet to touchdown and the variations from trim velocities remain tightly bounded, as compared to the magnitude of the disturbances. The height over ramp and touchdown dispersion criteria were satisfied, as shown in table V.

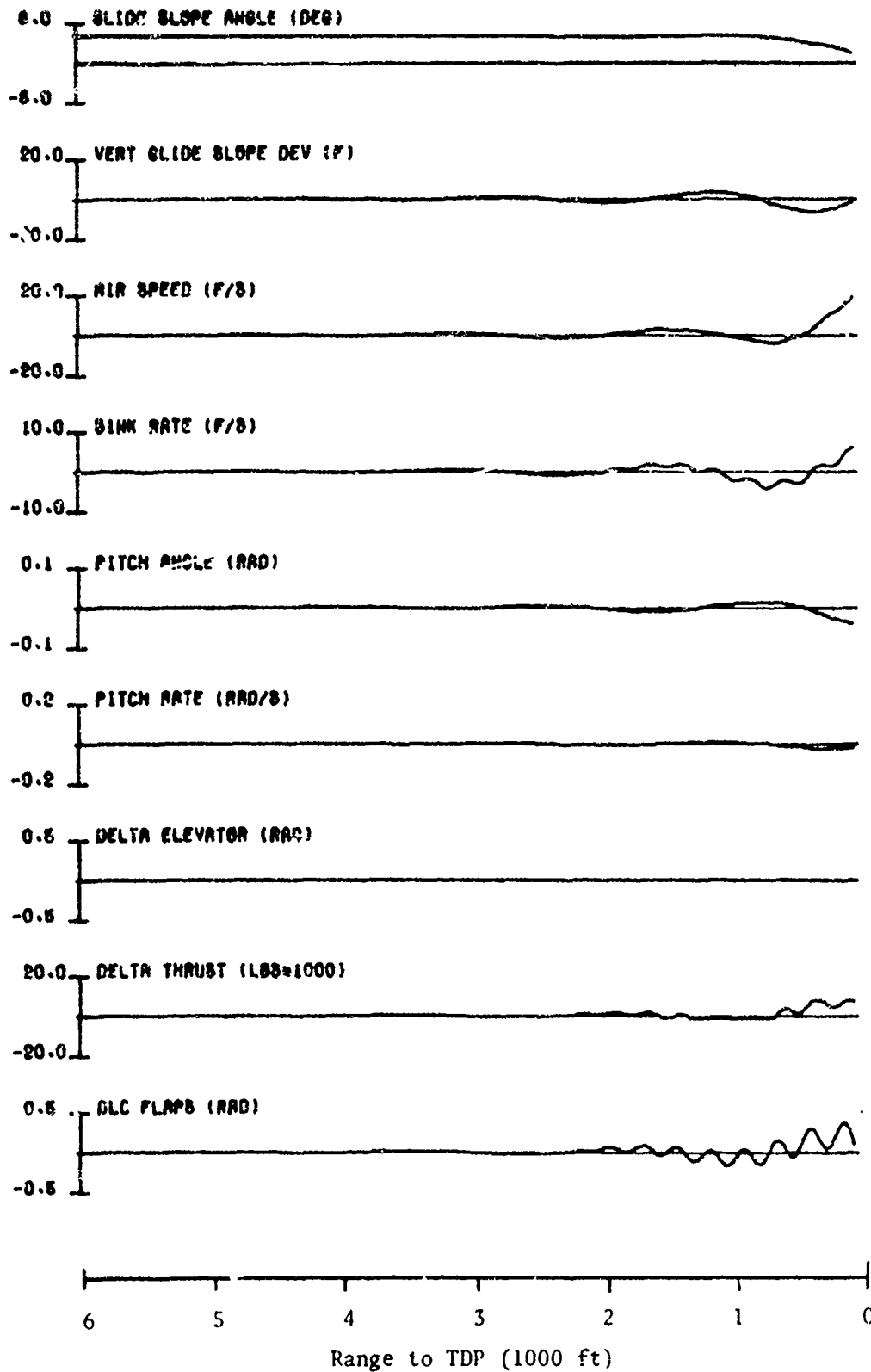
	SYSTEM 5 (Simple Airframe)	SYSTEM 6 (Simple Airframe)
$ \Delta H_R $ (ft)	4.2	4.4
$ \Delta H_D $ (ft)	0.5	0.95

TABLE V GLIDE SLOPE DEVIATIONS (A/D alone)

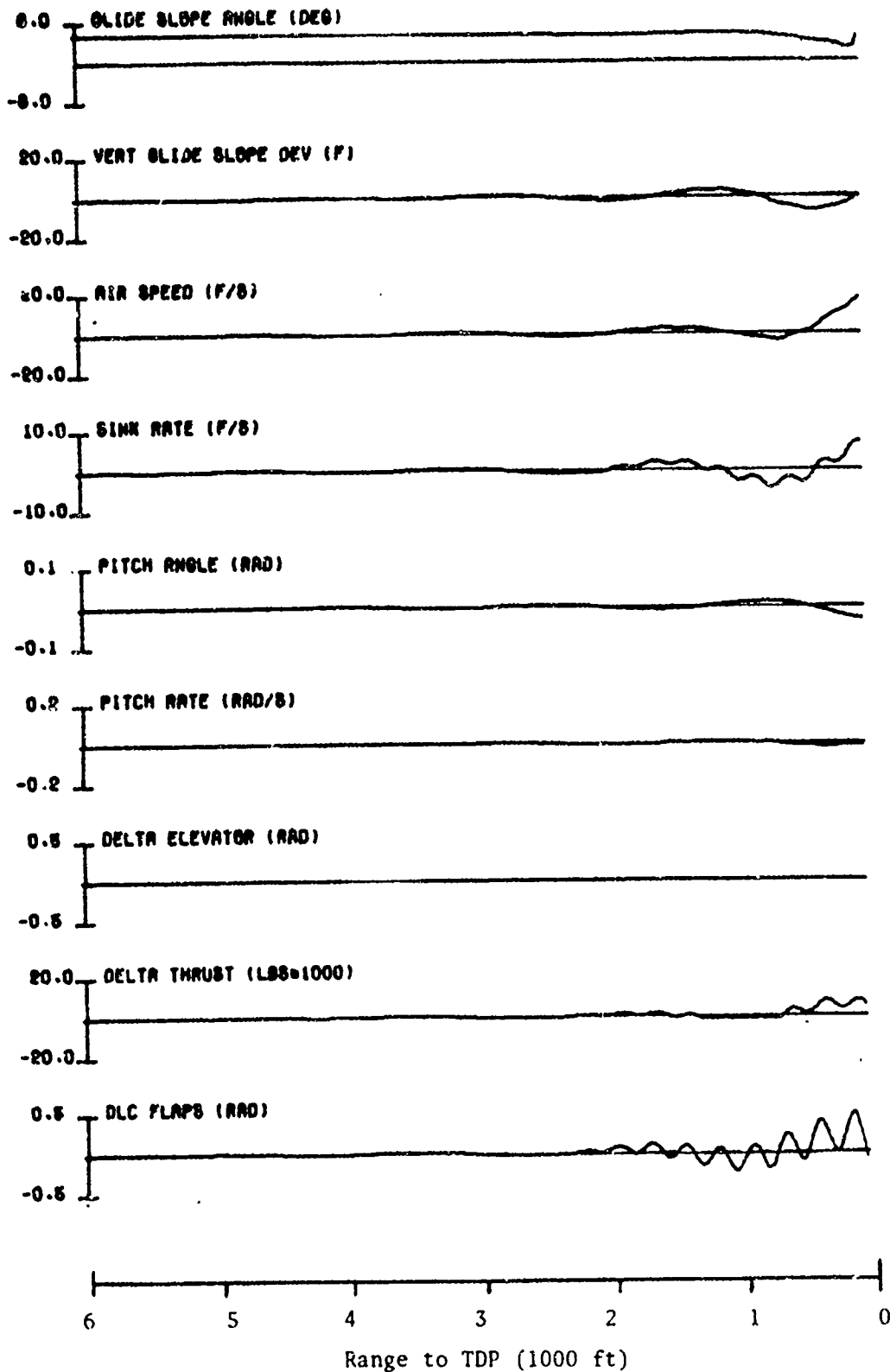
Pitch rate response and elevator deflection were minimal. The DLC flap deflection remained within operational bounds; however, the thrust limitations were exceeded. Since the periods of thrust limit exceedance were of short duration, the response was classed as acceptable and the next step in the design procedure was initiated.

The airplane model was expanded to include lags from the control surface actuators and engine, and the hard limiters on the controller outputs. The specific values of the lags and limits are included in appendix D. Figure 22 and 23 show time histories for systems 5 and 6 respectively. These time histories are quite similar to the previous set. The criteria on ΔH_D and ΔH_R are still satisfied, as shown in table VI. The trim velocity variations are again well bounded and in general smoother than the previous set. Thrust output is only limited over a small segment of the

NADC-SD-7153



FIGURE(22) SYSTEM 5. WITH ACTUATORS AND LIMITERS



FIGURE(23) SYSTEM 6. WITH ACTUATORS AND LIMITERS

response and exhibits linear control over the majority of the final one thousand feet. The DLC flap controller operates entirely in its linear region. With these simulations satisfactorily completed, the two candidate AMOAC designs are next evaluated as ACLS components.

	SYSTEM 5 (Simple Airframe)	SYSTEM 6 (Simple Airframe)
$ \Delta H_R $ (ft.)	5.1	5.2
$ \Delta H_D $ (ft.)	-0.45	0.25

Table VI - Glide Slope Deviations
(A/C Plus Actuators and Limiters)

Equation (41) defines the simple ACLS guidance equation used in the ACLS simulation. In order to find a proper value of guidance gain k , a root locus of the guidance loop was constructed according to equation (42). Figures 24 and 25 show the root loci for systems 5 and 6 respectively. In order to be consistent with the ten second recovery requirement on glide slope control, closed loop system roots should have negative real parts with magnitudes greater than 0.2 radians per second; however, magnitudes in excess of 1.0 radian per second seem unnecessary. Inspection of figures 24 and 25 show that only guidance gain values between 0.2 and 0.6 need be investigated. Figures 26, 27 and 28 show 20 foot low approaches of system 5 with guidance gains of 0.2, 0.25 and 0.3 respectively. Figures 29, 30, 31 and 32 show 20 foot low approaches of system 6 for guidance gains of 0.2, 0.25, 0.30 and 0.35 respectively.

Inspection of figures 26 through 32 show the expected quickening of glide slope recovery with increasing guidance gain k . However, as k is

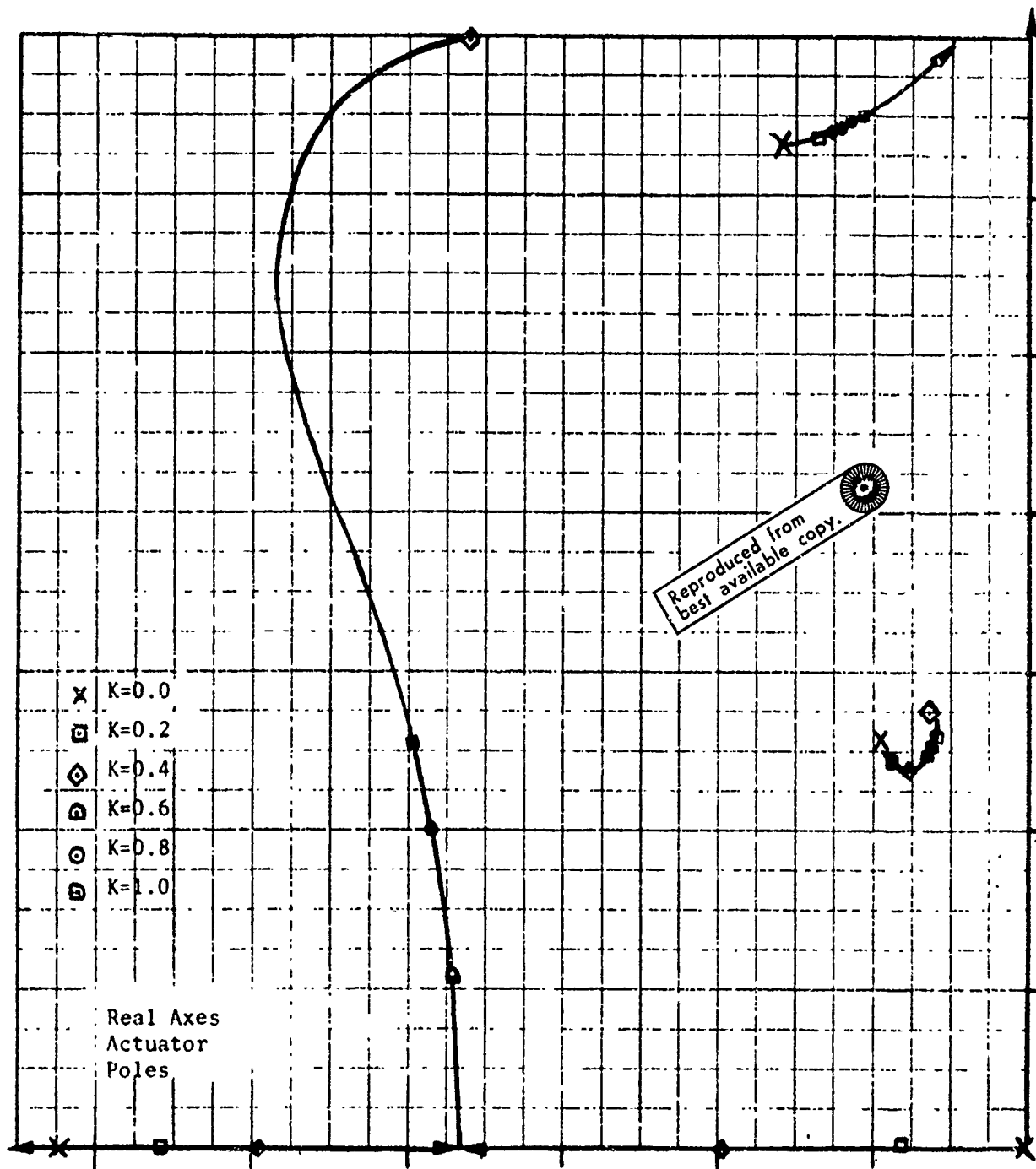


FIGURE 24. SYSTEM 5 GUIDANCE LOOP CLOSURE

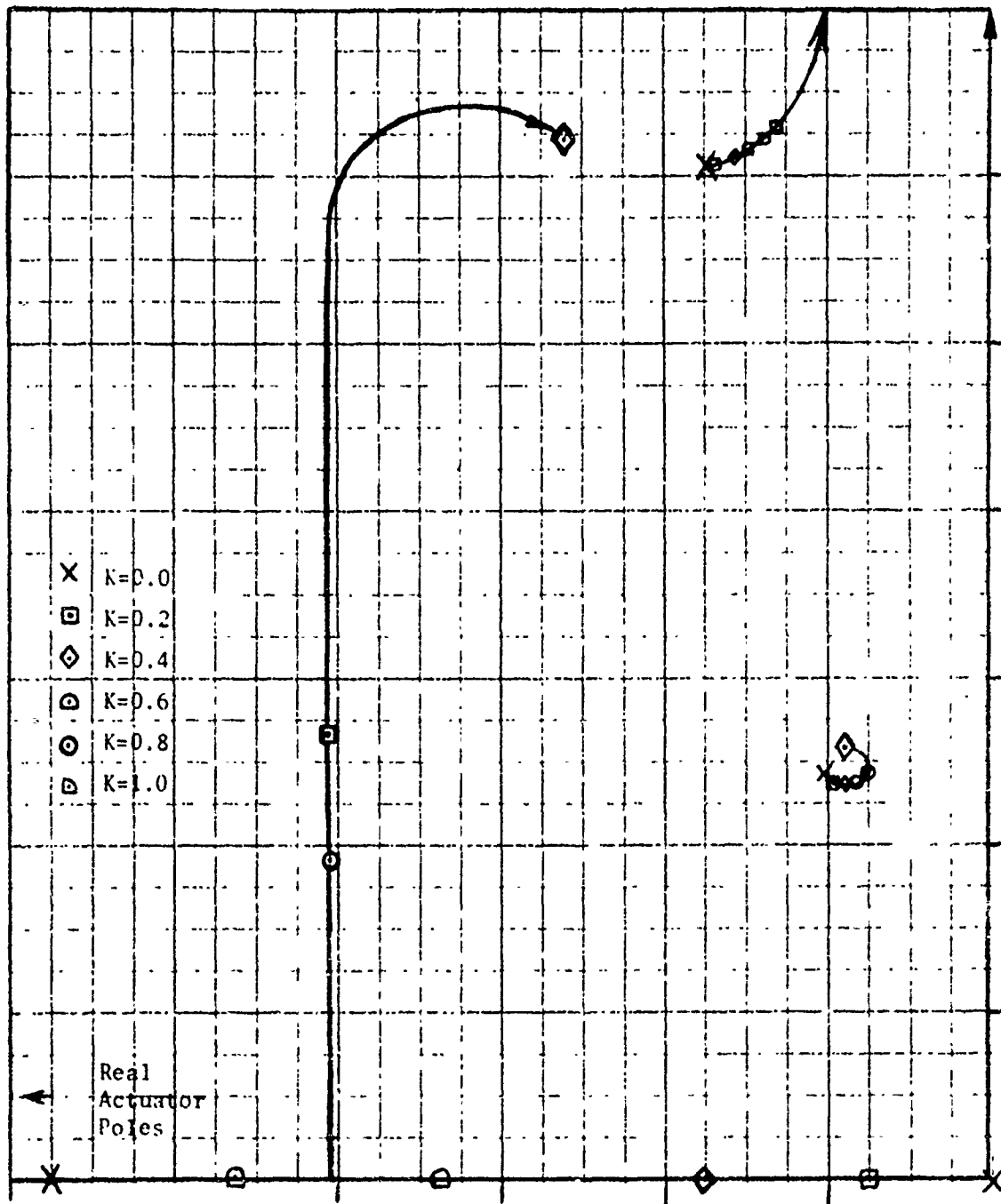
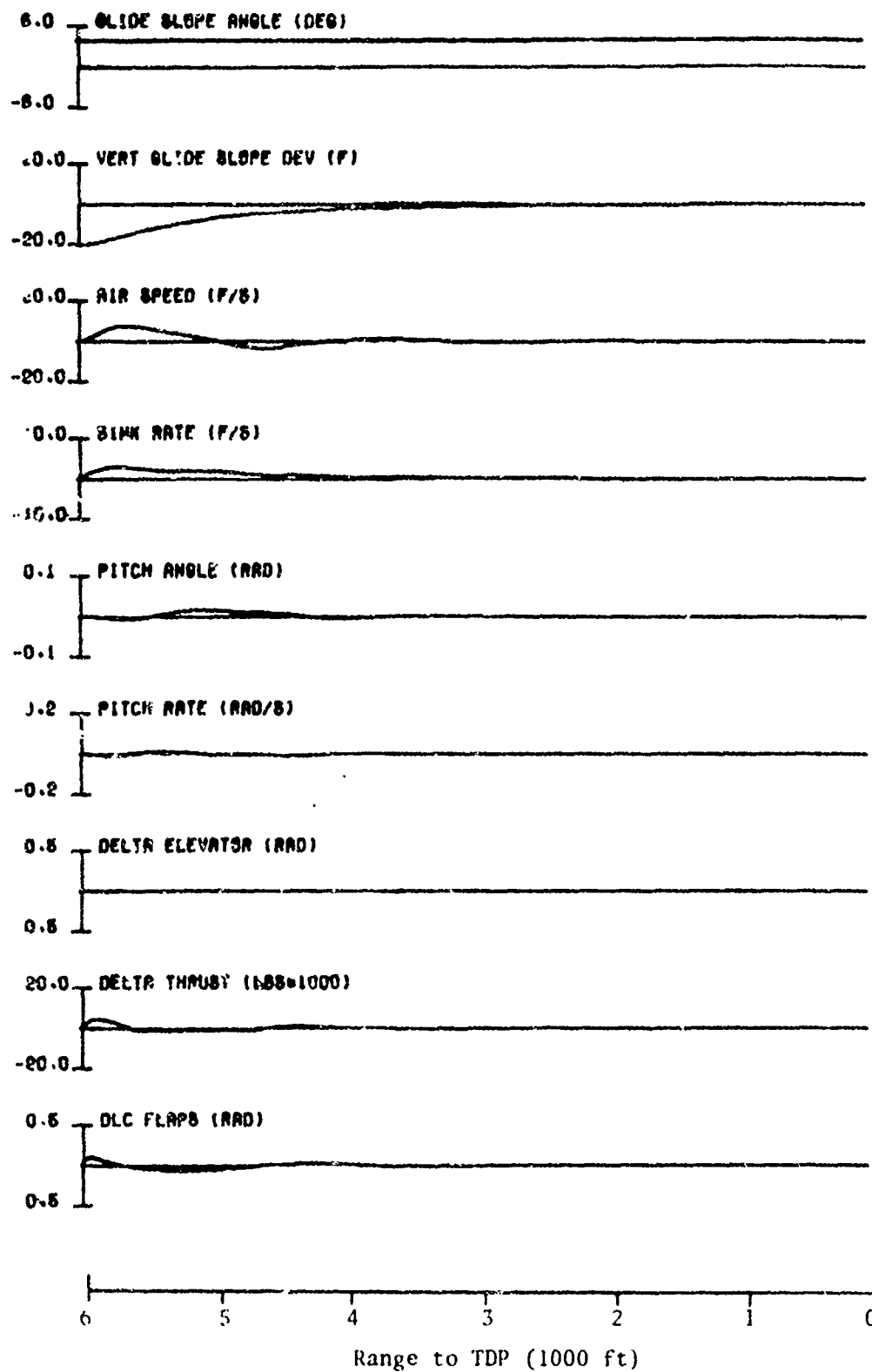
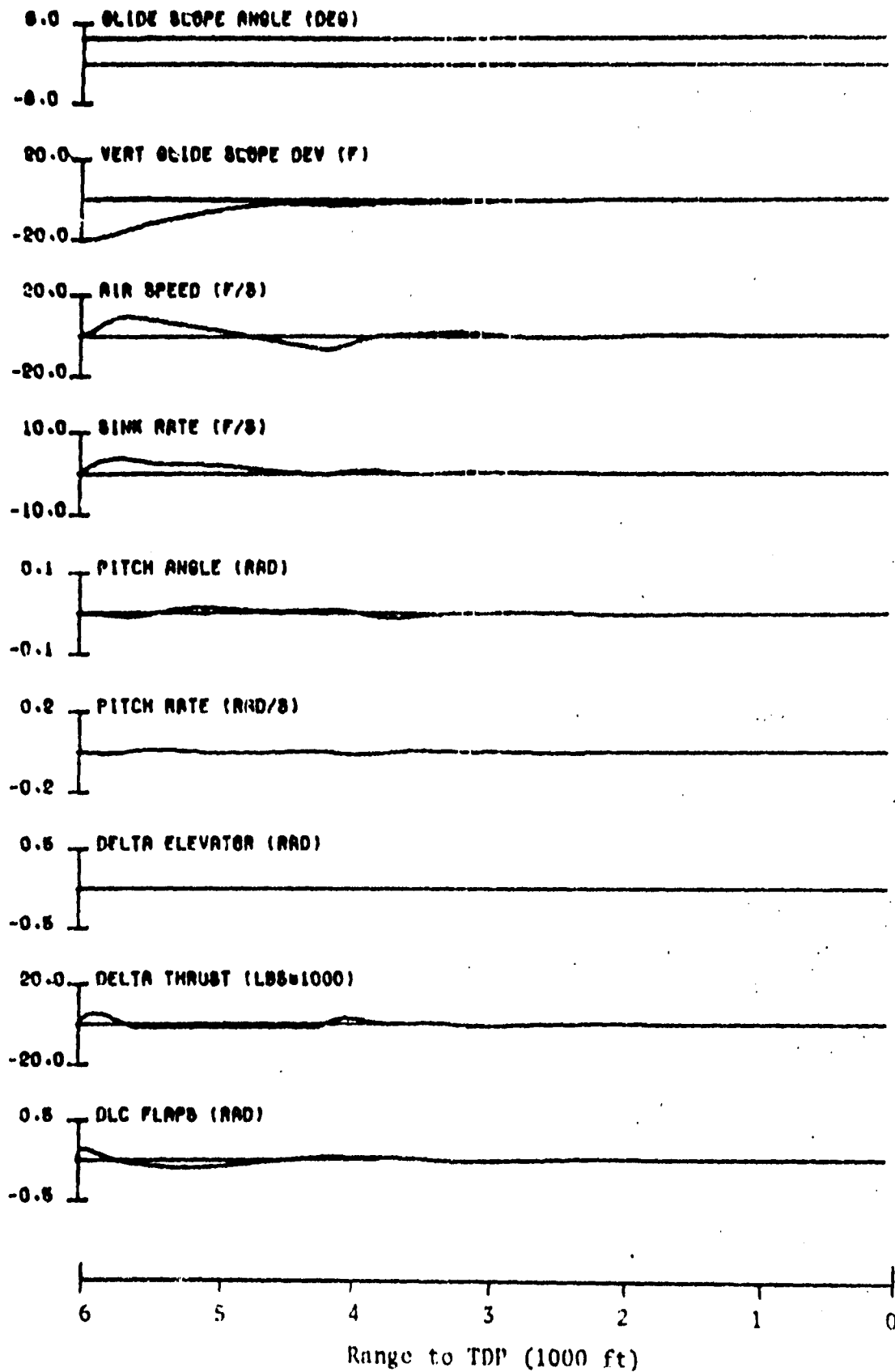
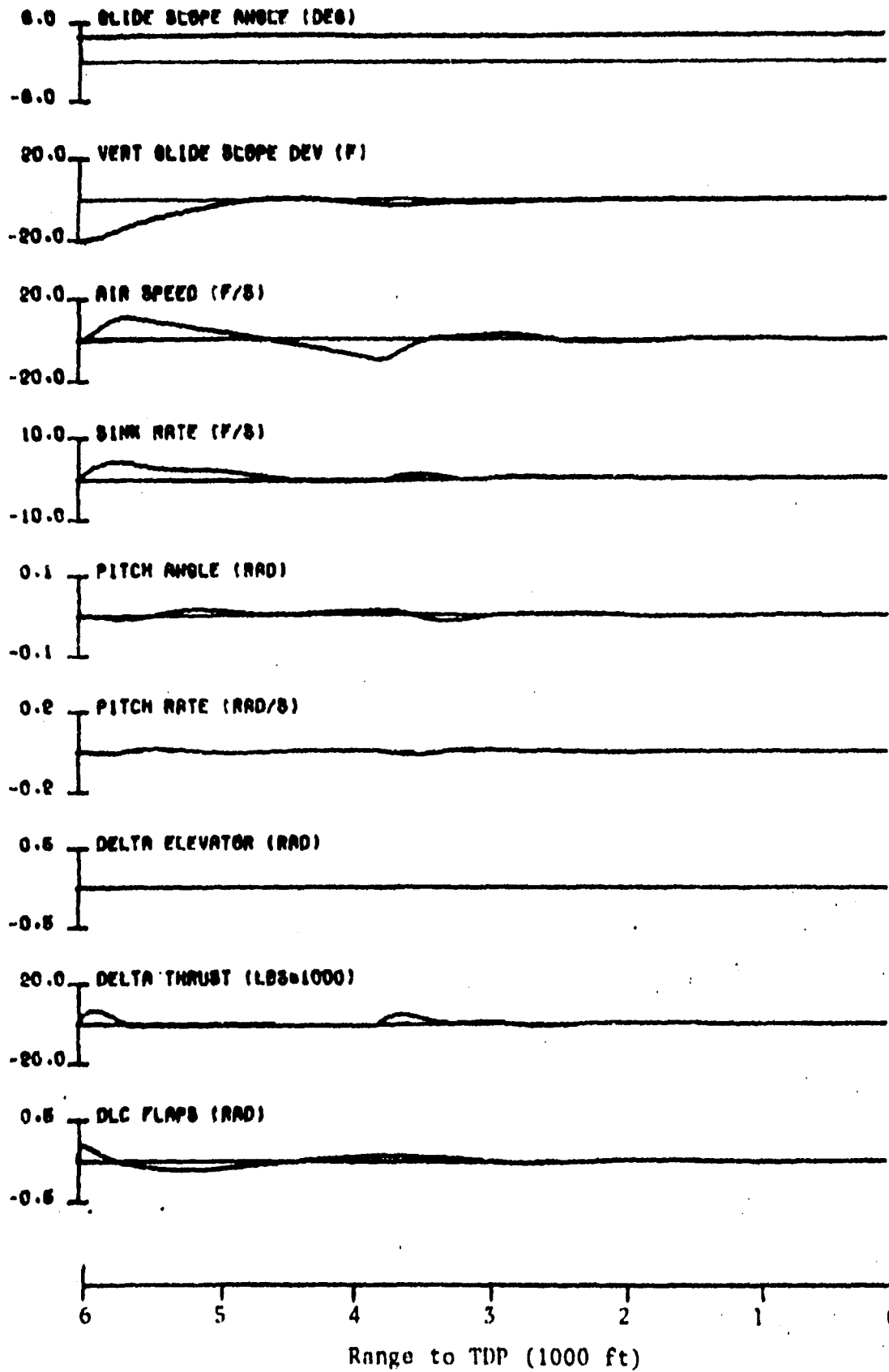


FIGURE 25. SYSTEM 6 GUIDANCE LOOP CLOSURE

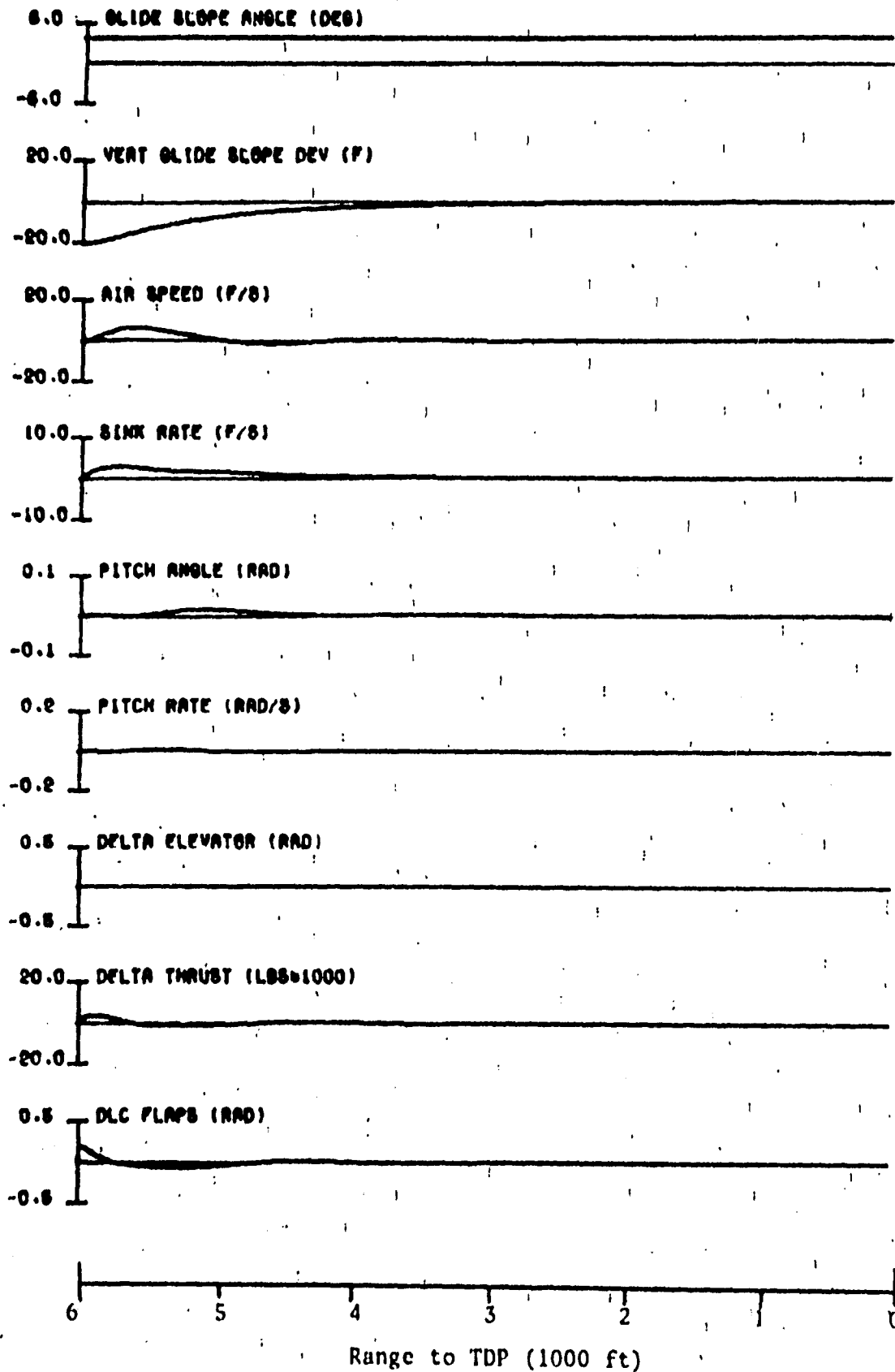


FIGURE(26) SYSTEM 5, ACLS ($K=.20$), 20.0 FEET LOW

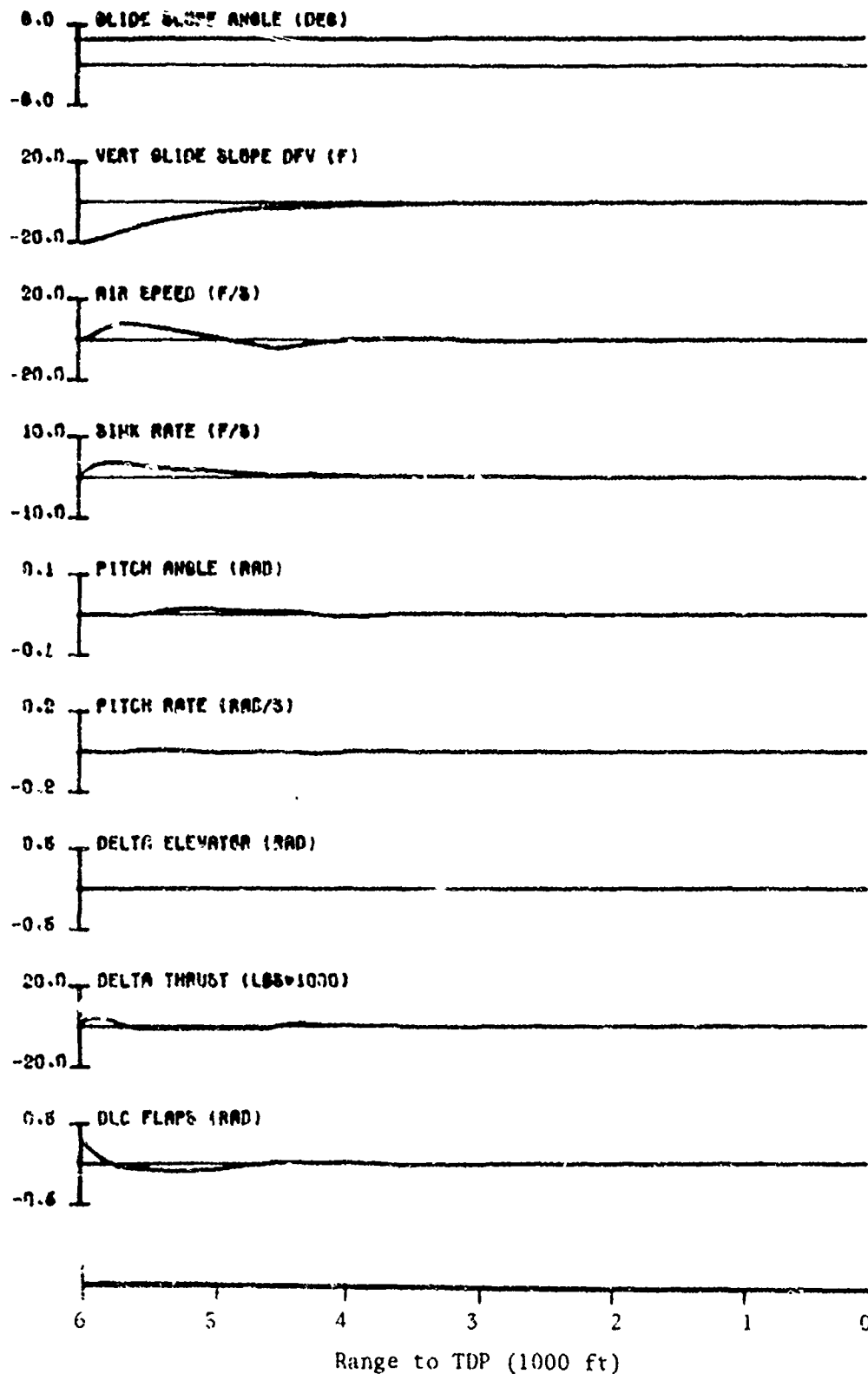
FIGURE(27) SYSTEM 6, ACLS ($K=.26$), 20.0 FEET LOW



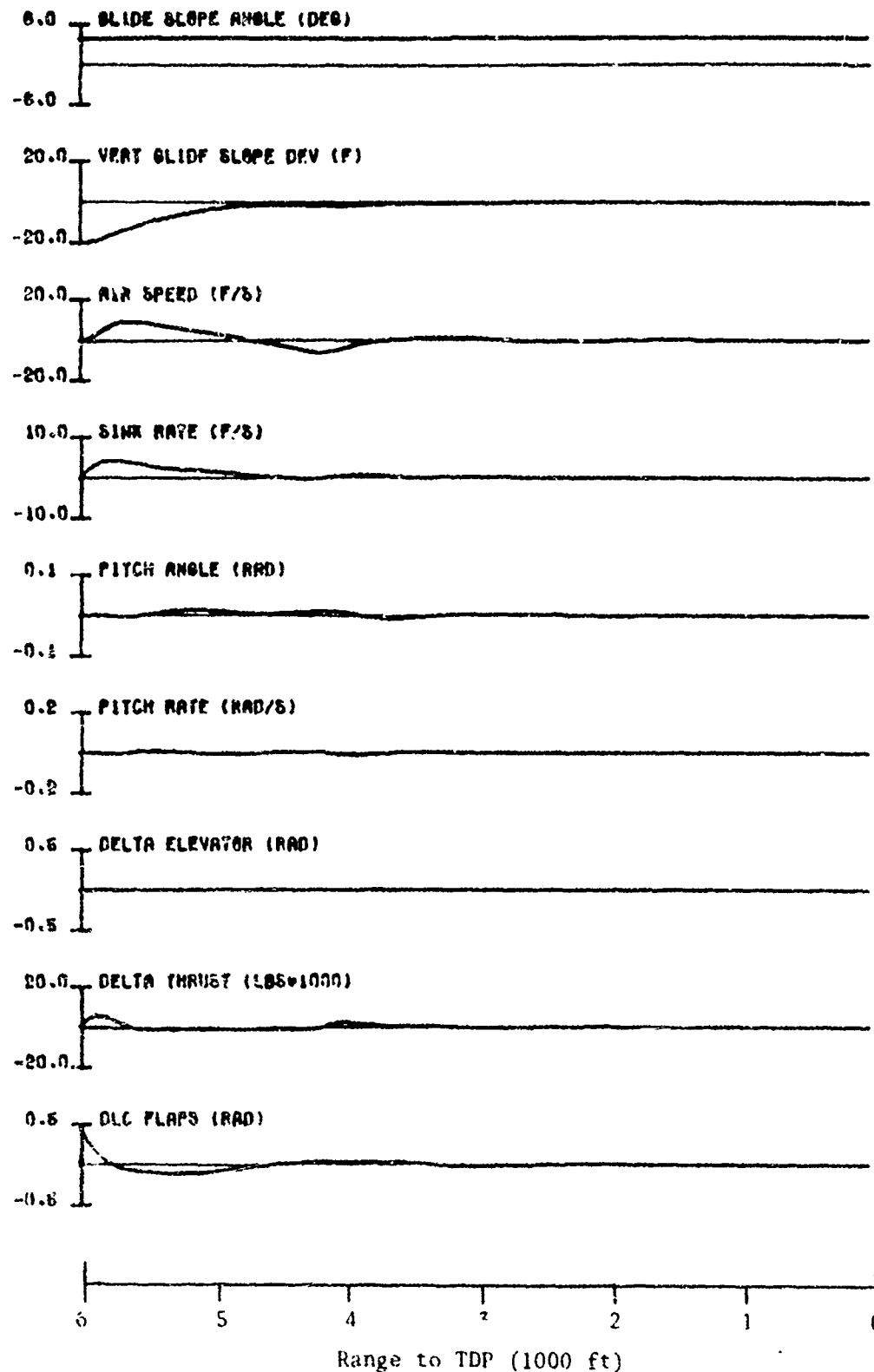
FIGURE(28) SYSTEM 5. ACLS (K=.30), 20.0 FEET LOW

FIGURE(29) SYSTEM 6, ACLS ($K=.20$), 20.0 FEET LOW

NADC-SD-7153



FIGURE(30) SYSTEM 6, ACLS (K=.25), 20.0 FEET LOW

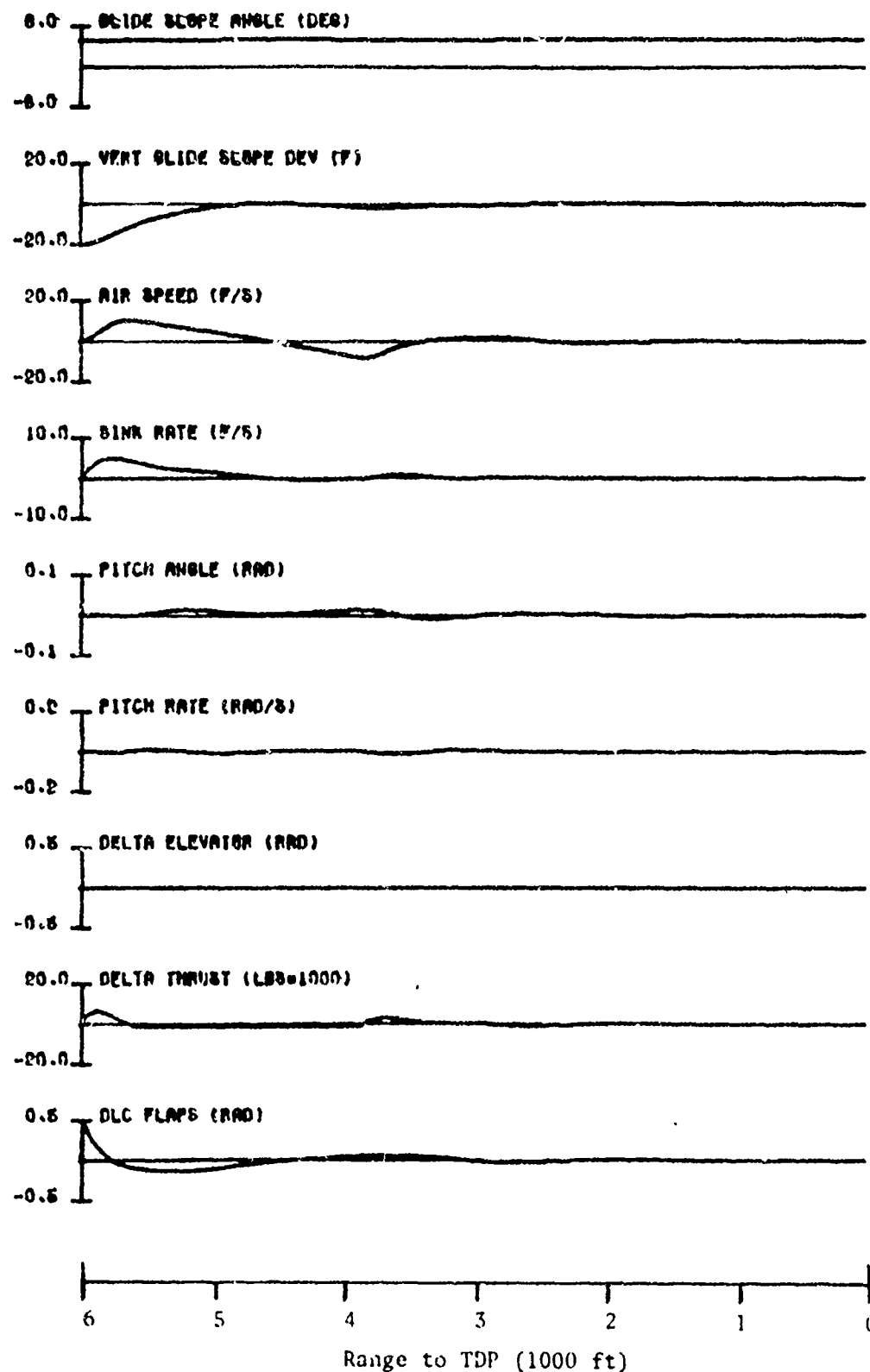


FIGURE(31) SYSTEM 5, ACLS (K=.30). 20.0 FEET LOW

increased, non-linear effects build up and prolong the recovery of airspeed and sink rate. In particular, the large asymmetry in thrust limits combines with the large engine lag effect airspeed response adversely. As k is increased, the system uses the large positive thrust limit to null positional errors quickly. The resulting speed-up takes considerable time to null out when thrust is reduced to its small negative limit. Since the glide slope response time and the airspeed response time trends oppose each other, there must exist a value of k for each system with fastest overall response. Figure 33 shows these trends and the resulting optimum response times. Inspection of figure 33 shows that system 6 responds 1.6 seconds faster than system 5. Though neither system can match the ten second criterion, figures 34 and 35 show that system 6 comes within 0.2 seconds of compliance, and engineering judgment dictates acceptance of this performance. Thus, system 5 was dropped from consideration for failing to provide fast glide slope response, and system 6 was retained.

The ACLS employing system 6 and the optimum guidance gain, $k = 0.24$, was then simulated in a fully automatic carrier approach. Figure 36 shows a carrier approach from a 20 foot initial glide slope error, through the burble to the TDP. For this run, all of the landing requirements were satisfied. The height over the ramp error, ΔH_R , was 3.8 feet and the touchdown height error, ΔH_D , was 2.34 feet. The carrier motion height dispersion σ_h was calculated according to equation (39) to be 0.2 feet, a small number relative to the design criterion.

Thus, the control law represented by the system 6 feedback matrix has been shown to be an effective carrier approach controller, and the AMOAC



FIGURE(32) SYSTEM 6, ACLS ($K=.36$), 20.0 FEET LOW

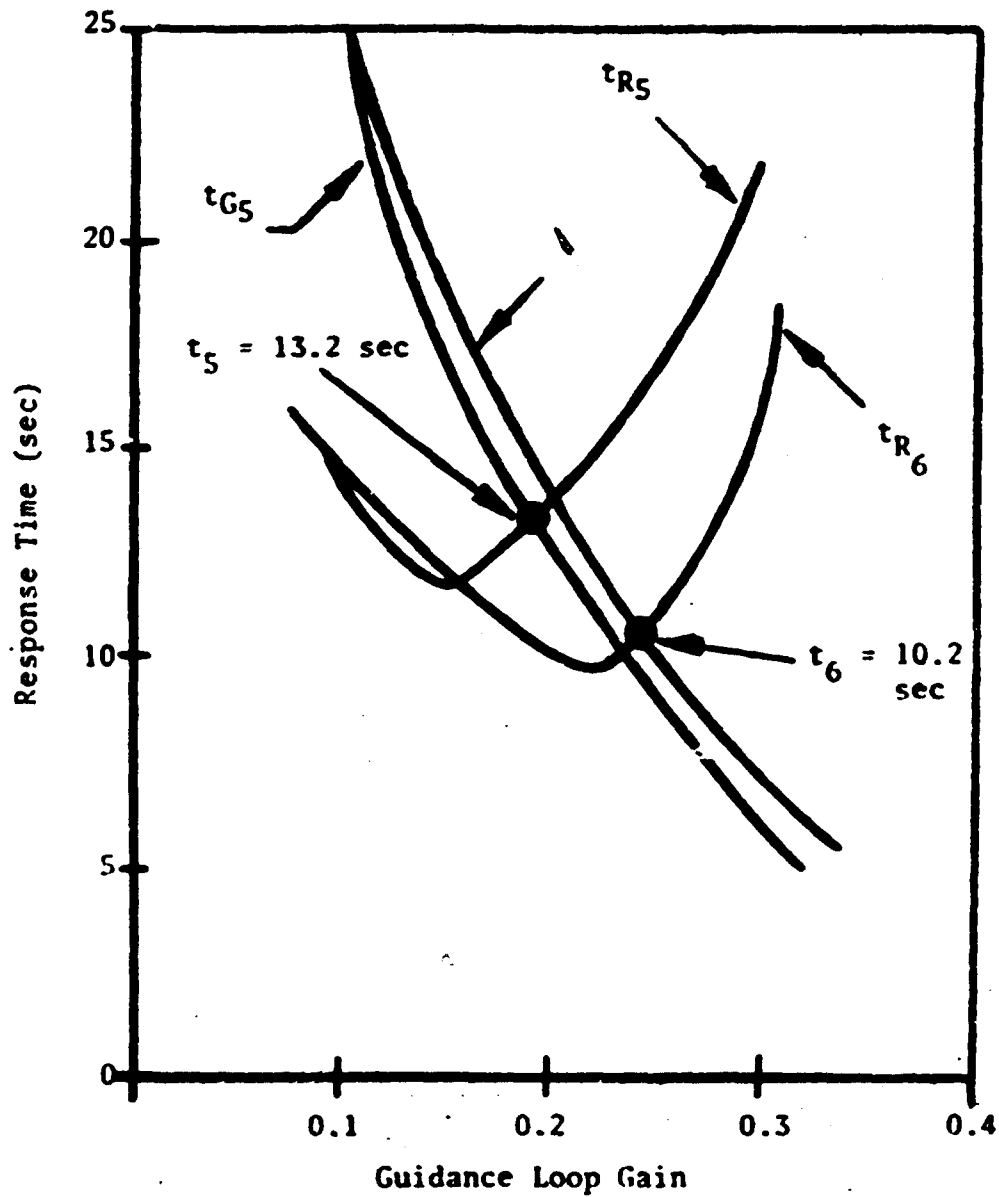
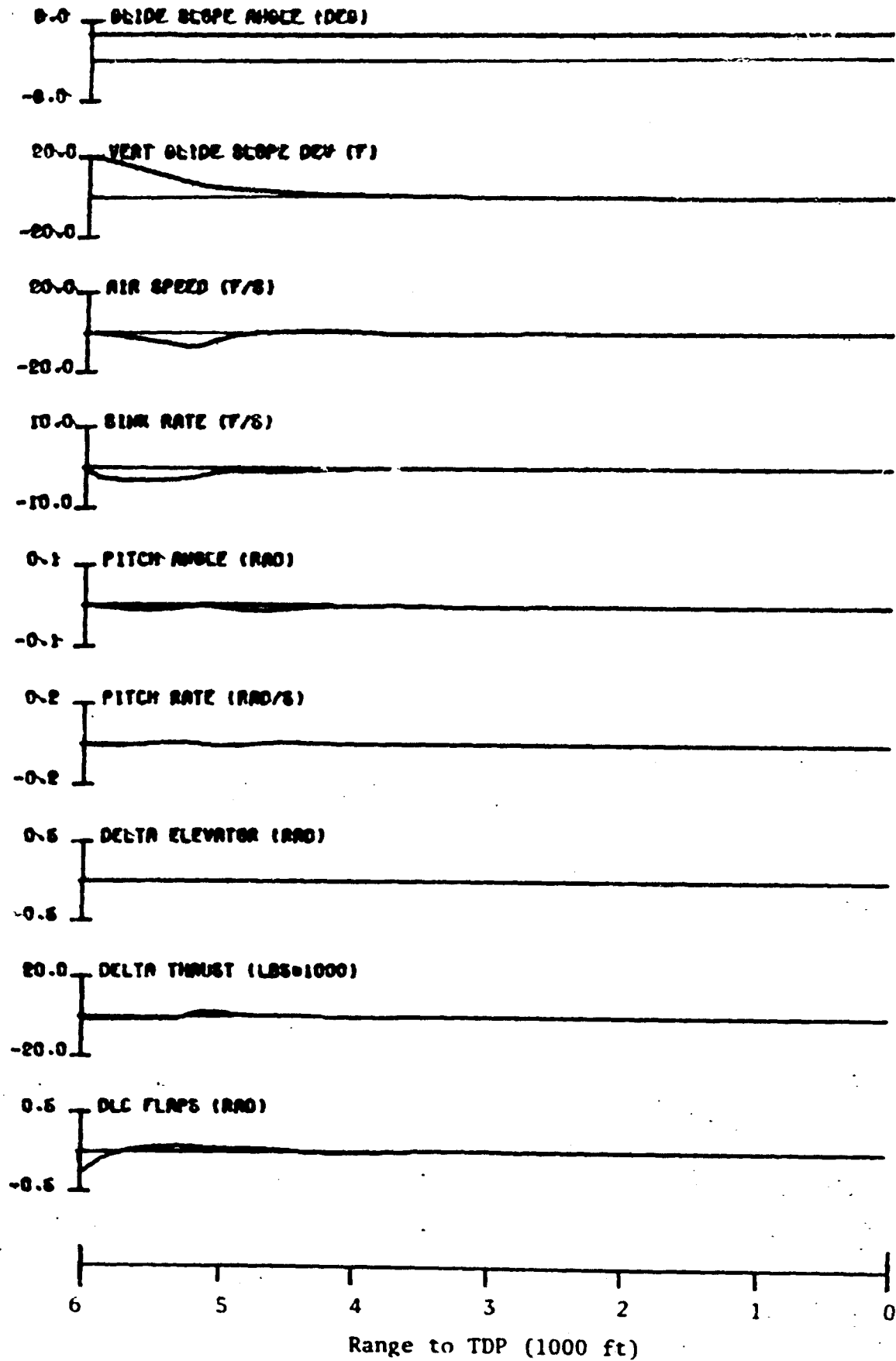
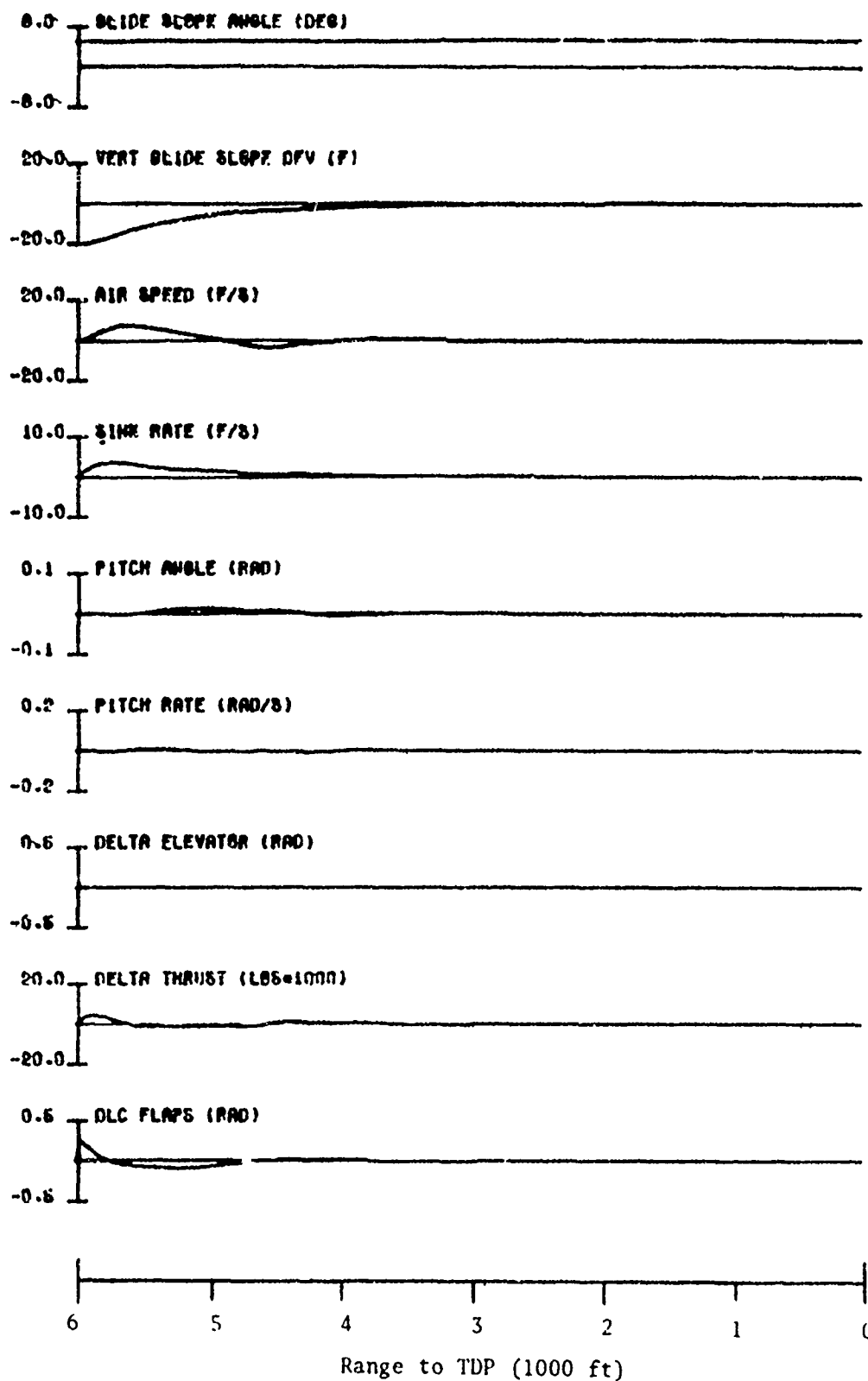


FIGURE 33. RESPONSE TIMES FOR CLOSED LOOP ACLS

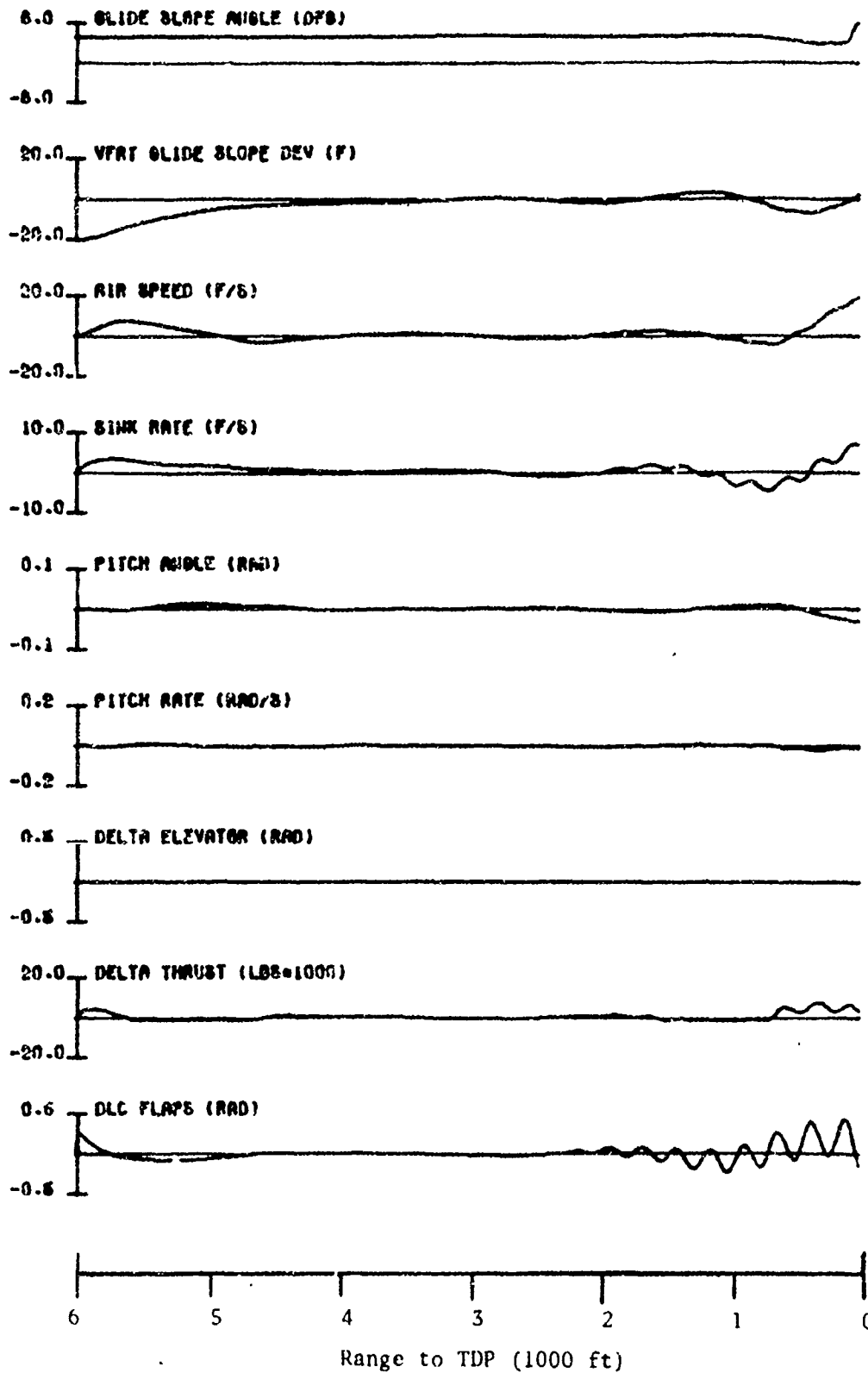


FIGURE(34) SYSTEM 6, ACLS (K=.24), 20.0 FEET HIGH

NADC-Sd-7153



FIGURE(35) SYSTEM 6. ACLS (K=.24), 20.0 FEET LOW

FIGURE(36) SYSTEM 6, ACLS ($K=.24$), LOW APPROACH

NADC-SD-7153

design procedure demonstrated as a valuable automatic flight control tool.

PART IV
CONCLUSIONS

The feasibility of the AMOAC design procedure has been demonstrated by its application to the control of the longitudinal axis of the F-8C fighter aircraft.

The blending of optimal control theory and modern state variable analysis techniques have allowed the synthesis of a complex twelve parameter feedback control system, with the ease and simplicity of a four parameter design technique. The iterative nature of the design logic was shown to converge rapidly in the F-8C application. After the original use of the root square locus this design tool was used only once in updating the design parameters. In spite of the implicit assumption of system linearity, the AMOAC design procedure was successful in treating the nonlinearities of the F-8C airframe and propulsion. The resulting glide slope control is very precise. Variations of aircraft position from the nominal glide slope is held to a tight tolerance in the presence of severe carrier burble. The AMOAC control system has demonstrated its ability to correct a 20 foot vertical glide slope error in under eleven seconds. In addition, this system responds well to carrier deck motions. The use of an AMOAC system in actual carrier approaches should yield a substantial improvement to present automatic carrier landing capability. The results of Appendix I show that similar closed loop dynamics can be expected for other carrier based, high performance aircraft. In particular, it is felt that the AMOAC design procedure has potential for rapid and straightforward application to the A-5A and the F-4 aircraft.

The results indicate that the following areas should be investigated in greater depth. These areas are: determining the effects of carrier-deck motion prediction, determining the effects of deleting the less important feedback gains and the applying an AMOAC type design procedure to the lateral-directional mode of a powered approach.

PART V

Literature Cited

- (a) Abrams, C. R., *Multiple Loop Control of the F-8C During a Power Approach*, Naval Air Development Center, Report No. NADC-AM-6743, 21 December 1967.
- (b) Rynski, E. G., et al., *The Theory and Application of Linear Optical Control*, Cornell Aeronautical Laboratory, Inc., Report No. IH-1943-F-1, October 1965.
- (c) Potter, J. E., *Matrix Quadratic Solutions*, SIAM Journal on Applied Mathematics, Vol. 14, May 1966.
- (d) Powell, F. D., et al., *Study of an Automatic Carrier Landing Environment with the AN/SPN-10 Landing Control Central*, Bell Aerosystems Company, Report No. 6026-932001, April 1965.
- (e) Durand, T. S., *Carrier Landing Analyses*, Systems Technology, Inc., Report No. 137-2, February 1967.

PART VI

Bibliography

- (1) Athans, M., et al, *Optimal Control*, McGraw-Hill Book Company, New York, 1966.
- (2) Davenport, W., et al, *Random Signals and Noise*, McGraw-Hill Book Company, New York, 1958.
- (3) DeRusso, P., et al, *State Variables for Engineers*, John Wiley and Sons, Inc., New York, 1965.
- (4) Dorf, R. C., *Modern Control Systems*, Addison-Wesley Publishing Company, Massachusetts, 1967.
- (5) Eney, J., *Comparative Flight Evaluation of Longitudinal Handling Qualities in Carrier Approach*, Princeton University Department of Aerospace and Mechanical Sciences, Report No. 777, May 1966.
- (6) Etkin, B., *Dynamics of Flight*, John Wiley and Sons, Inc., New York, 1959.
- (7) Hamming, R. W., *Numerical Methods for Scientists and Engineers*, McGraw-Hill Book Company, New York, 1962.
- (8) Schultz, D., et al, *State Functions and Linear Control Systems*, McGraw-Hill Book Company, New York, 1967.

APPENDIX A
AERODYNAMIC PARAMETERS

A Definition of Dimensional Derivatives

$$X_u = - \frac{\rho S_w q}{m V_o} (C_D + C_{D_u}) \quad 1/\text{sec}$$

$$X_w = \frac{S_w q}{m V_o} (C_L - C_{D_\alpha}) \quad 1/\text{sec}$$

$$X_\alpha = V_o X_w \quad \text{ft/sec}^2$$

$$X_{\delta_E} = - \frac{S_w q}{m} C_{D_{\delta_E}} \quad \text{ft/sec}^2$$

$$X_{\delta_F} = - \frac{S_w q}{m} C_{D_{\delta_F}} \quad \text{ft/sec}^2$$

$$X_{\delta_T} = \frac{\cos(i_w + \xi)}{m} \quad \frac{\text{ft/sec}^2}{\text{lb}}$$

$$Z_u = \frac{\rho S_w q}{m V_o} (C_L + C_{L_u}) \quad 1/\text{sec}$$

$$Z_w = \frac{S_w q}{m V_o} (C_D + C_{L_\alpha}) \quad 1/\text{sec}$$

$$Z_{\delta_E} = \frac{S_w q}{m} C_{L_{\delta_E}} \quad \text{ft/sec}^2$$

$$Z_{\delta_F} = \frac{S_w q}{m} C_{L_{\delta_F}} \quad \text{ft/sec}^2$$

$z_{\delta T}$	$= - \frac{\sin(i_w + \xi)}{m}$	$\frac{\text{ft/sec}^2}{\text{lb}}$
M_u	$= \frac{2S_w \bar{c} q}{I_y V_o} (C_m + C_{m_u})$	$\frac{\text{rad/sec}^2}{\text{ft/sec}}$
M_w	$= \frac{S_w \bar{c} q}{I_y V_o} C_{m_\alpha}$	$\frac{\text{rad/sec}^2}{\text{ft/sec}}$
$M_{\dot{\alpha}}$	$= V_o M_w$	$1/\text{sec}^2$
$M_{\dot{w}}$	$= \frac{S_w \bar{c}^2 q}{2I_y V_o^2} C_{m_\alpha}$	$\frac{\text{rad/sec}^2}{\text{ft/sec}}$
$M_{\dot{\alpha}}$	$= V_o M_{\dot{w}}$	$1/\text{sec}$
M_q	$= \frac{S_w \bar{c}^2 q}{2I_y V_o} C_{m_q}$	$1/\text{sec}$
$M_{\delta E}$	$= \frac{S_w c q}{I_y} C_{m_{\delta E}}$	$1/\text{sec}^2$
$M_{\delta F}$	$= \frac{S_w \bar{c} q}{I_y} C_{m_{\delta F}}$	$1/\text{sec}^2$
$M_{\delta T}$	$= \frac{l z}{I_y}$	$\frac{\text{rad/sec}^2}{\text{lb}}$
q	$= 1/2 \rho V_o^2$	lb/ft^2

B. Aerodynamics of Power Approach (F-8C)

Physical Constants

$$\begin{aligned}
 W &= 20,000 \text{ lbs} \\
 I_y &= 90,000 \text{ slug-ft}^2 \\
 S_w &= 375 \text{ ft}^2 \\
 \bar{c} &= 11.78 \text{ ft} \\
 i_w &= 7.0 \text{ deg} \\
 \xi &= 0.85 \text{ deg} \\
 l_z &= -0.424 \text{ ft}
 \end{aligned}$$

Initial Conditions

$$\begin{aligned}
 V_o &= 134 \text{ knots} = 226 \text{ ft/sec} \\
 \gamma_o &= -4 \text{ deg} \\
 \alpha_o &= \alpha_w = 13.6 \text{ deg} \\
 \alpha_{fus} &= \alpha_w - i_w = 6.6 \text{ deg} \\
 \theta_o &= \alpha_o + \gamma_o = 9.6 \text{ deg} \\
 \delta E_o &= -7 \text{ deg} \\
 \delta F_o &= -15 \text{ deg} \\
 T_o &= 2494 \text{ lbs @ 80\% rpm}
 \end{aligned}$$

C. Dimensional Derivatives for F-8C

For $q = 60.7 \text{ lbs/ft.}$, and c.g. = 27 percent of \bar{c} .

$$\begin{aligned}
 X_u &= -0.0506 \\
 X_w &= -0.0072 \\
 X_\alpha &= 1.63 \\
 X_{\delta E} &= -0.672 \\
 X_{\delta F} &= -6.72
 \end{aligned}$$

NADC-SD-7153

$X_{\delta T}$	=	0.001595
Z_u	=	0.264
Z_w	=	-0.554
$Z_{\delta E}$	=	-19.95
$Z_{\delta F}$	=	-18.9
$Z_{\delta T}$	=	-0.0002194
M_α	=	1.074
M_w	=	-0.000189
M_α	=	-0.043
M_q	=	-0.347
$M_{\delta E}$	=	-2.20
$M_{\delta F}$	=	0
$M_{\delta T}$	+	-4.71×10^{-6}

D. Approach Parameters for Various High Performance Aircraft

Physical Constants

<u>Airplane</u>	<u>F-4B</u>	<u>A-5A</u>	<u>F-111B</u>
I (lbs)	34,000	38,500	57,800
ly (slug-ft)	111,273	252,512	312,000
S_w (ft ²)	530	700	550
\bar{c} (ft)	16.04	15.2	8.8
i_w (deg)	1.0	0	1.0
ζ (deg)	4.25	1.24	1.20
l_z (ft)	-0.364	0.08	0.71
c.g (MAC)	30.0	30.6	35.5
V^* (ft/sec)	226	223	200

Dimensional Derivatives

<u>Airplane</u>	<u>F-4B</u>	<u>A-5A</u>	<u>F-111B</u>
X_u	-0.094	-0.0544	-0.0456
X_α	4.94	12.57	16.45
$X_{\delta T}$	9.43×10^{-4}	8.36×10^{-4}	5.57×10^{-4}
$X_{\delta F}$	N.A.	-5.16	-4.93
Z_u	-0.305	-0.274	-0.309
Z_α	-83.6	-146.7	-99.8
$Z_{\delta T}$	-8.67×10^{-5}	-1.82×10^{-5}	-1.89×10^{-5}
$Z_{\delta F}$	N.A.	-26.75	-32.25
M_u	1.8×10^{-4}	-8.0×10^{-5}	-2.05×10^{-4}
M_α	-1.298	-0.88	-0.08
M_W	-3.49×10^{-4}	-4.62×10^{-4}	-4.28×10^{-4}
M_α	-0.0789	-0.103	-0.0856
M_q	-0.433	-0.288	-0.436
$M_{\delta T}$	-3.27×10^{-6}	$+3.7 \times 10^{-8}$	2.26×10^{-6}

NOTE: N.A. means Not Applicable

APPENDIX B

OPTIMAL CONTROL EQUATIONS

A. Euler Equations

For a given set of differential constraints of the form

$$\dot{\underline{x}} = \underline{f}(\underline{x}, \underline{u}) \quad \underline{x}(0) = \underline{c} \quad (\text{B-1})$$

and a convex functional, $J(\underline{x}, \underline{u})$, of the form

$$J(\underline{x}, \underline{u}) = \int_0^\infty L(\underline{x}, \underline{u}) dt \quad (\text{B-2})$$

it is desired to find vector functions $\underline{u}^*(t)$ and $\underline{x}^*(t)$ that simultaneously satisfy equation (B-1) and minimize $J(\underline{x}, \underline{u})$. For this development, the constraint equation (B-1) becomes the open loop, longitudinal airframe equation evaluated along the nominal approach glide path. The vector \underline{x} is expressed in the airplane's stability axis coordinates, see figure (1).

The functional $J(\underline{x}, \underline{u})$, is the performance index defined by equation (4).

$$\dot{\underline{x}} = \underline{A}\underline{x} + \underline{B}\underline{\delta} \quad \underline{x}(0) = \underline{c} \quad (\text{B-3a})$$

$$J = 1/2 \int_0^\infty [\underline{x}^T \underline{K} \underline{x} + \underline{\delta}^T \underline{D} \underline{\delta}] dt \quad (\text{B-3b})$$

A new set of functions, $\underline{p}(t)$ are introduced to adjoin the constraint equation to the performance index.

$$J' = 1/2 \int_0^\infty [\underline{x}^T \underline{K} \underline{x} + \underline{\delta}^T \underline{D} \underline{\delta} - 2\underline{p}^T (\dot{\underline{x}} - \underline{A}\underline{x} - \underline{B}\underline{\delta})] dt \quad (\text{B-4})$$

It should be noted that when \underline{x} and $\underline{\delta}$ satisfy (B-3a), $J' = J$ regardless of \underline{p} . The calculus of variations states that a necessary condition for J to take on a minimum value is that the first order difference of $J(\underline{x}^*, \underline{\delta}^*) - J(\underline{x}, \underline{\delta})$ be zero

$$\begin{aligned} \Delta J &= J(\underline{x}^*, \underline{\delta}^*) - J(\underline{x}, \underline{\delta}) \\ &= 1/2 \int_0^\infty [\underline{x}^{*T} \underline{K} \underline{x}^* - \underline{x}^T \underline{K} \underline{x} + \underline{\delta}^{*T} \underline{D} \underline{\delta}^* - \underline{\delta}^T \underline{D} \underline{\delta} + \\ &\quad - 2\underline{p}^T (\dot{\underline{x}}^* - \dot{\underline{x}} - \underline{A}\underline{x}^* + \underline{A}\underline{x} - \underline{B}\underline{\delta}^* + \underline{B}\underline{\delta})] dt \end{aligned} \quad (\text{B-5})$$

Using Taylor's theorem

$$\begin{aligned}\underline{x}^{*T} \underline{K} \underline{x}^* - \underline{x}^T \underline{K} \underline{x} &= (2\underline{K} \underline{x}^*)^T (\underline{x}^* - \underline{x}) + \text{higher order terms} \\ &= (2\underline{K} \underline{x}^*)^T \underline{\Delta x} + O(|\underline{\Delta x}|^2)\end{aligned}$$

Similarly

$$\underline{\delta}^{*T} \underline{D} \underline{\delta}^* - \underline{\delta}^T \underline{D} \underline{\delta} = (2\underline{D} \underline{\delta}^*)^T \underline{\Delta \delta} + O(|\underline{\Delta \delta}|^2)$$

Substituting into equation (B-5)

$$\begin{aligned}\Delta J &= \int_0^\infty [(\underline{K} \underline{x}^* + \underline{A}^T \underline{p})^T \underline{\Delta x} + (\underline{D} \underline{\delta}^* + \underline{B}^T \underline{p})^T \underline{\Delta \delta} - \underline{p}^T \underline{\Delta x}] dt \\ &\quad + \int_0^\infty [O(|\underline{\Delta x}|^2) + O(|\underline{\Delta \delta}|^2)] dt\end{aligned}$$

Using integration by parts

$$\int_0^\infty \underline{p}^T \underline{\Delta \dot{x}} dt = - \int_0^\infty \dot{\underline{p}}^T \underline{\Delta x} dt + \underline{p}^T \underline{\Delta x} \Big|_0^\infty$$

Since there is no perturbation in the initial value of $\underline{x}(t)$, i.e., $\underline{\Delta x}(0) = 0$

equation (B-5) becomes

$$\begin{aligned}\Delta J &= \int_0^\infty [(\underline{K} \underline{x}^* + \underline{A}^T \underline{p} + \dot{\underline{p}})^T \underline{\Delta x} + (\underline{D} \underline{\delta}^* + \underline{B}^T \underline{p})^T \underline{\Delta \delta}] dt \\ &\quad + \underline{p}^T(\infty) \underline{\Delta x}(\infty) + \int_0^\infty [O(|\underline{\Delta x}|^2) + O(|\underline{\Delta \delta}|^2)] dt\end{aligned}\quad (B-6)$$

The relation between $\underline{\Delta x}$ and $\underline{\Delta \delta}$ is

$$\underline{\Delta x} = \underline{A} \underline{\Delta x} + \underline{B} \underline{\Delta \delta} \quad \underline{\Delta x}(0) = 0$$

Since $\underline{\Delta \delta}$ is unconstrained but small in magnitude the resulting $\underline{\Delta x}$

spans the entire \underline{x} region about \underline{x}^* . Thus, the requirement that the first

order difference vanish yields the following necessary conditions on \underline{x}^*

and $\underline{\delta}^*$.

$$\dot{\underline{p}} = -\underline{A}^T \underline{p} - \underline{K} \underline{x}^* \quad \underline{x}(\infty) = 0 \quad (B-7a)$$

$$0 = \underline{D} \underline{\delta}^* + \underline{B}^T \underline{p} \quad (B-7b)$$

$$\underline{x} = \underline{A} \underline{x}^* + \underline{B} \underline{\delta}^* \quad \underline{x}(0) = \underline{c} \quad (B-7c)$$

Equations (B-7a, b and c) are the Euler equations for the optimal system.

B. Riccati Equation and Feedback Gains

The solution of equations (B-7a, b and c) has the form

$$\begin{bmatrix} p & (t) \\ \underline{x}^*(t) \end{bmatrix} = \begin{bmatrix} \phi_{11}(t) & \phi_{12}(t) \\ \phi_{21}(t) & \phi_{22}(t) \end{bmatrix} \begin{bmatrix} p(0) \\ \underline{x}(0) \end{bmatrix} \quad \underline{x}(\infty) = \underline{0}$$

Solving this equation for p in terms of x yields

$$p(t) = - [\phi_{11}(-t) + \Gamma \phi_{21}(-t)]^{-1} [\phi_{12}(-t) + \Gamma \phi_{22}(-t)] \underline{x}^*(t)$$

$$\text{where } \Gamma = \lim_{T \rightarrow \infty} \phi_{21}(-T) \phi_{22}^{-1}(T)$$

Thus

$$p(t) = P(t) \underline{x}^*(t) \quad (B-8)$$

where $P(t)$ is the $n \times n$ Ricatti matrix. Combining equation (B-7c) and equation (B-7b)

$$\dot{p} = -A^T p - K \underline{x}^* \quad (B-9a)$$

$$\underline{x}^* = A \underline{x}^* - B D^{-1} B^T p \quad (B-9b)$$

Combining equations (B-8) and (B-9) gives

$$-\dot{P} \underline{x}^* = (PA + A^T P + K - PBD^{-1} B^T P) \underline{x}^* \quad (B-10)$$

Since equation (B-10) is independent of the initial choice of \underline{x} , the Riccati matrix must satisfy the following equation.

$$-\dot{P} = PA + A^T P + K - PBD^{-1} B^T P \quad (B-11)$$

Equation (B-7b) shows the form of the optimal feedback control law

$$\underline{u}^*(t) = -D^{-1} B^T p = -D^{-1} B^T P(t) \underline{x}(t) \quad (B-12)$$

For this report, the time interval of interest is $0 \leq t \leq \infty$, as such, the optimal control $\underline{\delta}_2^*(t)$ corresponding to a disturbance $\underline{x}(t)$ and the optimal control $\underline{\delta}_2^*(t)$ corresponding to $\underline{x}(t + \alpha)$ are related by $\underline{\delta}_2^*(t) = \underline{\delta}_2^*(t + \alpha)$ (B-13)

This states the feedback control law is time invariant or that the Riccati matrix is a matrix of constants. Thus $P(t) = P$ and the Riccati equation reduces to

$$0 = PA + A^T P + K - PBD^{-1}B^T P \quad (B-14)$$

and

$$\underline{\delta}^*(t) = -D^{-1}B^T P \underline{x} \quad (B-15)$$

APPENDIX C

ROOT SQUARE LOCUS EQUATION

In Appendix B, the differential equations of the optimal system, equations (C-7a, b and c) were derived, and may be written as:

$$\begin{bmatrix} \dot{\underline{x}} \\ 0 \\ \dot{\underline{p}} \end{bmatrix} = \begin{bmatrix} A & B & 0 \\ 0 & D & B^T \\ -K & 0 & -A^T \end{bmatrix} \begin{bmatrix} \underline{x} \\ \underline{\delta} \\ \underline{p} \end{bmatrix} \quad (C-1)$$

This equation completely determines the closed loop roots of the control system and its adjoint. In order to demonstrate the nature of the closed loop roots, it is necessary to solve the characteristic polynomial of equation (C-1). Laplace transforming equation (C-1) yields:

$$\begin{bmatrix} Is - A & -B & 0 \\ 0 & -D & -B^T \\ -K & 0 & -Is - A^T \end{bmatrix} \begin{bmatrix} \underline{x}(s) \\ \underline{\Delta}(s) \\ -\underline{p}(s) \end{bmatrix} = 0 \quad (C-2)$$

whose characteristic polynomial is:

$$\det \begin{bmatrix} Is - A & -B & 0 \\ 0 & -D & -B^T \\ -K & 0 & -Is - A^T \end{bmatrix} = 0 \quad (C-3)$$

This $(2n + m)$ dimensional matrix is divided into nine parts. The first n rows correspond to the airframe; the next m rows to the control vector $\underline{\Delta}(s)$, and the last n rows to the adjoint variables $\underline{p}(s)$. Adding a linear combination of the first n rows to the last n rows does not alter the determinant. Thus equation (C-3) can be simplified to:

$$\det \begin{bmatrix} Is - A & -B & 0 \\ 0 & -D & -B^T \\ 0 & -K[Is - A]^{-1}B & -Is - A^T \end{bmatrix} = 0$$

or

$$\det (Is - A) \det \begin{bmatrix} -D & -B^T \\ -K[Is - A]^{-1}B & -Is - A^T \end{bmatrix} = 0$$

Further simplification yields

$$0 = \det (Is - A) \det \begin{bmatrix} -D & -B^T[-Is - A^T]^{-1}K[Is - A]^{-1}B & 0 \\ -K[Is - A]^{-1}B & -Is - A^T \end{bmatrix}$$

or $\det (Is - A) \det (-Is - A^T) \det (D + B^T[-Is - A^T]^{-1}K[Is - A]^{-1}B) = 0$

The characteristic equation has three factors. The first two factors are the characteristic polynomials of the open loop system and its adjoint and are non-zero for the closed loop system. Thus equation (C-3) becomes:

$$\det [D + ((-Is - A)^{-1}B)^T K (Is - A)^{-1}B] = 0 \quad (C-4)$$

In equation (C-4), the terms $(Is - A)^{-1}B$ have particular significance. Laplace transforming the airframe equation yields:

$$(Is - A) \underline{X}(s) = B \underline{\Delta}(s)$$

$$\text{or} \quad \underline{X}(s) = (Is - A)^{-1}B \underline{\Delta}(s) \quad (C-5)$$

This equation is identical in form with equation (8), the definition of the open loop transfer matrix. Inspection of both equations shows that:

$$M(s) = (Is - A)^{-1}B$$

Substituting this into equation (D-4) yields

$$\det [D + M(-s)^T K M(s)] = 0 \quad (C-6)$$

Equation (C-6) is the basic equation of the root square locus

APPENDIX D

Carrier Approach Simulation Equations

For definitions of position coordinates and axis systems, refer to figure (6).

A. Positional Coordinates

The nominal glide slope is a four degree glide path starting 6000.0 feet behind and 419.4 feet above the touchdown point of a stationary aircraft carrier. The aircraft's closing velocity is 180.0 feet per second

Upper case letters denote nominal glide slope quantities and lower case letters are aircraft centered variables.

$$X = 6000.0 - 180.0t \quad (D-1a)$$

$$Z = 419.4 - 12.58t \quad (D-1b)$$

The aircraft's deviation from the glide slope is

$$\Delta x = \int_0^t u \, dt \quad (D-2a)$$

$$\Delta h = \int_0^t h \, dt \quad (D-2b)$$

Relative to the carrier, the aircraft is positioned as follows:

$$x = X + \Delta x \quad (D-3a)$$

$$h = Z + \Delta h \quad (D-3b)$$

$$R = (x^2 + h^2)^{1/2} \quad (D-3c)$$

$$\Gamma = \tan^{-1} (h/x) \quad (D-3d)$$

B. Aircraft State Variables

The state variables of the aircraft are the same as in Section II A. At each instant of time the starred quantities represent the aircraft variables relative to the aircraft carrier burble.

$$\underline{u}^* = \underline{u} + \underline{Ug}(R) \quad (D-4a)$$

$$\dot{\underline{h}}^* = \dot{\underline{h}} + \underline{Wg}(R) \quad (D-4b)$$

where

$$\underline{Ug} = \begin{cases} -23.0 e^{-R/1154} + 17.5 e^{-R/75} & R \geq 2000 \text{ ft} \\ -23.0 e^{-R/1154} + 17.5 e^{-R/75} + (1.8 - 0.009R) \sin(26.0 - R/41.7) & R < 2000 \text{ ft} \end{cases}$$

$$\underline{Wg} = \begin{cases} -7.0 e^{-R/1154} \cos(R/255) & R \geq 2306 \text{ ft} \\ -7.0 e^{-R/1154} \cos(R/255) + (4.15 - 0.00185R) \sin(26.0 - R/41.7) & R < 2306 \text{ ft} \end{cases}$$

The aircraft's equations of motion are then

$$\dot{\underline{x}} = \underline{A} \underline{x} + \underline{B} \underline{\delta} \quad (D-5)$$

C. Control Law

When the aircraft is not engaged in a closed loop ACLS, the control law is identical to the one in equation (8). Thus:

$$\underline{\delta} = -\underline{H} \underline{x}^* \quad (D-6)$$

is used in the simulation.

When the ACLS mode is used, a quantity proportional to the vertical glide slope error is added to the sink rate feedback term.

$$\dot{\underline{h}}_{fb} = \dot{\underline{h}}^* + k(\underline{h} - 0.069R) \quad (D-7)$$

Thus the ACLS control law is:

$$\underline{\delta} = -\underline{H} \underline{x}_{fb} \quad (D-8)$$

D. Airframe Model

The linearized airframe equation (D-5) is employed only in the initial simulation exercise. Further exercised use a more complicated, nonlinear model. This model includes first order lags for elevator and flap actuators and engine thrust build up, and control authority limiters.

In the following equations, upper case subscripts denote controller command and lower case subscripts denote controller outputs, primed quantities have been subjected to authority limitations

Actuators

$$\begin{bmatrix} \dot{\delta}_e \\ \dot{\delta}_t \\ \dot{\delta}_f \end{bmatrix} = \begin{bmatrix} -12.5 & 0 & 0 \\ 0 & -0.867 & 0 \\ 0 & 0 & -25 \end{bmatrix} \begin{bmatrix} \delta_e \\ \delta_t \\ \delta_f \end{bmatrix} + \begin{bmatrix} 12.5 & 0 & 0 \\ 0 & 0.867 & 0 \\ 0 & 0 & 25 \end{bmatrix} \begin{bmatrix} \delta_E \\ \delta_T \\ \delta_F \end{bmatrix} \quad (D-9)$$

or

$$\dot{\delta}_i = -L \delta_i + L \delta_{i1} \quad (D-10)$$

Limiters

$$\delta_{\lambda} = \begin{bmatrix} \lambda_e() & 0 & 0 \\ 0 & \lambda_t() & 0 \\ 0 & 0 & \lambda_f() \end{bmatrix} \delta_i \quad (D-11)$$

where figure (D-1) illustrates the functional relationship $\lambda_e()$, $\lambda_t()$ and $\lambda_f()$. Thus the entire nonlinear model is represented as:

$$\begin{bmatrix} \dot{x} \\ \dot{\delta}_i \end{bmatrix} = \begin{bmatrix} A & 0 \\ 0 & -L \end{bmatrix} \begin{bmatrix} x \\ \delta_i \end{bmatrix} + \begin{bmatrix} 0 & B \\ L & 0 \end{bmatrix} \begin{bmatrix} \delta_I \\ \delta_{\lambda} \end{bmatrix} \quad (D-12)$$

$$\begin{bmatrix} \delta_I \\ \delta_{\lambda} \end{bmatrix} = \begin{bmatrix} -H & 0 \\ 0 & \Lambda_i() \end{bmatrix} \begin{bmatrix} x \\ \delta_i \end{bmatrix} \quad (D-12)$$

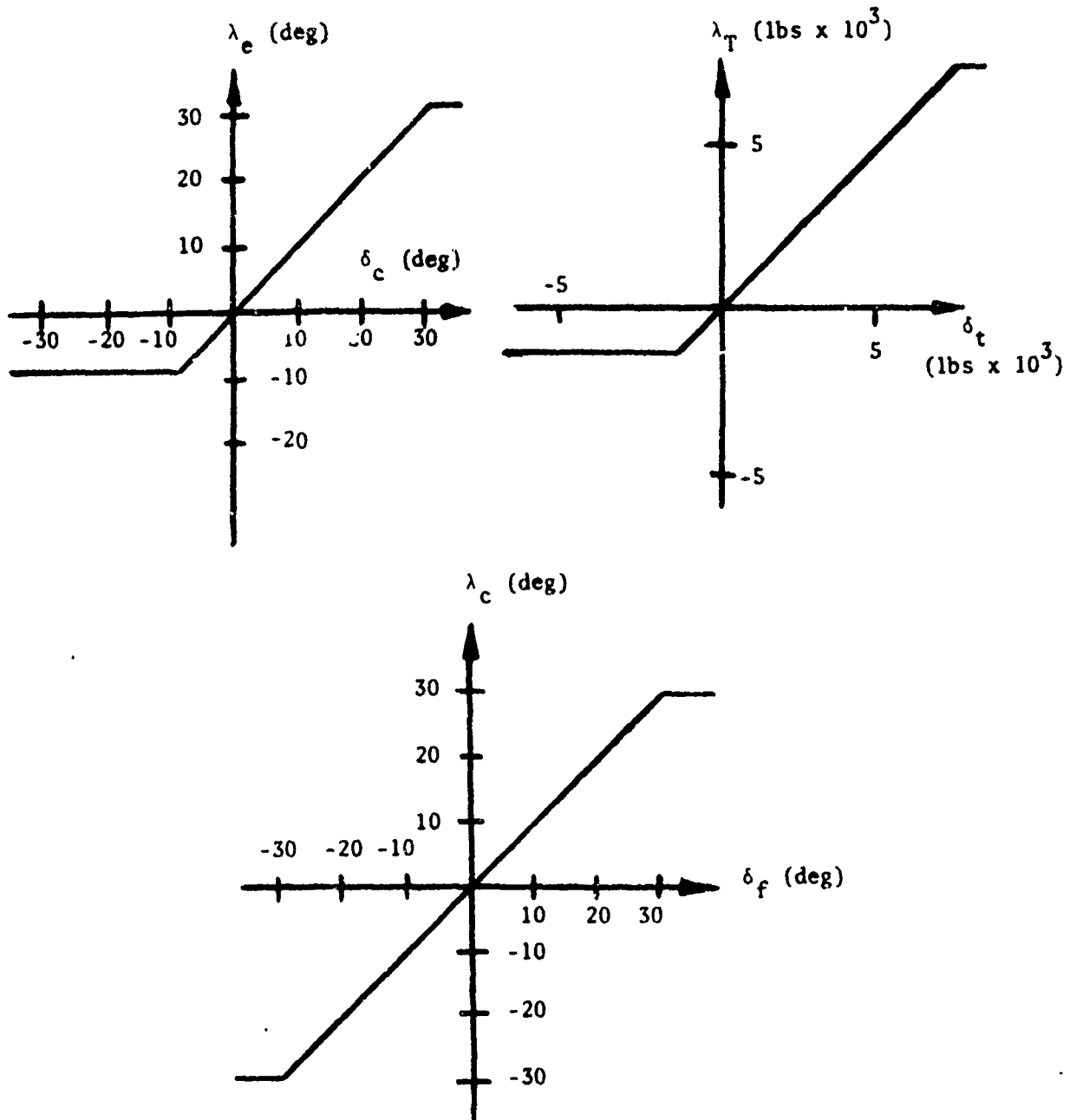


FIGURE 37 . CONTROLLER LIMITATIONS

APPENDIX E

Carrier Motion Dispersion

Appendix B described the system equations of the AMOAC controller used in the ACLS mode. In this appendix a method is derived for computing the carrier motion induced glide slope error. If $\underline{\dot{x}}$ is a vector of the aircraft's state variables plus position variables

$$\underline{\dot{x}} = \text{column } (\dot{x}, \dot{h}, \dot{u}, \dot{h}, \dot{\theta}, \dot{\theta}) \quad (\text{E-1})$$

and $\underline{\dot{x}}_{cm}$ is a vector of the aircraft carrier's motion

$$\underline{\dot{x}}_{cm} = \text{column } (\dot{x}_{cm}, \dot{h}_{cm}, 0, 0, 0, 0) \quad (\text{E-2})$$

and e_i is a unit vector with zeros in all but the i -th position, i.e.

$$e_2 = \text{column } (0, 1, 0, 0, 0, 0) \quad (\text{E-3})$$

Then the desired vertical error term is

$$h_d = h - h_{cm} = e^T (\underline{\dot{x}} - \underline{\dot{x}}_{cm}) \quad (\text{E-4})$$

A good measure of vertical dispersion is the one sigma variable distance

$$\sigma_{hd} = \left[\int_{-\infty}^{\infty} S_{hd}(\omega) d\omega \right]^{\frac{1}{2}} \quad (\text{E-5})$$

where

$$S_{hd}(\omega) = \int_{-\infty}^{\infty} dt \left[\lim_{T \rightarrow \infty} \frac{1}{2T} \int_{-T}^T h_d(t+\tau) h_d(\tau) dt e^{-j\omega\tau} \right] \quad (\text{E-6})$$

is the power spectral density of the glide slope error.

The airframe equations are as follows:

$$\underline{\dot{x}} = \underline{\hat{A}} \underline{\dot{x}} + \underline{\hat{B}} \underline{\dot{\delta}} \quad (\text{E-6})$$

$$\underline{\dot{\delta}} = -\underline{\hat{H}}(\underline{\dot{x}} - \underline{\dot{x}}_{cm}) \quad (\text{E-7})$$

Combining equations (E-6) and (E-7) and Fourier transforming yields

$$\underline{\dot{X}} = (\underline{I}j - \underline{\hat{A}} + \underline{\hat{B}}\underline{\hat{H}})^{-1} \underline{\hat{B}}\underline{\dot{X}}_{cm} \quad (\text{E-8})$$

Laplace transforming equation (E-4) and substituting equation (E-8) yields

$$H_d(\omega) = e_2^T \left[(I\omega - \hat{A} + \hat{B}\hat{H})^{-1} \hat{B}\hat{H} - I \right] \underline{X} \quad (E-9)$$

Upon rearranging

$$H_d(\omega) = e_2^T \Lambda(\omega) \underline{X}(\omega) \quad (E-10)$$

where

$$\Lambda(\omega) = \left[(I\omega I - A + BH)^{-1} (I\omega I - A) \right]$$

Expanding equation (E-10) yields

$$H_d(\omega) = \Lambda_{21}(\omega) X_{cm}(\omega) + \Lambda_{22}(\omega) H_{cm}(\omega) + \Lambda_{23}(\omega) \theta_{cm}(\omega)$$

where

$$\Lambda_{ij}(\omega) = e_i^T \Lambda(\omega) e_j$$

Thus the resulting power spectral density is

$$S_{hd}(\omega) = \left| \Lambda_{21}(\omega) \right|^2 S_{xcm}(\omega) + \left| \Lambda_{22}(\omega) \right|^2 S_{hcm}(\omega) + \left| \Lambda_{23}(\omega) \right|^2 S_{\theta cm}(\omega) + \text{Cross Spectral density terms} \quad (E-12)$$

Since the complete set of cross spectral density functions is not available, their contribution was dropped from equation (E-12), thus yielding:

$$S_{hd} = \left(\int_{-\infty}^{\infty} \left[\left| \Lambda_{21}(\omega) \right|^2 S_{xcm}(\omega) + \left| \Lambda_{22}(\omega) \right|^2 S_{hcm}(\omega) + \left| \Lambda_{23}(\omega) \right|^2 S_{\theta cm}(\omega) \right] d\omega \right)^{\frac{1}{2}} \quad (E-13)$$

All the matrices and functions used in obtaining equation (E-13) are defined in section V of this report.

Appendix F

Guidance Loop Equations

When the AMOAC control system is engaged in an ACLS mode, the system behavior is altered in accordance with the guidance loop. An equation for the closed loop ACLS roots is derived in this section.

The optimal system is characterized by

$$\underline{\dot{x}} = A \underline{x} + B \underline{\delta} \quad (F1a)$$

$$\underline{\delta} = -H \underline{x} \quad (F1b)$$

where

$$\underline{x} = \text{column } (u, h, \dot{h}, 0) \text{ and } \underline{\delta} = \text{column } (\delta_E, \delta_T, \delta_F)$$

The guidance command adds vertical position error to the sink rate feedback.

$$\dot{h}_{fb} = \dot{h} + k h \quad (F-2)$$

laplace transforming equation (F-2) and combining with equation (F1b) yields

$$\underline{u} = H(I + \frac{e_2 e_2^T}{s} \frac{k}{s}) \underline{x} \quad (F-3)$$

where

$$\underline{e}_2 = \text{column } (0, 1, 0, 0).$$

And the closed loop ACLS equation becomes

$$\left[Is - A + BH(I + \frac{e_2 e_2^T}{s} \frac{k}{s}) \right] \underline{x} = 0 \quad (F-4)$$

Upon rearranging equation (F-4)

$$\frac{1}{s} \left[(Is - A + BH)s + kBH e_2 e_2^T \right] \underline{x} = 0 \quad (F-5)$$

Equation (F-5) is obtained which results in the characteristic equation.

$$\det \left[(Is - A + BH)s + kBH \frac{e_2 e_2^T}{s} \right] = 0 \quad (F-6)$$

or

$$\det (Is - A + BH) \det (Is + k(Is - A + BH)^{-1} BH \frac{e_2 e_2^T}{s}) = 0 \quad (F-7)$$

However, the first factor in equation (F-7) is the open loop characteristic equation and equals zero only when k equals zero, thus

$$\det \left[Is + k \left[(Is - A + BH)^{-1} B \right] H e_2 e_2^T \right] = 0 \quad (F-8)$$

The bracketed term in equation (F-8) is the closed loop transfer matrix of equation (12), and consists of the numerator polynomial matrix $(N_{ij}(s))$ divided by the characteristic polynomial of the optimal system.

$$\det \left[Is + k \frac{N(s) H e_2 e_2^T}{\det(Is - A + BH)} \right] = 0 \quad (F-9)$$

However

$$N(s) H e_2 e_2^T = \begin{bmatrix} 0 & \sum_i N_{1i}(s) h_{i2} & 0 & 0 \\ 0 & \sum_i N_{2i}(s) h_{i1} & 0 & 0 \\ 0 & \sum_i N_{3i}(s) h_{i1} & 0 & 0 \\ 0 & \sum_i N_{4i}(s) h_{i2} & 0 & 0 \end{bmatrix}$$

which yields

$$\det \begin{bmatrix} s & \frac{k \sum_i N_{1i}(s) h_{i2}}{\Delta(s)} & 0 & 0 \\ 0 & \frac{k \sum_i N_{2i}(s) h_{i2} + s}{\Delta(s)} & 0 & 0 \\ 0 & \frac{k \sum_i N_{3i}(s) h_{i2}}{\Delta(s)} & s & 0 \\ 0 & \frac{k \sum_i N_{4i}(s) h_{i2}}{\Delta(s)} & 0 & s \end{bmatrix} = 0$$

Reproduced from
best available copy.

F-10

where

$$\Delta(s) = \det (Is - A + BH)$$

or

$$s^2 \Delta(s) + k \sum_i N_{2i}(s) h_{i2} = 0 \quad (F-12)$$

Thus the closed ACLS guidance loop is characterized by

$$0 = s \det(Is - A + BH) + k \sum_{i=1}^u N_{2i}(s) h_{i2} \quad (F-13)$$

Appendix G

Open Loop Transfer MatrixA Definition

$$M(s) = (Is - A)^{-1} \cdot B$$

B Airframe Matrices

$$A = \begin{bmatrix} X_{11} & -X_w & X_\alpha - g \cos \gamma_o & 0 \\ Z_u & Z_w & g \sin \gamma_o - Z_w V_o & 0 \\ 0 & 0 & 0 & 1 \\ M_u + M_w Z_u & -(M_w + M_w Z_w) & M_\alpha + M_w Z_w V_o - g \sin \gamma_o & M_q + M_u \end{bmatrix}$$

$$B = \begin{bmatrix} X_{\delta E} & X_{\delta T} & X_{\delta F} \\ -Z_{\delta E} & -Z_{\delta T} & -Z_{\delta F} \\ 0 & 0 & 0 \\ M_{\delta E} + M_w Z_{\delta E} & M_{\delta T} + M_w Z_{\delta T} & M_{\delta F} + M_w Z_{\delta F} \end{bmatrix}$$

Substituting values from Appendix (A) for the F-8C

$$A = \begin{bmatrix} -0.0506 & 0.0072 & -33.8 & 0 \\ -0.264 & -0.554 & 127.4 & 0 \\ 0 & 0 & 0 & 1.0 \\ -5.83 \times 10^{-4} & 0.00465 & -1.051 & -0.390 \end{bmatrix}$$

$$B = \begin{bmatrix} -0.672 & 0.001595 & -6.72 \\ 19.95 & 2.194 \times 10^{-4} & 18.9 \\ 0 & 0 & 0 \\ -2.196 & -4.67 \times 10^{-6} & 0.0357 \end{bmatrix}$$

C TRANSFER MATRIX ELEMENTS

$$M_{11}(s) = \frac{0.672}{\Delta(s)} (s^3 + 0.730s^2 - 109.5s - 53.9)$$

$$M_{21}(s) = \frac{-19.95}{\Delta(s)} (s^3 + 0.432s^2 - 13.0s + 0.300)$$

$$M_{31}(s) = \frac{2.20}{\Delta(s)} (s^2 + 0.562s + 0.0243)$$

$$M_{41}(s) = \frac{2.20s}{\Delta(s)} (s^2 + 0.562s + 0.0243)$$

$$M_{12}(s) = \frac{-0.0016}{\Delta(s)} (s^3 + 0.945s^2 + 1.37s + 0.021)$$

$$M_{22}(s) = \frac{0.000219}{\Delta(s)} (s^3 + 2.37s^2 - 0.895s + 1.67)$$

$$M_{32}(s) = \frac{4.67 \times 10^{-6}}{\Delta(s)} (s^2 + 0.586s - 0.295)$$

$$M_{42}(s) = \frac{4.67 \times 10^{-6}}{\Delta(s)} s(s^2 + 0.586s - 0.295)$$

$$M_{13}(s) = \frac{6.72}{\Delta(s)} (s^3 + 0.924s^2 + 1.44s - 0.505)$$

$$M_{23}(s) = \frac{-18.9}{\Delta(s)} (s^3 + 0.347s^2 + 1.27s - 0.434)$$

$$M_{33}(s) = \frac{-0.0357}{\Delta(s)} (s^2 + 3.18s - 0.0218)$$

$$M_{43}(s) = \frac{-0.0357}{\Delta(s)} s(s^2 + 3.18s - 0.0218)$$

$$\Delta(s) = s^4 + 0.995s^3 + 1.319s^2 + 0.0329s + 0.0286$$

Appendix H

AMOAC Design DataSystem 0A. Performance Index Parameters

$$b_1 = 1.0 \times 10^{-13}$$

$$b_2 = 1.0 \times 10^{-13}$$

$$k_1 = 4.0 \times 10^{+7}$$

$$k_2 = 1.0 \times 10^{+10}$$

B. Feedback Gains

	Airspeed	Sink Rate	Pitch	Pitch Rate
Elevator	-0.000282	-0.000807	-0.0679	-0.1259
Thrust	1451.0	4977.0	13,590.0	222,600.0
DLC Flap	0.0000199	0.0000876	0.00671	0.00892

C. Numerator Zeros

$\frac{\theta(s)}{\delta_E(s)}$	$N(s) = k_1 (s + 1.408) (s + 2.352)$
$\frac{u(s)}{\delta_T(s)}$	$N(s) = k_2 (s + 0.220) (s + 0.494 \pm 1.091j)^2$
$\frac{\dot{h}(s)}{\delta_T(s)}$	$N(s) = k_3 (s + 2.86) (s - 0.120 \pm 0.66j)^2$
$\frac{\dot{h}(s)}{\delta_F(s)}$	$N(s) = k_4 (s + 1.68) (s + 0.119 \pm 1.403j)^2$

System IA Performance Index Parameters

$$b_1 = 1.0 \times 10^{-13}$$

$$b_2 = 1.0 \times 10^{-12}$$

$$k_1 = 4.0 \times 10^{+7}$$

$$k_2 = 1.0 \times 10^{+10}$$

B Feedback Gains

	Airspeed	Sink Rate	Pitch	Pitch Rate
Elevator	-0.000278	-0.000794	-0.0669	-0.124
Thrust	1433.0	4918.0	9653.0	214,200.0
DLC Flap	0.000196	0.000866	0.0663	0.0877

C. Numerator Zeros

$\frac{\theta(s)}{\delta_E(s)}$	$N(s) = k_1 (s + 1.411) (s + 2.324)$
$\frac{u(s)}{\theta_T(s)}$	$N(s) = k_2 (s + 0.235) (s + 0.493 \pm 1.09j)^2$
$\frac{h(s)}{\delta_T(s)}$	$N(s) = k_3 (s + 2.86) (s - 0.116 + 0.658j)^2$
$\frac{h(s)}{\delta_F(s)}$	$N(s) = k_4 (s + 1.673) (s + 0.127 \pm 1.398j)^2$

System 2A Performance Index Parameters

$$b_1 = 1.0 \times 10^{-1}$$

$$b_2 = 2.0 \times 10^{-1}$$

$$k_1 = 4.0 \times 10^{-7}$$

$$k_2 = 1.0 \times 10^{-10}$$

B Feedback Gains

	Airspeed	Sink Rate	Pitch	Pitch Rate
Elevator	-0.000271	-0.000775	-0.0654	-0.121
Thrust	1410.0	4863.0	7190.0	205.700.0
DLC Flap	0.000382	0.00170	0.130	0.171

C Numerator Zeros

$\frac{\theta(s)}{\delta_E(s)}$	$N(s) = k_1 (s + 1.423) (s + 2.281)$
$\frac{u(s)}{\delta_T(s)}$	$N(s) = k_2 (s + 0.250) (s + 0.491 \pm 1.091j)^2$
$\frac{h(s)}{\delta_F(s)}$	$N(s) = k_3 (s + 2.86) (s - 0.113 \pm 0.655j)^2$
$\frac{h(s)}{\delta_F(s)}$	$N(s) = k_4 (s + 1.66) (s - 0.132 \pm 1.391j)^2$

System 3A. Performance Index Parameters

$$b_1 = 1.0 \times 10^{-13}$$

$$b_2 = 1.0 \times 10^{-11}$$

$$k_1 = 4.0 \times 10^{+7}$$

$$k_2 = 1.0 \times 10^{+10}$$

B. Feedback Gains

	Airspeed	Sink Rate	Pitch	Pitch Rate
Elevator	-0.000228	-0.000649	-0.0560	-0.103
Thrust	1255.0	4510.0	-7316.0	150,600.0
DLC Flap	0.00160	0.00756	0.574	0.724

C. Numerator Zeros

$\frac{\theta(s)}{\delta_E(s)}$	$N(s) = k_1 (S + 1.539) (S + 1.958)$
$\frac{u(s)}{\delta_T(s)}$	$N(s) = k_2 (S + 0.359) (S + 0.480 \pm 1.086j)^2$
$\frac{\dot{h}(s)}{\delta_T(s)}$	$N(s) = k_3 (S + 2.839) (S - 0.089 \pm 0.632j)^2$
$\frac{\dot{h}(s)}{\delta_F(s)}$	$N(s) = k_4 (S + 1.570) (S + 0.169 \pm 1.342j)^2$

System 4A. Performance Index Parameters

$$b_1 = 1.0 \times 10^{-13}$$

$$b_2 = 2.0 \times 10^{-11}$$

$$k_1 = 4.0 \times 10^{+7}$$

$$k_2 = 1.0 \times 10^{+10}$$

B. Feedback Gains

	Airspeed	Sink Rate	Pitch	Pitch Rate
Elevator	-0.0001894	-0.000538	-0.0476	-0.0866
Thrust	1116.0	4209.0	-17,030.0	103.100.0
DLC Flap	0.00267	0.0134	1.007	1.212

C. Numerator Zeros

$\frac{\theta(s)}{\delta_E(s)}$	$N(s) = k_1 (S + 1.664 \pm 0.210j)^2$
$\frac{u(s)}{\delta_T(s)}$	$N(s) = k_2 (S + 0.475) (S + 0.467 \pm 1.080j)^2$
$\frac{h(s)}{\delta_T(s)}$	$N(s) = k_3 (S + 2.818) (S - 0.065 + 0.613j)^2$
$\frac{h(s)}{\delta_F(s)}$	$N(s) = k_4 (S + 1.478) (S + 0.201 \pm 1.294j)^2$

System 5A. Performance Index Parameters

$$b_1 = 1.0 \times 10^{-13}$$

$$k_1 = 4.0 \times 10^{+7}$$

$$b_1 = 1.0 \times 10^{-10}$$

$$k_1 = 1.0 \times 10^{+10}$$

B Feedback Gains

	Air Speed	Sink Rate	Pitch	Pitch Rate
Elevator	-0.0000803	-0.000215	-0.0221	-0.0399
Thrust	688.6	3378.0	-17,090.0	-22,900.0
DLC Flap	0.00577	0.0406	2.708	2.617

C. Numerator Zeros

$\frac{\theta(s)}{\delta_E(s)}$	$N(s) = k_1 (S + 1.365) (S + 1.635)$
$\frac{u(s)}{\delta_T(s)}$	$N(s) = k_2 (S + 1.101) (S + 0.387 \pm 1.060j)^2$
$\frac{\dot{h}(s)}{\delta_T(s)}$	$N(s) = k_3 (S + 2.684) (S + 0.039 \pm 0.563j)^2$
$\frac{h(s)}{\delta_F(s)}$	$N(s) = k_4 (S + 1.111) (S + 0.296 \pm 1.120j)^2$

System 6A. Performance Index Parameters

$$b_1 = 1.0 \times 10^{-13}$$

$$b_2 = 2.0 \times 10^{-13}$$

$$k_1 = 4.0 \times 10^{+7}$$

$$k_2 = 1.0 \times 10^{+10}$$

B Feedback Gains

	Airspeed	Sink Rate	Pitch	Pitch Rate
Elevator	-0.0000465	-0.000112	-0.0134	-0.0249
Thrust	530.6	3070.0	2312.0	-54,380.0
DLC Flap	0.00691	0.0618	3.579	3.006

C. Numerator Zeros

$\frac{\theta(s)}{\delta_E(s)}$	$N(s) = k_1 (s + 0.963) (s + 2.131)$
$\frac{u(s)}{\delta_T(s)}$	$N(s) = k_2 (s + 1.600) (s + 0.336 \pm 1.063j)$
$\frac{h(s)}{\delta_T(s)}$	$N(s) = k_3 (s + 2.538) (s + 0.099 + 0.549j)^2$
$\frac{h(s)}{\delta_F(s)}$	$N(s) = k_4 (s + 0.913) (s + 0.327 \pm 1.049j)^2$

APPENDIX 1

Design Limitations of Root Square LocusTechnique for the Carrier Approach

In order to gain satisfactory phugoid loci in the outer loop closure of the root square locus design, it is necessary to have a lightly damped complex root pair in the sink rate loop. This complex pair is obtained from the complex zeros of the sink rate to flap and the sink rate to thrust transfer functions. A method of testing these transfer functions for suitable phugoid-control zeros is derived in this appendix.

A. Development of Phugoid-Control Zeros

For the derivation of $N_{23}(s)$ and $N_{22}(s)$, equation (2) is simplified as follows: Since γ_0 is approximately 4 degrees, $\cos \gamma_0$ is assumed equal to unity. It is further assumed that a suitable mechanical flap-to-elevator interconnect will cancel the $M_{\delta F}$ effect. The following inequalities are properties of the aerodynamics:

$$\left| Z_{\alpha} \right| > \left| g \sin \gamma_0 \right| \quad (a)$$

$$\left| M_{\alpha} \right| > \left| M_w' Z_{\alpha} \right| > \left| M_w' g \sin \gamma_0 \right| \quad (b)$$

$$\left| M_q \right| > \left| M_{\dot{\alpha}} \right| \quad (c)$$

Table VII lists the values of these parameters for the F-8C, the A-5A, and the F-4E. Inequalities (a) through (c) are used to further simplify equation (2). Thus, the airframe equation becomes:

$$\dot{\underline{x}} = \begin{bmatrix} X_u & -X_w & X_\alpha - g & 0 \\ -Z_u & Z_w & -Z_w V_o & 0 \\ 0 & 0 & 0 & 1 \\ (M_u + M_w Z_u) & -M_w + M_w Z_w & M_\alpha & M_q \end{bmatrix} \underline{x} + \begin{bmatrix} X_{\delta E} & X_{\delta T} & X_{\delta F} \\ -Z_{\delta E} & -Z_{\delta T} & -Z_{\delta F} \\ 0 & 0 & 0 \\ \begin{pmatrix} M_{\delta E} + \\ +M_w Z_{\delta E} \end{pmatrix} & \begin{pmatrix} M_{\delta T} + \\ +M_w Z_{\delta T} \end{pmatrix} & M_w Z_{\delta F} \end{bmatrix} \underline{\delta}$$

or

$$\underline{\dot{x}} = \underline{A'} \underline{x} + \underline{B'} \underline{\delta} \quad (I-1)$$

Laplace transforming equation (I-1) and solving for \underline{x} yields:

$$\underline{x}(s) = [Is - \underline{A'}]^{-1} \underline{B'} \underline{\Delta}(s)$$

Airplane	Z_α	$g \sin \gamma_o$	M_α	$M_w Z_\alpha$	M_q	M_α'
F-8C	125.2	2.25	1.074	0.0237	0.347	0.043
F-4B	83.6	2.25	1.298	0.0292	0.433	0.0789
A-5A	146.7	2.25	0.88	0.0678	0.288	0.103
F-111B	92.8	2.25	0.08	0.041	0.436	0.0856

TABLE VII AERODYNAMIC PARAMETERS FOR VARIOUS NAVY AIRCRAFT

or

$$X_j(s) = \sum_{k=1}^3 \left[\frac{1}{\Delta(s)} \sum_{i=1}^4 C_{ij}(s) b_{ik} \right] \Delta_k(s) \quad (I-2)$$

where $C_{ij}(s)$ is the i, j th cofactor of $[Is - A]$. If k is fixed at a specific number, i.e., $k = l$, and $\Delta_k(s)$ is set equal to zero for $k \neq l$, equation (I-2) becomes

$$X_j(s) = \frac{1}{\Delta(s)} \sum_{i=1}^4 C_{ij}(s) b_{il} \Delta_l(s)$$

or

$$\frac{X_j(s)}{\Delta_l(s)} \underset{i \neq l}{\Delta_i(s) = 0} = \frac{1}{\Delta(s)} \sum_{i=1}^n C_{ij}(s) b_{il} \quad (I-3)$$

Equation (I-3) is the definition of the i, j th element of the transfer matrix, $M_{ij}(s)$. Substituting into equation (I-3)

$$M_{jl}(s) = \frac{N_{jl}(s)}{\Delta(s)}$$

yields the desired numerator polynomial

$$N_{jl}(s) = \sum_{i=1}^n C_{ij}(s) b_{il} \quad (I-4)$$

Since the derivation in this appendix considers only sink rate transfer functions (i.e., $j = 2$) and noting that $b_{23} = 0$, only $C_{12}(s)$, $C_{22}(s)$ and $C_{42}(s)$ need be calculated.

$$C_{12}(s) = - \det \begin{bmatrix} Z_u & Z_w V_o & 0 \\ 0 & s & -1 \\ -\beta & -M_\alpha & S-M_q \end{bmatrix}$$

where

$$\beta = M_u + M_w Z_u$$

$$C_{12}(s) = -Z_u (s^2 - M_q s - M_\alpha) - \beta Z_w V_o$$

The magnitude of $Z_u M_\alpha$ and $\beta Z_w V_o$ are compared for the selected aircraft in Table VIII.

Airplane	$\beta Z_w V_o$	$Z_u M_\alpha$
F-8C	0.073	0.284
F-4B	0.032	0.396
A-5A	0.00683	0.0479
F-111B	0.00743	0.0247

TABLE VIII CONSTANT TERMS OF $C_{12}(s)$

This comparison allows the simplification

$$C_{12}(s) = -Z_u (s^2 - M_q s - M_\alpha) \quad (I-5a)$$

$$C_{22}(s) = \det \begin{bmatrix} s - X_u & -X_\alpha + g & 0 \\ 0 & s & -1 \\ -\beta & -M_\alpha & s - M_q \end{bmatrix}$$

$$C_{22}(s) = s^3 - (X_u + M_q) s^2 + (X_u M_q + M_\alpha) s + X_u M_\alpha + (g - X_\alpha) \beta$$

The magnitude of terms in the coefficients are compared in Table IX.

Airplane	X_u	M_q	$X_u M_q$	M_α	$X_u M_\alpha$	$(g - X_\alpha) \beta$
F-8C	0.0506	0.347	0.0176	1.074	0.0543	0.0196
F-4B	0.094	0.433	0.0407	1.298	0.122	0.00759
A-5A	0.0544	0.288	0.0157	0.83	0.0479	0.000914
F-111B	0.0456	0.436	0.0199	0.08	0.00365	0.00117

TABLE IX COEFFICIENT TERMS OF $C_{22}(s)$

Thus $C(s)$ is approximately

$$C_{22}(s) = s^3 - M_q s^2 - M_\alpha s + X_u M_\alpha \quad (I-5b)$$

$$C_{42}(s) = \det \begin{bmatrix} s - X_u & g - X_\alpha & 0 \\ Z_u & Z_w V_o & 0 \\ 0 & s & -1 \end{bmatrix}$$

$$C_{42}(s) = -Z_w V_o s + Z_w V_o X_u + Z_u (g - X_\alpha) \quad (I-5c)$$

B. Sink Rate to Thrust Numerator $N_{22}(s)$

$$N_{22}(s) = \sum_{i=1}^4 C_{i2}(s) b_{i2}$$

$$N_{22}(s) = -Z_{\delta T} s^3 + (Z_{\delta T} M_q - Z_u X_{\delta T}) s^2 +$$

$$[Z_u Z_{\delta T} M_q + Z_{\delta T} (M_\alpha - Z_w V_o M_w^*) - Z_w V_o M_{\delta T}] s +$$

$$[Z_u M_\alpha X_{\delta T} - Z_{\delta T} X_u M_\alpha + (g - X_\alpha) Z_u (M_{\delta T} + M_w^* Z_{\delta T}) +$$

$$+ Z_w V_o X_u (M_{\delta T} + M_w^* Z_{\delta T})]$$

Table X lists the magnitude of the various coefficient terms.

$N_{22}(s)$ may be simplified to

$$N_{22}(s) = -Z_{\delta T} [s^3 + Z_u \eta_T s^2 + (Z_w V_o \epsilon_T - Z_u M_q \eta_T - M_\alpha) s - M_\alpha \eta_T Z_u] \quad (I-6)$$

for all aircraft listed in Table X except the F-111B, η_T and ϵ_T are defined as follows:

$$\eta_T = \frac{X_{\delta T}}{Z_{\delta T}} \quad \text{and} \quad \epsilon_T = \frac{M_{\delta T}}{Z_{\delta T}}$$

The extremely small value of M_α for the F-111B negates the constant term approximation of equation (I-6). This approximation will be retained and justified later on for the F-111B.

CONSTANT TERMS							S TERMS		S ² TERMS	
Air planes	$Z_u M_\alpha$ $X_{\delta T}$	$X_u M_\alpha$ $Z_{\delta T}$	$(g-X_\alpha)$ $Z_u M_{\delta T}$	$(g-X_\alpha) Z_u$ $M_w Z_{\delta T}$	$X_u Z_w$ $V_o M_{\delta T}$	$X_u Z_w V_o$ $M_w Z_{\delta T}$	M_α	$Z_w V_o$ M_w	Z_u $X_{\delta T}$	$M Z_q$
F-8C	4.51×10^{-4}	1.19×10^{-5}	4.20×10^{-5}	3.70×10^{-7}	2.98×10^{-5}	2.63×10^{-7}	1.074	0.0237	0.000461	0.0000701
F-4B	3.72×10^{-4}	1.06×10^{-5}	2.72×10^{-5}	2.52×10^{-7}	2.57×10^{-5}	2.38×10^{-7}	1.298	0.0292	0.000288	0.0000375
A-5A	2.01×10^{-4}	8.71×10^{-7}	1.71×10^{-7}	4.52×10^{-8}	2.53×10^{-7}	6.71×10^{-8}	0.88	0.0678	0.000229	0.0000524
F-111B	1.38×10^{-5}	6.89×10^{-8}	1.09×10^{-5}	3.94×10^{-8}	1.03×10^{-5}	3.68×10^{-8}	0.08	0.0427	0.000172	0.0000824

TABLE X COEFFICIENT TERMS OF N_{22} (s)

AIRPLANE	NUMERATOR POLYNOMIALS
F-8C	$N_{22}(s) = -Z_{\dot{\epsilon}_T} (s^3 + 1.92 s^2 - 0.95s + 2.06)$
F-4B	$N_{22}(s) = -Z_{\delta_T} (s^3 + 3.32 s^2 - 0.42s + 4.31)$
A-5A	$N_{22}(s) = -Z_{\dot{\epsilon}_T} (s^3 + 12.59s^2 + 4.76s + 11.08)$
F-111B	$N_{22}(s) = -Z_{\dot{\epsilon}_T} (s^3 + 9.10s^2 + 15.94s + 0.729)$

TABLE XI $N_{22}(s)$ FOR VARIOUS NAVY AIRCRAFT

For the F-8C, $N_{22}(s)$ has a complex root pair in the right-half s plane. Inspection of $N_{22}(s)$ in Table XI shows that the quadratic term formed by deleting the s^3 term also yields a complex root pair in the right-half s plane. Table XII lists the roots of $N_{22}(s)$ when this quadratic term is assumed as a factor of $N_{22}(s)$ and also when the original cubic equation is solved.

Airplane	Quadratic Approximation	Original Cubic
F-8C	$+ 0.25 + 1.01j$ -2.39	$+ 0.34 + 0.82j$ -2.59
A-5A	$-0.19 + 0.92j$ -12.20	$-0.16 + 0.96j$ -12.28
F-4B	$+0.07 + 1.14j$ -3.43	$+0.20 + 1.07j$ -3.74
F-111B	$-1.71 - .05$ -7.35	$-2.30 - .047$ -6.76

TABLE XII ROOTS OF $N_{22}(s)$

Using the approximate quadratic factor, the phugoid-control zeros of $N_{22}(s)$ are described by

$$s + \left(\frac{Z_w V_o M_{\delta T} - M_{\alpha} Z_{\delta T}}{Z_u X_{\delta T}} - M_q \right) s - M_{\alpha} = 0 \quad (I-7)$$

For the phugoid locus to pass through the desired region of figure 12, the numerator roots should have a natural frequency greater than 0.707 radians per second and a damping ratio no greater than $|0.35|$. Thus, the phugoid-control zeros which determine the numerator roots should have a damping ration between -0.35 and 0.35 and a natural frequency greater than 0.707 radians per second, resulting in the following specifications:

$$-M_{\alpha} \geq 0.5 \quad (I-8a)$$

$$\Lambda = \frac{Z_w V_{\alpha} M_{\delta T} - M_{\alpha} Z_{\delta T}}{Z_u X_{\delta T}} - M_q \geq 0.5 \quad (I-8b)$$

C. Sink Rate to Flap Numerator $N_{23}(s)$

$$N_{23}(s) = \sum_{i=1}^4 C_{i2} b_{i3}$$

$$\begin{aligned} N_{23}(s) = & -Z_{\delta F} s^3 - (Z_u X_{\delta F} - M_q Z_{\delta F}) s^2 + \\ & + (M_q Z_u X_{\delta F} + M_{\alpha} Z_{\delta F} - M_w^* Z_w V_{\alpha} Z_{\delta F}) s + \\ & + (Z_u M_{\alpha} X_{\delta F} - X_u M_{\alpha} Z_{\delta F} + M_w^* Z_w V_{\alpha} X_u Z_{\delta F} + g Z_u M_w^* Z_{\delta F}) \end{aligned}$$

Table XIII lists the magnitudes of the coefficient terms. Dropping the less significant terms yields

$$N_{23}(s) = Z_{\delta F} [s^3 + (Z_u n_F - M_q) s^2 - M_{\alpha} s - M_{\alpha} (Z_u n_F - X_u)] \quad (I-9)$$

where

$$n_F = \frac{X_{\delta F}}{Z_{\delta F}}$$

Table XIV lists $N_{23}(s)$ for the F-8C, A-5A and F-111B. The F-4B is excluded due to the nonlinearity of its flap effectiveness curve.

Inspection of N_{23} in Table XIV discloses a difference of two orders of magnitude between the linear term in s and the constant term. This fact strongly indicates that it may be approximately factored as follows:

	CONSTANT TERMS						S TERMS				S TERMS		
	$Z_u X_a \delta F$	$X_u M_a \delta F$	$M_w Z_w X_u \delta F$	$(g-X_c) Z_u M_w Z_w \delta F$	$M_q Z_q X_u \delta F$	$M_a Z_a \delta F$	$M_w Z_w \delta F$	$M_q Z_q \delta F$	$Z_u X_u \delta F$	$Z_u X_u \delta F$	$M_q Z_q \delta F$	$M_q Z_q \delta F$	$M_q Z_q \delta F$
Air-plane													
F-8C	1.905	1.027	0.0226	0.0319	0.616	20.299	0.447		1.774		6.558		
A-5A	1.244	1.281	0.0986	0.0664	0.407	23.540	1.813		1.414		7.704		
F-111B	0.122	0.118	0.0633	0.0672	0.664	2.58	1.278		1.523		14.061		

TABLE VIII: COEFFICIENT TERMS OF $N_2(s)$

$$N_{23}(s) = -Z_{\delta F} [s^2 + (Z_u \eta_F - M_q)s^2 - M_\alpha s - M_\alpha (Z_u \eta_F + X_u)]$$

$$= -Z_{\delta F} [s^2 + (Z_u \eta_F - M_q)s - M_\alpha] (s - Z_u \eta_F + X_u)$$

Airplane	NUMERATOR POLYNOMIAL
F-8C	$N_{23}(s) = -Z_{\delta F} (s^2 + 0.25s^2 + 1.07s - 0.047)$
A-5A	$N_{23}(s) = -Z_{\delta F} (s^2 + 0.24s^2 + 0.88s - 0.000136)$
F-111B	$N_{23}(s) = -Z_{\delta F} (s^2 + 0.389s^2 - 0.008s - 0.000134)$

TABLE XIV $N_{23}(s)$ FOR VARIOUS NAVY AIRCRAFT

Table XV lists the roots of $N_{23}(s)$. The first column is determined by the approximation, and the second column by solving the original cubic equation.

Airplane	Approximate Factorization	Original Cubic
F-8C	$-0.13 + 1.03j$ $+0.043$	$-0.15 + 1.03j$ $+0.043$
A-5A	$-0.22 + 0.93j$ -0.000155	$-0.22 + 0.93j$ 0.000155
F-111B	$-0.195 + 0.205j$ -0.00168	$-0.194 + 0.205j$ -0.00169

TABLE XV Roots of $N_{23}(s)$

Thus the phugoid control zeros of $N_{\delta}(s)$ may be described by

$$s^2 + (Z_u n_F - M_q)s - M_{\alpha} = 0 \quad (1-10)$$

For the roots of equation (1-10) to have a damping ratio between -0.35 and 0.35 and a natural frequency greater than 0.5 radians per second, the following inequalities must be satisfied:

$$-M_{\alpha} \geq 0.5 \quad (1-11a)$$

$$\zeta = \frac{Z_u X_{\delta F} - M_q Z_{\delta F}}{Z_{\delta F} \sqrt{-M_{\alpha}}} \geq 0.7 \quad (1-11b)$$

D. Operational limitations

To assure closed loop phugoid roots which satisfy equation (2b), a lightly damped complex zero pair is needed in the sink rate loop. Since the elevator zeros are characteristically real, this pair must come from either the flap zeros or the thrust zeros. Alternatively, the aerodynamic derivatives of the airplane in question must satisfy either conditions (1-8) or conditions (1-11). Since conditions (1-8a) and (1-11a) are identical, it appears that $-M_{\alpha} \geq 0.5$ is an essential requirement for satisfactory closed loop phugoid roots. Table XVI lists the results obtained when these conditions are applied to the F-8C, the F-4B, the A-5A and the F-111B, each for a single approach configuration. The results indicate that the Root Square Locus technique can be applied to design satisfactory automatic approach controllers for the F-8C, F-4B, A-5A and similar aircraft. In the case of the F-111B, however, the very low magnitude of M_{α} indicates that adequate phugoid bandwidth cannot be obtained via root square locus design.

This particular value of $-M = 0.08$ is for a specific loading condition as shown in Table XVI. Examination of the entire range of center of gravity locations and airspeeds of the F-111B approach configurations indicate that the value of M_α is always unsatisfactorily small. This may be demonstrated as follows:

$$\left| M_\alpha \right| = - \frac{S_w c_D}{2ly} V_o^2 C_{m_\alpha} \text{ and} \quad (I-12)$$

$$C_m = - C_L \left(\frac{x_{np}}{c} - \frac{x_{cg}}{c} \right) \quad (I-13)$$

Substituting into (I-13)

$$\left| M_\alpha \right| = \left(\frac{S_w C_{L_\alpha}}{2ly} \right) V_o^2 (x_{np} - x_{cg}) \quad (I-14)$$

Airplane	Landing Conditions	$-M_\alpha$	Λ	Ω
F-8C	$V_o = 226 \text{ ft/sec}$ $cg = 27\% \text{ MAC}$	1.074	0.494	0.25?
F-1B	$V_o = 226 \text{ ft/sec}$ $cg = 30.0\% \text{ MAC}$	1.298	0.210	Not calculated
A-52	$V_o = 223 \text{ ft/sec}$ $cg = 30.6\% \text{ MAC}$	0.88	0.378	0.251
F-111B	$V_o = 200 \text{ ft/sec}$ $cg = 35.5\% \text{ MAC}$	0.08	1.755	1.374

NOTE: Satisfactory zeros require

$$-M_\alpha \leq 0.5, \Lambda \leq 0.5 \text{ and } \Omega \leq 0.7$$

TABLE XVI CRITERIA FOR SATISFACTORY PHUGOID-CONTROL ZEROS

In the approach configuration, C_{L_α} is independent of the center of gravity location and airspeed. Therefore

$$M_\alpha = k_1 V_o^2 (x_{np} - x_{cg}) \quad (I-15)$$

Substituting the numerical values of Appendix A into equation (I-14) yields

$$x_{np} = 0.372\bar{c}$$

Thus,

$$M_\alpha = 4.43 \left(\frac{V_o}{200} \right) \left(0.372 - \frac{x_{cg}}{c} \right) \quad (I-15)$$

Typical approach conditions for the F-111B are

$$0.555 \leq \frac{x_{cg}}{c} \leq 0.420 \quad (I-16a)$$

and

$$V_o = 250 \text{ ft/sec} \quad (I-16b)$$

which yield

$$|M_\alpha| = 0.332$$

Thus, the magnitude of M_α for the F-111B is unsatisfactory for any center of gravity location and approach airspeed, in terms of root square optimal design.

Condition (I-8a) was derived from the approximation of $N_z(s)$ defined in equation (I-6). This approximation was found to be poor for the F-111B for the flight condition given in Appendix A. Several components of the constant term are similar in magnitude to $n_T Z_u M_\alpha$ at this flight condition. However, for the power approach conditions stated in equations (I-17) all of the components of the constant term except $n_T Z_u M_\alpha$ remain near the values listed in Table X, while $n_T Z_u M_\alpha$ increases by a factor of five. Thus, a natural frequency of sufficient magnitude (i.e., $\omega_n = 0.707$) can only be provided by the $n_T Z_u M_\alpha$ term. Condition (I-8a) is thus a valid criterion for the F-111B airplane.